Universitetet i Stavanger

FACULTY OF SCIENCE AND TECHNOLOGY

MASTER'S THESIS

Study programme/specialisation: Petroleum Engineering/ Reservoir Engineering	Spring semester, 2018 ~~Open~~/Confidential
Author: Jone Urdal	..... (signature of author)
Programme coordinator: Steinar Evje Supervisor(s): Jahn-Otto Waldeland	
Title of master's thesis: A Three-Phase Model for Tumor Cell Migration	
Credits: 30	
Keywords: Cell migration, Chemokine, Chemotaxis, ECM remodeling, Fibroblast, Interstitial fluid, Multiphase flow, TGF, Viscous coupling	Number of pages: 102 Stavanger, 15.06.2018 date/year

A Three-Phase Model for Tumor Cell Migration

Jone Urdal

Department of Energy and Petroleum Engineering
Faculty of Science and Technology
University of Stavanger

June 15, 2018

This thesis is submitted for the degree of Master of Science.

Abstract

Flow of interstitial fluid (IF) has proven to have a significant effect on the migration of cancer cells through tissue due to the tumor cells ability to sense flow by secreting chemokines that convect in the flow direction (autologous chemotaxis). It has become increasingly popular to model this (and other) phenomena using multiphase models based on e.g. Darcy's law, the Brinkman equation or more general mixture theory approaches.

Recent experimental work suggests that fibroblast cells present in vivo might influence the ability of cancer cells to invade the surrounding tissue. The objective of this thesis is to expand a two-fluid model used to investigate autologous chemotaxis of cancer cells to a three-phase model where also the effect of the fibroblasts can be accounted for.

First, relevant experimental results will be analyzed, followed by a general model formulation using mass and momentum balance based on mixture theory. The approach is inspired by that of modeling hydrocarbon flow in underground reservoirs. Finally, we will implement a numerical solution for a simplified 1-D version of the model and compare the simulated output to experimental results to elucidate some of the mechanism(s) behind fibroblast-enhanced tumor cell invasion. Special focus we will be on investigating the fibroblasts ability to remodel the ECM and also viscous coupling between cells and fibroblasts.

Acknowledgements

I would like to express my sincere gratitude to Professor Steinar Evje and PhD student Jahn-Otto Waldeland at the Department of Energy and Petroleum Engineering for presenting me with this very interesting topic. I also appreciate all our discussions and the information, comments, and suggestions provided. Your guidance and knowledge have been of immense help. Thank you!

Contents

List of Figures

List of Tables

Nomenclature

Abbreviations

BL =	Buckley-Leverett
ECM =	extracellular matrix
Fb =	fibroblast
IF =	interstitial fluid
MG =	Matrigel
MMP =	matrix metalloproteinase
ODE =	ordinary differential equation
TC =	tumor cell
TGF =	transforming growth factor

Roman

A =	parameter in $\hat{k}_c$, -
B =	parameter in $\hat{k}_c$, -
$\mathbf{b}_i$ =	net body force per unit mass, m/s^2
C =	concentration of chemokine, kg/m^3 or -
C_M =	maximum concentration of chemokine, kg/m^3 or -
C^* =	reference concentration of chemokine, kg/m^3
D_C =	diffusion coefficient of chemokine, m^2/s or -
D_G =	diffusion coefficient of protease, m^2/s or -
D_H =	diffusion coefficient of TGF, m^2/s or -
D^* =	reference diffusion coefficient, m^2/s
$\mathbf{f}_{ij}$ =	momentum transfer from phase j into phase i, Pa/m
$\hat{f}_c$ =	fractional flow of cell phase, -
$\hat{f}_f$ =	fractional flow of fibroblast phase, -
$\hat{f}_w$ =	fractional flow of IF phase, -
G =	concentration of protease, kg/m^3 or -
G_M =	maximum concentration of protease, kg/m^3 or -
G^* =	reference concentration of protease, kg/m^3
H =	concentration of TGF, kg/m^3 or -

H_M = maximum concentration of TGF, kg/m^3 or -
H^* = reference concentration of TGF, kg/m^3
I_c = static parameter of the cell-ECM interaction, Pas/m^2 or -
I_f = static parameter of the fibroblast-ECM interaction, Pas/m^2 or -
I_w = static parameter of the IF-ECM interaction, Pas/m^2 or -
I_{cf} = static parameter of the cell-fibroblast interaction, Pas/m^2 or -
$\mathbf{I}$ = identity matrix, -
K = absolute permeability of tissue, m^2
k_{cf} = volume conversion rate from fibroblast to cell, 1/s
k_{cw} = volume conversion rate from IF to cell, 1/s
k_{fc} = volume conversion rate from cell to fibroblast, 1/s
k_{fw} = volume conversion rate from IF to fibroblast, 1/s
k_{rl} = relative permeability of phase l, -
k_{wc} = volume conversion rate from cell to IF, 1/s
k_{wf} = volume conversion rate from fibroblast to IF, 1/s
$\hat{k}_c$ = dynamic parameter of the cell-ECM interaction, -
$\hat{k}_f$ = dynamic parameter of the fibroblast-ECM interaction, -
$\hat{k}_w$ = dynamic parameter of the IF-ECM interaction, -
$\mathbf{k}$ = absolute permeability tensor, m^2
L = length of domain, m or -
L^* = reference length, m
$\mathbf{m}_i$ = momentum transfer to phase i, from all other phases, Pa/m
n_w = Corey water saturation exponent, -
P_l = pressure of phase l, Pa or -
P^* = reference pressure, Pa
Q_l = source term of phase l, 1/s
Q_v = production of IF from the vascular system, 1/s
Q_l = adsorption of IF to the lymphatic system, 1/s
R_c = relation between cell-ECM and cell-fibroblast force, -
R_f = relation between fibroblast-ECM and cell-fibroblast force, -
R_w = relation between IF-ECM and cell-fibroblast force, -
r_c = parameter describing cell-ECM interaction, -
r_f = parameter describing fibroblast-ECM interaction, -
r_i = mass transfer to phase i, from all other phases, Pas/m^2
r_w = parameter describing IF-ECM interaction, -
r_{cf} = parameter describing viscous coupling between cells and fibroblasts, -
r_{fc} = parameter describing viscous coupling between cells and fibroblasts, -
S_c = cell source term, 1/s or -
S_f = fibroblast source term, 1/s or -
S_o = oil saturation, -
S_w = water saturation, -
T = time of simulation, s or -
T^* = reference time, s

t = time, s or d or -
$\mathbf{t}$ = stress tensor of phase i, Pa
U_l = Darcy velocity of phase l, m/s or -
U_T = total velocity, m/s or -
u_l = interstitial velocity of phase l, m/s or -
u^* = reference velocity, m/s
x = distance, m or -
$\bar{x}_c$ = cell volume center, m or -

Greek

α_c = cell volume fraction, -
α_f = fibroblast volume fraction, -
α_w = IF volume fraction, -
γ = parameter in ΔP-function, Pa or -
Δ = forward-difference or gradient operator
ΔP_{cw} = cell-IF capillary pressure, Pa or -
ΔP_{fw} = fibroblast-IF capillary pressure, Pa or -
δ = central-difference operator or parameter in ΔP-function, -
$\hat{\zeta}_c$ = interaction coefficient between the cell phase and the ECM, Pas/m^2 or -
$\hat{\zeta}_f$ = interaction coefficient between the fibroblast phase and the ECM, Pas/m^2 or -
$\hat{\zeta}_w$ = interaction coefficient between the IF phase and the ECM, Pas/m^2 or -
$\hat{\zeta}_{cf}$ = viscous coupling between the cell and fibroblast phase, Pas/m^2 or -
Λ_C = potential function for chemotaxis of cells toward chemokine, Pa or -
Λ_{C0} = parameter characterizing Λ_C, Pa or -
Λ_{C1} = parameter characterizing Λ_C, Pa or -
Λ_H = potential function for chemotaxis of fibroblasts toward TGF, Pa or -
Λ_{H0} = parameter characterizing Λ_H, Pa or -
Λ_{H1} = parameter characterizing Λ_H, Pa or -
λ_{11} = proliferation of tumor cells, 1/s or -
λ_{12} = decay of tumor cells, 1/s or -
λ_{13} = decay of tumor cells, 1/s or -
λ_{21} = degradation of ECM, m^3/kgs or -
λ_{22} = reconstruction of ECM, 1/s or -
λ_{23} = release of ECM, 1/s or -
λ_{24} = release of ECM, 1/s or -
λ_{31} = decay of protease, 1/s or -
λ_{32} = cell production of protease, kg/m^{3}s or -
λ_{33} = logistic term constant (protease), kg/m^{3}s or -
λ_{41} = proteolytically freed chemokine, m^3/kgs or -
λ_{42} = logistic term constant (chemokine), m^3/kgs or -
λ_{43} = logistic term constant (chemokine), m^3/kgs or -

λ_{44} = cell consumption of chemokine, kg/m^{3}s or -
λ_{51} = decay of TGF, 1/s or -
λ_{52} = production of TGF, kg/m^{3}s or -
λ_{53} = logistic term constant (TGF), kg/m^{3}s or -
λ_l = Darcy-based mobility of phase l, m^2/(Pas)
$\hat{\lambda}_l$ = general mobility of phase l, m^2/(Pas)
μ_l = viscosity of phase l, Pa·s
ν_C = exponent in logistic function of chemokine, -
ν_G = exponent in logistic function of protease, -
ν_H = exponent in logistic function of TGF, -
ξ_1 = parameter characterizing Λ_C (dependence on C), m^3/kg or -
ξ_2 = parameter characterizing Λ_H (dependence on H), m^3/kg or -
ρ = density of ECM, kg/m^3 or -
ρ_l = density of phase l, kg/m^3
ρ_M = maximum density of ECM, kg/m^3 or -
ρ^* = reference density of ECM, kg/m^3
ϕ = porosity, -

Subscripts

0 = initial
C = chemokine
c = cell phase
f = fibroblast phase
H = TGF
i, j = dummy variables
l = phase index
M = maximal
T = total
w = interstitial fluid (IF) phase

Superscripts

x, y, z = coordinate directions
$*$ = reference parameter

Chapter 1

Introduction

It has been experimentally demonstrated that interstitial fluid (IF) flow (in the order of 1 μm/s) through the tissue may alter the tumor microenvironment and lead to a significant increase in the migration of cancer cells (Shieh, Rozansky, Hinz, & Swartz, 2011; Shieh & Swartz, 2011; Shields et al., 2007; Swartz & Fleury, 2007). An illustration of the tumor microenvironment is given in Figure 1.1. The IF flow apply stresses directly to the tumor cells by push and drag, but it also creates extracellular gradients of chemokines downstream, thus accelerating tumor progression in the direction of flow by means of *chemotaxis* (the ability of cells to move in a direction corresponding to a gradient of increasing or decreasing concentration of a particular substance).

More recently, it has been experimentally demonstrated that *fibroblast cells* (or just fibroblasts) also affects the progression of cancer cells (or just cells), making the tumor more aggressive (Shieh et al., 2011). Fibroblasts are one of the key components of the *tumor microenvironment* (the cellular environment in which the tumor exists), accompanied by e.g. immune cells, surrounding blood vessels, signaling molecules, IF and the *extracellular matrix* (ECM; consisting e.g. of collagen proteins which are fibers making up the skeleton of the tumor microenvironment). Fibroblasts are connective tissue cells that maintain the matrix enveloping most *epithelial tissues* (thin tissue covering all body surfaces, such as the outer surfaces of organs and blood vessels), and they are important e.g. in the process of wound healing. In cancer, fibroblasts synthesize and secrete the ECM molecules which make up the tumor stroma. They create an environment which is considerably different than healthy tissue, with higher concentrations of type I collagen, the main structural protein in the extracellular space. The possible interplay between the cancer cells and fibroblasts will be important in understanding the progression of tumors.

1.1 Objectives of this Thesis

Cancer cell migration driven by autologous chemotaxis was experimentally demonstrated by Shields et al. (2007). Later, autologous chemotaxis of cancer cells was investigated by Waldeland and Evje (2018) using a multiphase (cell and IF) model similar to those used

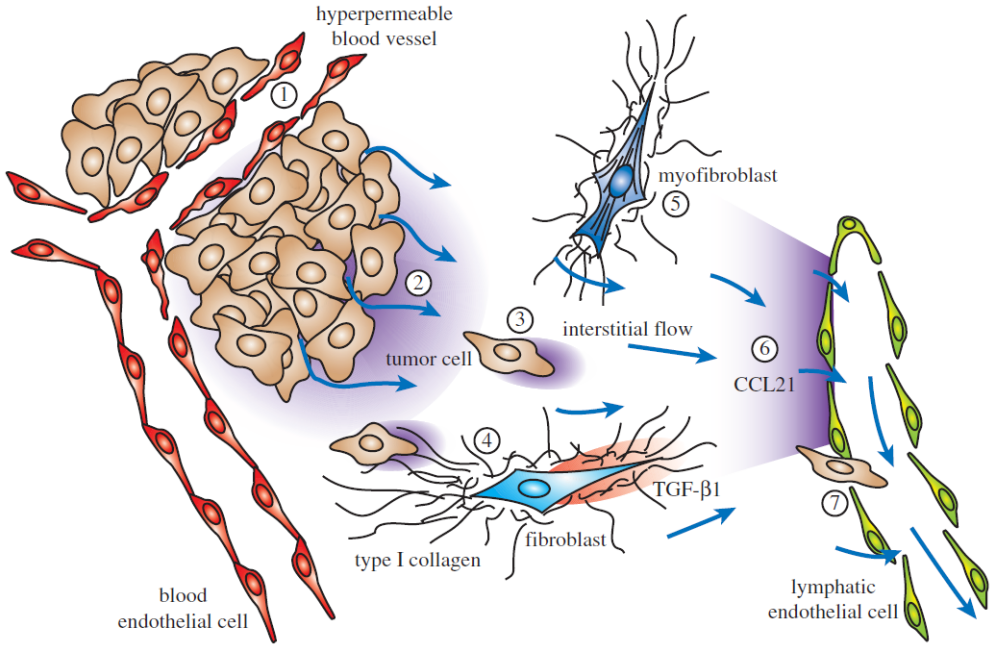

Figure 1.1: Tumor microenvironment: Leaky blood vessels inside the tumor and lymphatic vessels placed in the tissue acts as sources and sinks of interstitial fluid, creating a flow field across the tumor microenvironment. The tumor cells are able to sense the direction of flow by secreting chemokines into the flow field, and migrating downstream by means of autologous chemotaxis. The fibroblasts respond to the IF flow in a TGF-β1-dependent manner (also an example autologous chemotaxis). (Shieh & Swartz, 2011).

in the modeling of the simultaneous flow of water and oil in underground hydrocarbon reservoirs. The objective of this thesis is to expand upon the model given in that paper in order to study the simultaneous flow of cells, fibroblasts and IF. The model will then be solved numerically in a 1-D setting, and finally simulations will be compared with the experimental results by Shieh et al. (2011), summarized in Section 1.2.

1.2 Review of Paper by Shieh et. al., 2011

This section provides a review/summary of the most important results in the paper investigating the effects of fibroblasts on tumor cell invasion (Shieh et al., 2011). The authors of this paper did *in vitro* (outside body) experiments where they measured tumor cell invasion in an invasion assay consisting of tumor cells and/or fibroblasts cultured together with an ECM consisting of type I collagen and Matrigel (rich in chemokines). The experimental setup was exposed to an external pressure gradient resulting in interstitial flow of 0.5 μm/s. The following subsections sums up key results that could be useful when carrying out the simulation study.

1.2.1 Interstitial Flow Stimulates Fibroblast and Concomitant Tumor Cell Invasion

The main result of the experimental study was the increased tumor cell invasion in response to fibroblasts and flow being present. The results are summarized in Figure 1.2, and the main findings extracted from the article are given below.

1. IF flow stimulated tumor cell invasion, Figure 1.2A, but this effect was dependent on Matrigel. This is related to the chemotaxis of cells toward positive gradients in chemokine (which is bound to Matrigel), referred to as *autologous chemotaxis* by Shields et al. (2007). The tumor cells secrete protease, which react with the ECM to release surface-bound chemokines. The chemokine concentration is then skewed in the direction of IF flow, causing extracellular gradients, and inducing the chemotactic response of the tumor cells (in the direction of flow).

2. Cocultured fibroblasts increased tumor cell invasion under flow conditions, Figure 1.2B (left). In the absence of flow, or in the case when fibroblasts were cultured upstream, the effect was abolished. A similar effect was observed for the invasion of fibroblasts; IF flow stimulated fibroblast invasion, and even more so in the presence of tumor cells, Figure 1.2B (right). This suggests that the interaction between cells and fibroblasts go both ways.

3. Flow-enhanced fibroblast invasion was *independent* of chemokine (bound to Matrigel), Figure 1.2C (right), contrary to tumor cells. As a consequence, tumor cells continued to invade in the presence of fibroblasts and flow, even when Matrigel was absent, Figure 1.2C (left). Thus we can conclude that the mechanism behind the fibroblast-enhanced tumor cell invasion is independent of cell autologous chemotaxis, since it does not depend on the presence of Matrigel.

4. Tumor cell invasion was independent of fibroblast density under static conditions; however, in the presence of flow it increased fast at first but was insensitive at higher concentrations, Figure 1.2D.

These results make it very clear that fibroblasts have a significant impact on the aggressiveness of tumors, and explaining *why* is the main motivation for this thesis. Note that from these results it seems that the invasion of tumor cells correlates well with the migration of fibroblasts.

1.2.2 Flow- and Fibroblast-Enhanced Tumor Cell Invasion Depends on TGF

From the previous subsection it is clear that flow-enhanced fibroblast migration is due to some factor other than chemokine. To further investigate what kind of chemical signal the fibroblasts might respond to, the effect of TGF was explored, see results in Figure 1.3. Note that TGF is short for *transforming growth factor* (sometimes also tumor growth factor). There are two main types of transforming growth factors, TGFα and

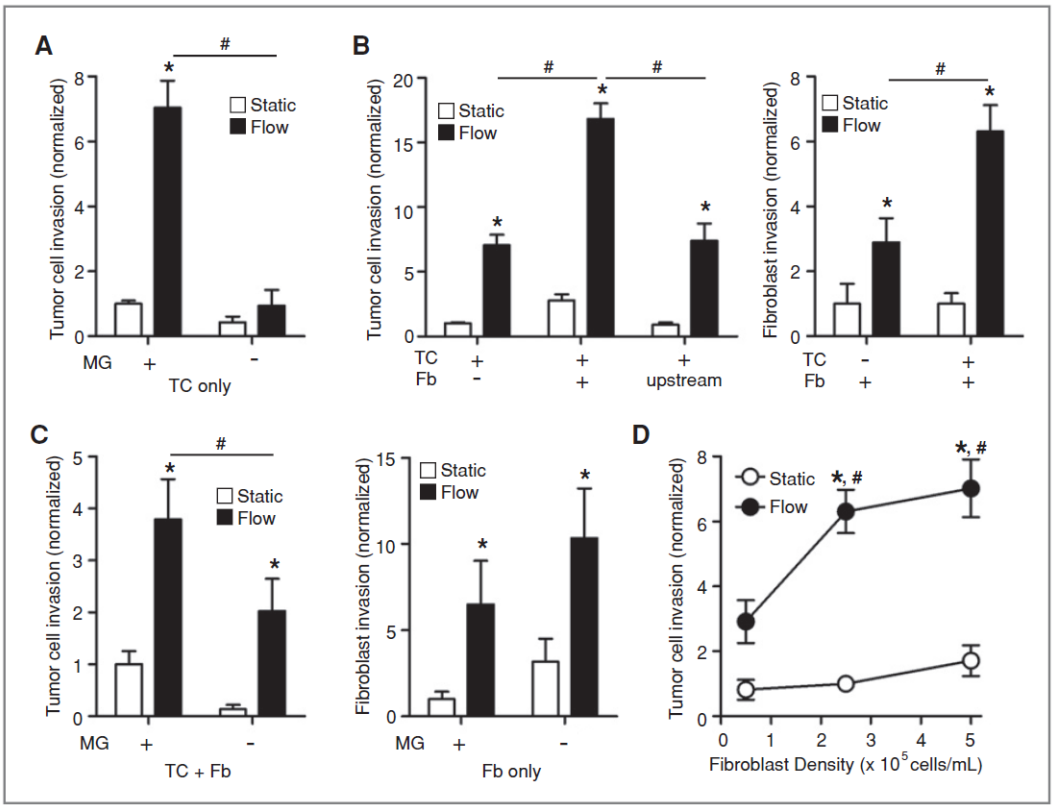

Figure 1.2: Fibroblasts enhance tumor cell invasion in the presence of interstitial flow (Shieh et al., 2011). Fb=fibroblast, MG=Matrigel, TC=tumor cell, +/−=present/absent.

TGFβ. The only type that we are going to consider is TGF-β1, which will sometimes be referred to as just TGF.

TGF are secreted by the fibroblasts themselves, but in latent form. It seems to be activated by e.g. shear stresses resulting from flow (Shieh et al., 2011; Shieh & Swartz, 2011). The main findings are listed below:

1. Blocking of TGF-β1 reduced tumor cell invasion when both flow and fibroblasts where present, otherwise it did not have any effect, Figure 1.3A (left). It also reduced the fibroblast invasion in the presence of flow, Figure 1.3A (right). Since tumor cells cultured alone did not respond to blocking of TGF, but fibroblasts alone, and tumor cells cocultured with fibroblasts did, it suggests that only the fibroblasts are directly affected. Tumor cells are indirectly influenced due to increased migration of fibroblasts.

2. The total amount of TGF-β1 increased in the presence of fibroblasts, Figure 1.3B. Increased activation was observed in the presence of flow, Figure 1.3C.

3. Invasion was only affected by TGF-β1 *gradients*. When exposed to uniform concentrations, the effect was negligible, Figure 1.3D. It is believed that the fibroblasts secrete TGF, which will then be transported in the direction of IF flow, causing localized gradients of the chemical agent to form and result in chemotaxis. Therefore, this is a type of autologous chemotaxis similar to that experienced by the cancer cells.

This suggest that fibroblasts chemotact toward TGF, and from previous results we know that they are unaffected by chemokine. The opposite is true for tumor cells; they follow chemokine concentrations, while being unaffected by TGF. It will be necessary to include equations in our model that can account for the transport and production/consumption of both chemokine and TGF.

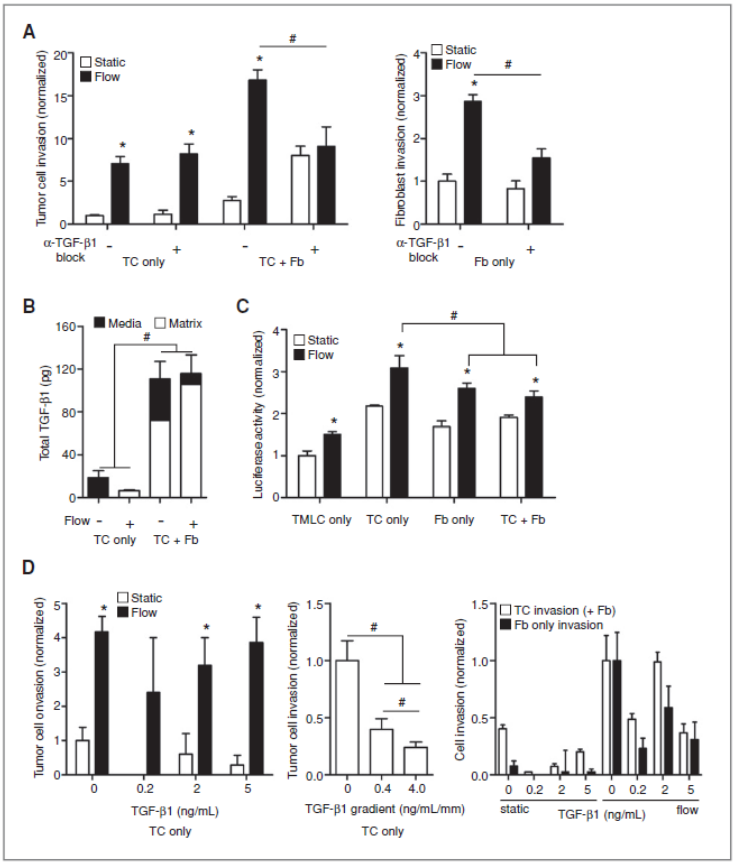

Figure 1.3: TGF-β1 is necessary for flow-enhanced tumor cell invasion only when fibroblasts are present (Shieh et al., 2011). TC=tumor cell, Fb=fibroblast, +/−=present/absent.

1.2.3 Fibroblast- and Flow-Enhanced Tumor Cell Invasion Depends on MMPs

Figure 1.4 shows that interstitial flow increased the amount of MMP-1, which in turn degrades the collagen in the matrix, and thus enhances the cell motility by reducing the resistance against flow through the tissue. Consequently, this may be considered as an increase of the absolute permeability of the porous medium.

We will not make any attempts to model this phenomenon individually, but rather as a combined effect together with the ECM remodeling which are discussed in Subsections 1.2.4-1.2.5.

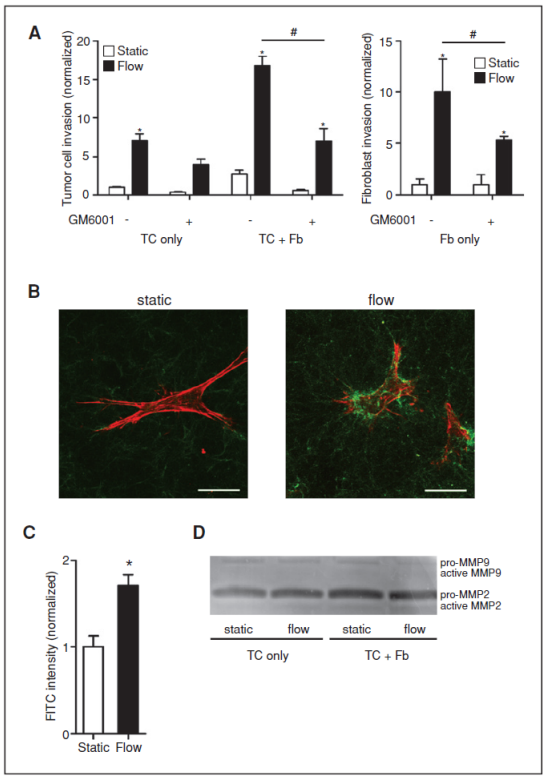

Figure 1.4: MMP activity is necessary for flow- and fibroblast-enhanced tumor cell migration (Shieh et al., 2011). Fibroblasts (red) and degraded collagen (green). TC=tumor cell, Fb=fibroblast, +/−=present/absent. Scale bar, 25 μm.

1.2.4 Rho-Dependent Fibroblast Contractility Drives Flow-Enhanced Tumor Cell Invasion

It is well-known that fibroblasts possess the ability to alter their surroundings by contracting the collagen fibers of the ECM (Kim, Lakshman, & Petroll, 2006). In order to determine if this is a necessary mechanism for flow- and fibroblast-enhanced tumor

cell invasion, Shieh et al. (2011) conducted experiments with different types of inhibitors affecting fibroblast contraction. Results are summarized in Figure 1.5.

1. When treating the fibroblasts with *C3 transferase* and *blebbistatin* (reagents inhibiting fibroblast contraction pathways), the morphology of the fibroblasts changed significantly, and collagen matrix contraction was reduced, Figure 1.5A.

2. Fibroblasts treated with C3 transferase and blebbistatin showed reduced tumor cell invasion, even if the migration of fibroblasts actually *increased*, Figure 1.5B and C. This proves that fibroblast migration alone is not sufficient to enhance tumor cell invasion.

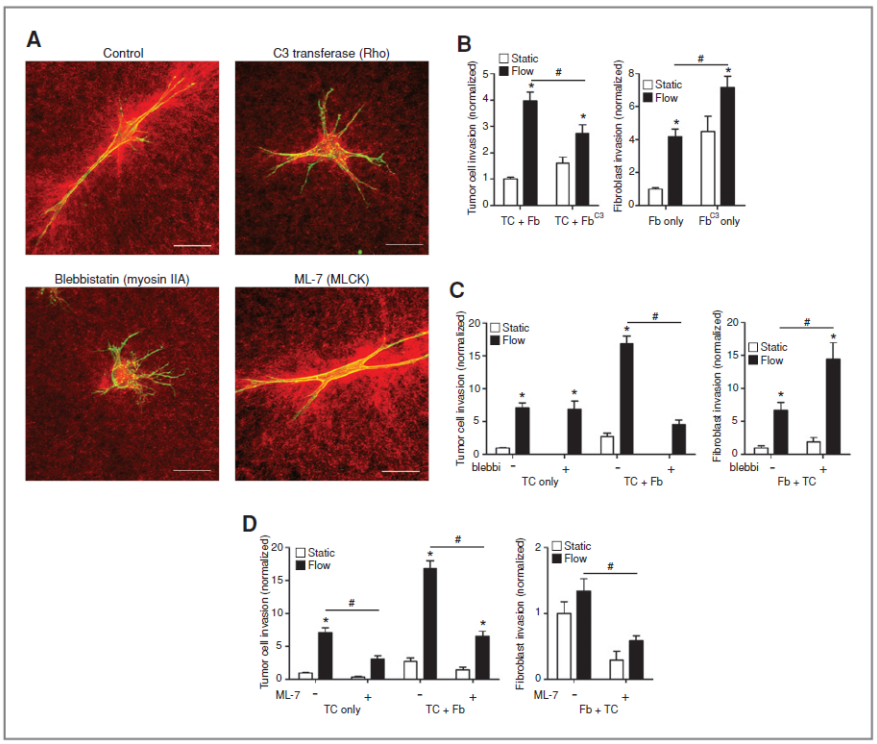

Figure 1.5: Flow- and fibroblast-enhanced tumor cell migration depends on Rho-mediated fibroblast contractility (Shieh et al., 2011). F-actin (green) and collagen matrix (red). TC=tumor cell, Fb=fibroblast, +/−=present/absent. Scale bar, 30 μm.

1.2.5 Fibroblasts Mediate ECM Reorganization

Figure 1.6 shows how the fibroblasts (red) locally contract the matrix (white) and interact with tumor cells (green). The tumor cells extend towards the fibroblasts in the direction of the contracted collagen fibers, and also align with the fibroblasts.

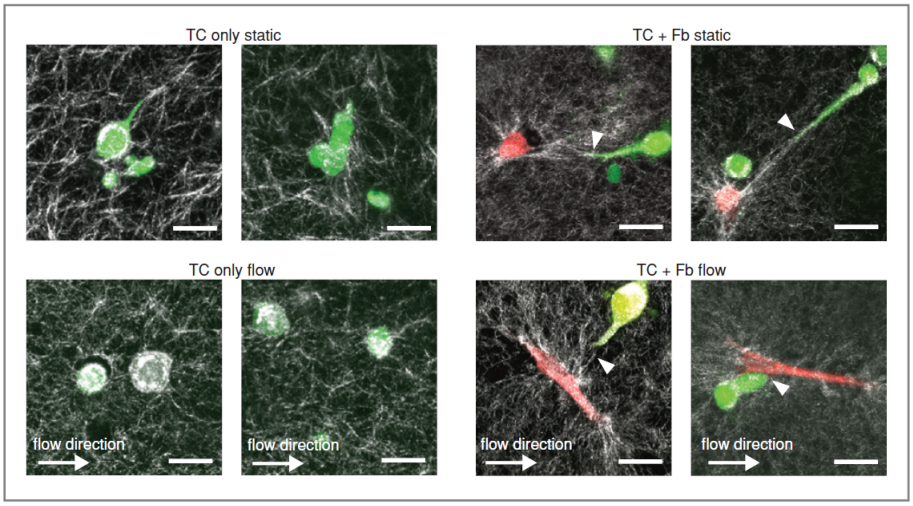

Figure 1.6: Fibroblasts locally contract the matrix and interact with tumor cells (Shieh et al., 2011). Tumor cells (TC; green), fibroblasts (Fb; red) and collagen matrix (white). Scale bar, 25 μm.

1.2.6 Proposed Mechanism

The proposed mechanism by Shieh et al. (2011) is summarized in Figure 1.7. This model can be explained through the following four steps:

1. Fibroblasts secrete latent TGF-β1 and contract the collagen fibers of the ECM.

2. When exposed to interstitial flow, the migration of fibroblasts increase significantly due to enhanced activation and availability of TGF-β1.

3. Flowing fibroblasts remodel the ECM.

4. Tumor cells migrate in the direction of flow due to autologous chemotaxis, and take advantage of the primed matrix to enhance their invasion.

Note that this model explains flow- and fibroblast-enhanced tumor cell invasion by focusing on the indirect interaction between the fibroblasts and cells, as a result of remodeling of the ECM. It does not say anything about the possible role played by the fluid-fluid interaction (also called *viscous coupling*) between the cells and fibroblasts, although it seems natural to think that this force should be present, as it plays a more or less significant role in the simultaneous flow of oil and water through rocks (Qiao, Andersen, Evje, & Standnes, 2018). This is also the mechanism suggested by Labernadie et al. (2017). If the strength of the viscous coupling is large enough, it could cause a direct drag force effect on the tumor cells from the fibroblasts.

Above is mentioned two different hypotheses that we want to test when doing the simulations, that is

1. indirect interaction due to ECM remodeling, and
2. direct interaction due to viscous coupling between cells and fibroblasts.

In the following chapter we will formulate the mathematical model relevant for exploring the two proposed models.

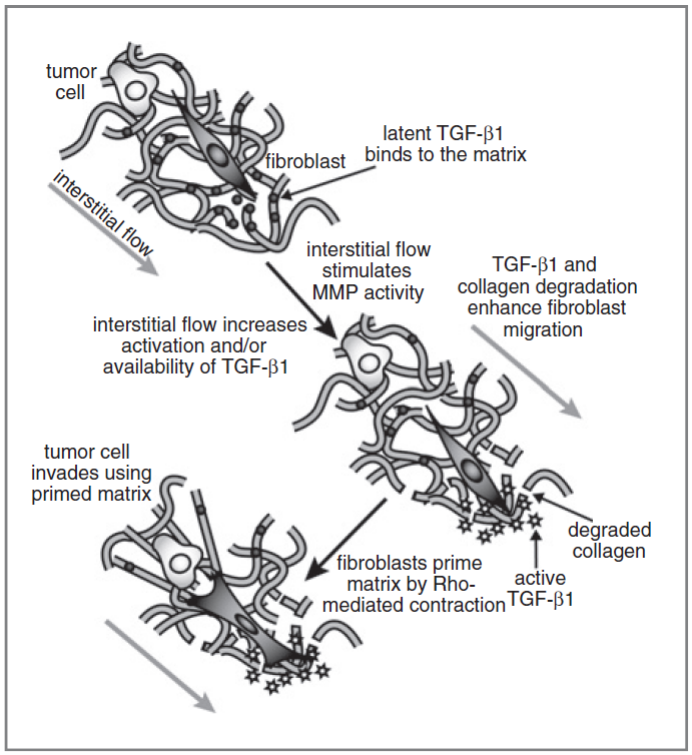

Figure 1.7: Proposed mechanism for flow- and fibroblast-enhanced tumor cell migration (Shieh et al., 2011).

Chapter 2

Mathematical Model

In this chapter, we develop the mathematical model describing the simultaneous flow of cell, fibroblast and interstitial fluid (IF), each represented by a phase. The approach is inspired by multiphase models used for flow of oil, water and gas in porous and permeable reservoir rocks. The tissue represent the "bulk" of the porous media, whereas the ECM is the solid/non-porous part (comparable to the solid rock matrix) and the porous portion is assumed to be completely saturated by the three phases cell, fibroblast, and IF. We do not differentiate between different types of tumor cells, such as alive or dead cells.

The model will be applied in a so-called "experimental setting", in which there is an externally imposed pressure gradient, causing IF flow across the domain, see Figure 2.1. This is different from a "tumor setting", in which there is no external pressure gradient, and flow of IF is generated by the vascular and lymphatic system, as shown in Figure 1.1.

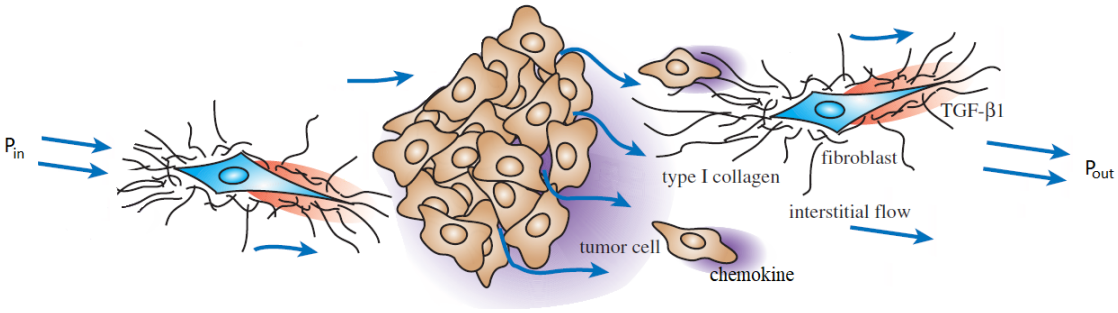

Figure 2.1: Tumor microenvironment (experimental setting). Figure modified from Shieh and Swartz (2011).

For each of the three phases, we formulate one mass and one momentum balance, summing to a total of six equations (we might treat the ECM as a fourth phase, but assuming it's stationary, we get the trivial momentum balance). In addition, we have three equations describing the evolution of the chemical agents; cell-secreted protease (G), surface-released chemokine (C), and fibroblast-secreted transforming growth factor

(H). The chemical components are subject to advection and diffusion, in addition to source terms representing production, decay and consumption. Finally, we have one equation representing dissolution of the extracellular matrix (ρ), as protease reacts with the ECM to release surface-bound chemokine (Fleury, Boardman, & Swartz, 2006).

2.1 Mass Balance Equations

The general continuity equation of phase i, assuming incompressibility, constant density, and constant porosity, is (Lemon, King, Byrne, Jensen, & Shakesheff, 2006)

$$\rho_i \left[\frac{\partial \alpha_i}{\partial t} + \nabla \cdot (\alpha_i \mathbf{u}_i) \right] = \sum_j k_{ij} \rho_j \alpha_j - \rho_i \alpha_i \sum_j k_{ji} + Q_i \rho_i, \tag{2.1}$$

where $\alpha_i, \mathbf{u}_i, \rho_i, Q_i$ is the volume fraction, interstitial velocity vector, density and mass transport across the boundary of the domain of phase i. k_{ij} is the volume conversion rate of material from phase j to phase i, which is a function of the volume fractions. The first term on the left-hand side represent the accumulation of phase i in an infinitesimal control volume and the second term describe flow of the particular phase across the boundaries of this volume element (positive when there is a net outflow of mass). The first term on the right-hand side is the mass conversion rate of material from phase j to phase i, summed over all phases j, and can be used to describe e.g. the production of cells or fibroblasts from IF. The second-to-last term is similar, but specifies the conversion rate from phase i to phase j, again summed over all phases j. Finally, the last term is a source term controlling mass transport of phase i to or from the outside of the domain (positive for net inflow).

Applying equation (2.1) to the cell, fibroblast and IF phases, we get

$$\begin{aligned}
\rho_c \left[\frac{\partial \alpha_c}{\partial t} + \nabla \cdot (\alpha_c \mathbf{u}_c) \right] &= \sum_{j=f,w} k_{cj} \rho_j \alpha_j - \rho_c \alpha_c \sum_{j=f,w} k_{jc} + Q_c \rho_c \\
\rho_f \left[\frac{\partial \alpha_f}{\partial t} + \nabla \cdot (\alpha_f \mathbf{u}_f) \right] &= \sum_{j=c,w} k_{fj} \rho_j \alpha_j - \rho_f \alpha_f \sum_{j=c,w} k_{jf} + Q_f \rho_f \\
\rho_w \left[\frac{\partial \alpha_w}{\partial t} + \nabla \cdot (\alpha_w \mathbf{u}_w) \right] &= \sum_{j=c,f} k_{wj} \rho_j \alpha_j - \rho_w \alpha_w \sum_{j=c,f} k_{jw} + Q_w \rho_w,
\end{aligned} \tag{2.2}$$

or, if we assume that cells and fibroblasts do not exchange mass, and that there are no supply/withdrawal of either of these phases across the outer boundaries of the domain,

we get

$$\begin{aligned}
\rho_c\left[\frac{\partial \alpha_c}{\partial t}+\nabla\cdot(\alpha_c\mathbf{u}_c)\right] &= k_{cw}\rho_w\alpha_w - k_{wc}\rho_c\alpha_c \\
\rho_f\left[\frac{\partial \alpha_f}{\partial t}+\nabla\cdot(\alpha_f\mathbf{u}_f)\right] &= k_{fw}\rho_w\alpha_w - k_{wf}\rho_f\alpha_f \\
\rho_w\left[\frac{\partial \alpha_w}{\partial t}+\nabla\cdot(\alpha_w\mathbf{u}_w)\right] &= -(k_{cw}\rho_w\alpha_w - k_{wc}\rho_c\alpha_c) - (k_{fw}\rho_w\alpha_w - k_{wf}\rho_f\alpha_f) + Q_w\rho_w.
\end{aligned} \tag{2.3}$$

Since IF basically is water, and tumor cells and fibroblasts are themselves mainly water (Lemon et al., 2006), it's fair to assume all densities to be equal, thus arriving at

$$\begin{aligned}
\frac{\partial \alpha_c}{\partial t}+\nabla\cdot(\alpha_c\mathbf{u}_c) &= S_c, \qquad S_c = k_{cw}\alpha_w - k_{wc}\alpha_c \\
\frac{\partial \alpha_f}{\partial t}+\nabla\cdot(\alpha_f\mathbf{u}_f) &= S_f, \qquad S_f = k_{fw}\alpha_w - k_{wf}\alpha_f \\
\frac{\partial \alpha_w}{\partial t}+\nabla\cdot(\alpha_w\mathbf{u}_w) &= -S_c - S_f + (Q_v - Q_l).
\end{aligned} \tag{2.4}$$

Here, α_c, α_f and α_w are the volume fractions of the cell, fibroblast and IF phase, respectively, and $\mathbf{u}_c, \mathbf{u}_f$ and $\mathbf{u}_w$ the corresponding (interstitial) velocity vectors, in 3-D having components $\mathbf{u}_l = (u_l^x, u_l^y, u_l^z)$, $(l = c, f, w)$. We have assumed that the porosity is constant in time and uniform is space, and that α_l is measured as a fraction of the volume available for fluids, i.e. the pore volume. It is also assumed that

$$\alpha_c + \alpha_f + \alpha_w = 1,$$

implying that there is no void space. The volume conversion terms S_c and S_f represent the (net) production of cells and fibroblasts; since cells profilerate and grow by absorbing water, it's as expected that similar terms, but opposite in sign, show up in the mass balance of IF. Q_v and Q_l are production and absorption of IF through the vascular and lymphatic system, respectively, but this is not relevant for the experimental setting.

2.2 Momentum Balance Equations

Fluid flow through tissue can be regarded as a type of porous media flow, similar to the flow of oil and water through a rock. For flow through porous rocks the multi-phase extension of Darcy's law (Muskat, Wyckoff, Botset, & Meres, 1937) is used, written as (neglecting gravity forces)

$$\mathbf{u}_l = -\frac{\mathbf{k}k_{rl}}{\mu_l}\nabla P_l,$$

where $\mathbf{u}_l, k_{rl}, \mu_l, P_l$ are the superficial velocity vector, relative permeability, viscosity and pressure of phase l, respectively, and $\mathbf{k}$ is the (absolute) permeability tensor. Using this equation we allow for different phase pressures due to capillary forces (Leverett, 1940).

The permeability tensor can be written as a diagonal matrix for coordinate systems oriented in the principal directions of permeability; for an anisotropic rock taking the form

$$\mathbf{k} = \begin{bmatrix} k_x & 0 & 0 \\ 0 & k_y & 0 \\ 0 & 0 & k_z \end{bmatrix}.$$

One disadvantage of the Darcy equation is that all information about the fluid-fluid and fluid-rock interactions are grouped into the relative permeability, thus making it impossible to investigate the effects of e.g. co- and counter-current flow. To overcome these restrictions, we will consider an approach based on the theory of mixtures (Allen III, Behie, & Trangenstein, 1988; Evje, 2017; Lemon et al., 2006; Qiao et al., 2018), in which we split the momentum balance equations into several terms, each accounting for different fluid-fluid and fluid-ECM interactions.

The basic idea of mixture theory is to model the system as a collection of overlapping continua, each representing a phase. The following general form of momentum balance then applies (Allen III, 1985; Allen III et al., 1988; Hilfer, 1998)

$$\phi\alpha_i\rho_i\frac{D^i\mathbf{u}_i}{Dt} - \nabla\cdot(\alpha_i\mathbf{t}_i) - \phi\alpha_i\rho_i\mathbf{b}_i = \mathbf{m}_i - \mathbf{u}_i r_i, \tag{2.5}$$

where $\mathbf{u}_i, \alpha_i, \rho_i$ are the interstitial velocity vector, saturation and density of phase i, and ϕ is the porosity of the porous medium, given as volume of fluids per unit volume of mixture (fluids and solid). $D^i/Dt = \partial/\partial t + \mathbf{u}_i\cdot\nabla$ is the material derivative operator, $\mathbf{t}_i$ is the stress tensor of phase i, whereas $\mathbf{b}_i$ expresses the net body force per unit mass acting on the body. $\mathbf{m}_i$ and r_i accounts for momentum and mass transfer, respectively, from all other phases into phase i.

We are going to make some simplifying assumptions to the expression in (2.5); *first* we assume that inertial effects can be ignored, i.e. setting

$$\frac{D^i\mathbf{u}_i}{Dt} = 0. \tag{2.6}$$

For typical porous media flows this is a good approximation since the velocities are small (Bear, 1988), an exception of course being the flow of gases, which have a lower viscosity and flows with higher rates, causing large Reynolds numbers and turbulence. In that case the Forchheimer equation, having an extra second-order term representing the kinetic energy of fluid, can be used (Teng & Zhao, 2000; Jambhekar, 2011). Throughout this thesis we will only be working with liquid-like phases and low flow velocities (in the order of $1\,\mu$m/s), justifying the assumption of negligible inertial effects (Jain, Martin, & Stylianopoulos, 2014).

Second, we assume momentum transfer via shear stresses to be negligible, such that the stress tensor becomes diagonal

$$\mathbf{t}_i = -P_i\mathbf{I} = -\begin{bmatrix} P_i & 0 & 0 \\ 0 & P_i & 0 \\ 0 & 0 & P_i \end{bmatrix},$$

with $\mathbf{I}$ being the identity matrix, and P_i the (isotropic) pressure of phase i. This is consistent with e.g. C. J. Breward, Byrne, and Lewis (2003); Byrne and Owen (2004); Evje (2017); Waldeland and Evje (2018). It follows that

$$-\nabla \cdot (\alpha_i \mathbf{t}_i) = \nabla(\alpha_i P_i). \tag{2.7}$$

Third, the only relevant body force is the gravitational acceleration. However, in order to arrive at the simplest possible model, we are going to neglect this effect by setting

$$\mathbf{b}_i = \mathbf{0}. \tag{2.8}$$

Fourth, we are going to neglect mass transfer between the different phases, i.e.

$$r_i = 0. \tag{2.9}$$

It could be relevant to include this effect in order to model *proliferation* (cell growth and division) and *apoptosis* (cell death) of tumor cells and fibroblasts, but again, we are going to neglect this to avoid a too complex model formulation.

Fifth, the transfer of momentum into phase i from the other phases can be expressed as

$$\mathbf{m}_i = P_i \nabla \alpha_i + \sum_{j \neq i} \mathbf{f}_{ij}, \tag{2.10}$$

where the first term is an interfacial force resulting from an averaging process (C. J. Breward et al., 2003; Byrne & Owen, 2004; Evje, 2017; Qiao et al., 2018), and $\mathbf{f}_{ij}$ is the drag force exerted by the jth phase on the ith phase, and should be summed over all phases $j \neq i$, including the solid phase (the ECM).

Finally, using the assumptions given in (2.6) through (2.10) to simplify (2.5), we arrive at the equation

$$\nabla(\alpha_i P_i) = P_i \nabla \alpha_i + \sum_{j \neq i} \mathbf{f}_{ij}, \tag{2.11}$$

or, by expanding the gradient on the LHS using the product rule

$$\alpha_i \nabla P_i = \sum_{j \neq i} \mathbf{f}_{ij}. \tag{2.12}$$

It now remains to specify the form of the drag force terms. Assuming creeping flow (Stokes flow), we can write (Evje, 2017; Waldeland & Evje, 2018)

$$\mathbf{f}_{ij} = \hat{\zeta}_{ij}(\mathbf{u}_j - \mathbf{u}_i) = -\mathbf{f}_{ji}, \tag{2.13}$$

consistent with Newtons third law of motion, which states that for every action, there is an equal and opposite reaction. We assume $\hat{\zeta}_{ij}$ to be proportional to the viscosity of the fluid(s).

Now, using equation (2.13), we can write equation (2.12) for the IF phase as

$$\alpha_w \nabla P_w = -\hat{\zeta}_w \mathbf{u}_w - \hat{\zeta}_{cw}(\mathbf{u}_w - \mathbf{u}_c) - \hat{\zeta}_{fw}(\mathbf{u}_w - \mathbf{u}_f). \tag{2.14}$$

Here, the right-hand side is separated into three terms: $\hat{\zeta}_w \mathbf{u}_w$, representing the resistance against flow felt by the water phase from the solid material of the porous medium, $\hat{\zeta}_{cw}(\mathbf{u}_w - \mathbf{u}_c)$ and $\hat{\zeta}_{fw}(\mathbf{u}_w - \mathbf{u}_f)$, representing the drag force exerted by the cells and fibroblasts on the water phase. The remaining momentum equations can be written as

$$\alpha_c \nabla(P_w + \Delta P_{cw} + \Lambda_C) = -\hat{\zeta}_c \mathbf{u}_c + \hat{\zeta}_{cw}(\mathbf{u}_w - \mathbf{u}_c) + \hat{\zeta}_{cf}(\mathbf{u}_f - \mathbf{u}_c) \tag{2.15}$$

for the cell phase, and

$$\alpha_f \nabla(P_w + \Delta P_{fw} + \Lambda_H) = -\hat{\zeta}_f \mathbf{u}_f - \hat{\zeta}_{cf}(\mathbf{u}_f - \mathbf{u}_c) + \hat{\zeta}_{fw}(\mathbf{u}_w - \mathbf{u}_f) \tag{2.16}$$

for the fibroblast phase. ΔP_{cw} and ΔP_{fw} are functions quantifying the elevated pressures seen in the cell and fibroblast phase, respectively, compared to water (IF). This is comparable to the capillary pressure functions used in the simulation of flow of water, oil and gas in hydrocarbon reservoirs (Allen III et al., 1988; Ertekin, Abou-Kassem, & King, 2001; Zolotukhin & Ursin, 2000). These terms give rise to diffusion-like behavior. The potential functions Λ_C and Λ_H have been added to the equations in (2.15) and (2.16) to represent the additional phase pressures due to chemotaxis (Byrne & Owen, 2004; Evje, 2017; Waldeland & Evje, 2018). The cells chemotact toward chemokine (C), whereas fibroblasts migrate toward increasing concentrations of TGF (H), consistent with Section 1.2.

Remark 2.1. *Note that e.g. growth factors, inhibitors and nutrients might have an indirect effect on cell motion as well, by stimulating tumor growth. This can be modeled through the terms S_c and S_f. When cells duplicate, the tumor has to expand outwards in order to make room for more cells (Ambrosi & Preziosi, 2002).*

Remark 2.2. *We have assumed that all phases are incompressible; however, previous works have demonstrated that solid stress may cause tighter packing of the cells and affect tumor growth (Helmlinger, Netti, Lichtenbeld, Melder, & Jain, 1997). A model accounting for such mechanical effects has been formulated by e.g. Ambrosi and Preziosi (2009).*

Constitutive relations will be given in a subsequent section, and the effects of Λ_C and Λ_H (chemotaxis), ΔP_{cw} and ΔP_{fw} (diffusion) as well as the viscous couplings and fluid-ECM interactions on the solution will become more clear later on when we will consider a simplified 1-D model.

2.3 Chemical Agents

We assume that protease is secreted by the cells, as described by Shields et al. (2007). As mentioned in Subsection 1.2.2, pt. 2, increased concentration and activation of TGF was observed in the presence of fibroblasts. The simplest model consistent with these observations is based on the assumption that TGF is secreted directly by the fibroblasts.

Remark 2.3. *Note that it might be more realistic to assume TGF to be produced in a manner similar to the production of chemokine (described below), in which case the fibroblasts would secrete their own type of protease, releasing surface-bound growth factors from the ECM. Also, we know that shear stresses are involved in the process of activating TGF (Ahamed et al., 2008; Wipff, Rifkin, Meister, & Hinz, 2007), so that could play a role as well.*

Finally, we are going to assume that protease, G, and TGF, H, moves in the water phase by advection and diffusion according to the following equations (Ambrosi & Preziosi, 2002; Waldeland & Evje, 2018)

$$\begin{aligned} G_t + \nabla \cdot (\mathbf{u}_w G) &= \nabla \cdot (D_G \nabla G) - \lambda_{31} G + \alpha_c \left(\lambda_{32} - \lambda_{33} \left(\frac{G}{G_M} \right)^{v_G} \right) \\ H_t + \nabla \cdot (\mathbf{u}_w H) &= \nabla \cdot (D_H \nabla H) - \lambda_{51} H + \alpha_f \left(\lambda_{52} - \lambda_{53} \left(\frac{H}{H_M} \right)^{v_H} \right). \end{aligned} \tag{2.17}$$

The second term on the right-hand side describes decay of the chemical component, whereas the last term is the growth term. Note that the production terms are dependent on the volume fractions of cell and fibroblast. G_M and H_M are included to put restrictions on the production of protease and TGF, respectively, and can thus be used to set the upper limits of the dissolved components in the aqueous phase.

The evolution of chemokine is described by (Waldeland & Evje, 2018)

$$C_t + \nabla \cdot (\mathbf{u}_w C) = \nabla \cdot (D_C \nabla C) + G\rho \left(\lambda_{41} - \lambda_{42} \left(\frac{C}{C_M} \right)^2 - \lambda_{43} \left(\frac{C}{C_M} \right)^{v_C} \right) - \lambda_{44} \alpha_c. \tag{2.18}$$

Again, C_M is a parameter that controls the maximal levels of chemokine. Note that production of chemokine is dependent on the concentration of both protease and ECM, consistent with Shields et al. (2007) and Fleury et al. (2006), which argue that chemokine initially is bound to the ECM, but will be released into the water phase upon reaction with cell-secreted protease. This gives rise to much larger transcellular gradients compared to when chemokines are secreted directly by the cells (Fleury et al., 2006). The ECM component is described by

$$\rho_t = -\lambda_{21} G \rho + \rho \left(\lambda_{22} - \lambda_{23} \alpha_c - \lambda_{24} \frac{\rho}{\rho_M} \right). \tag{2.19}$$

When protease reacts with the ECM to release chemokines into the water phase, some of the ECM dissolves, as described by the first term on the right-hand side. ρ_M here serves the same purpose as G_M, H_M and C_M in the previous equations. We will use a simplified version of (2.19) when we solve the model in a 1-D setting in Chapter 3.

Remark 2.4. *Note that $\lambda_{11}, \lambda_{12}$ and λ_{13} has already been reserved for the description of S_c (Waldeland & Evje, 2018).*

2.4 The Three-Phase Model

Now the final, three-dimensional, three-phase cell-fibroblast-IF model takes the following form

$$
\begin{aligned}
\alpha_{ct} + \nabla \cdot (\alpha_c \mathbf{u}_c) &= S_c \\
\alpha_{ft} + \nabla \cdot (\alpha_f \mathbf{u}_f) &= S_f \\
\alpha_{wt} + \nabla \cdot (\alpha_w \mathbf{u}_w) &= -S_c - S_f + (Q_v - Q_l) \\
\alpha_c \nabla (P_w + \Delta P_{cw} + \Lambda_C) &= -\hat{\zeta}_c \mathbf{u}_c + \hat{\zeta}_{cf}(\mathbf{u}_f - \mathbf{u}_c) \\
\alpha_f \nabla (P_w + \Lambda_H) &= -\hat{\zeta}_f \mathbf{u}_f - \hat{\zeta}_{cf}(\mathbf{u}_f - \mathbf{u}_c) \\
\alpha_w \nabla P_w &= -\hat{\zeta}_w \mathbf{u}_w \\
\rho_t &= -\lambda_{21} G \rho + \rho \left(\lambda_{22} - \lambda_{23} \alpha_c - \lambda_{24} \frac{\rho}{\rho_M} \right) \\
G_t + \nabla \cdot (\mathbf{u}_w G) &= \nabla \cdot (D_G \nabla G) - \lambda_{31} G + \alpha_c \left(\lambda_{32} - \lambda_{33} \left(\frac{G}{G_M} \right)^{v_G} \right) \\
C_t + \nabla \cdot (\mathbf{u}_w C) &= \nabla \cdot (D_C \nabla C) + G\rho \left(\lambda_{41} - \lambda_{42} \left(\frac{C}{C_M} \right)^2 - \lambda_{43} \left(\frac{C}{C_M} \right)^{v_C} \right) - \lambda_{44} \alpha_c \\
H_t + \nabla \cdot (\mathbf{u}_w H) &= \nabla \cdot (D_H \nabla H) - \lambda_{51} H + \alpha_f \left(\lambda_{52} - \lambda_{53} \left(\frac{H}{H_M} \right)^{v_H} \right), \qquad (2.20)
\end{aligned}
$$

where we have assumed $\hat{\zeta}_{cw} = \hat{\zeta}_{fw} = \Delta P_{fw} = 0$. The motivation for ignoring the viscous couplings are related to the fact that in two-phase flow of either cell or fibroblast together with IF, flow-enhanced migration practically vanish when removing the effect of chemotaxis, see Figure 1.2A and 1.3A (right). This suggests that the effect of mechanical coupling with IF is negligible (at least compared to chemotaxis). Also, we assume that fibroblasts do not possess the ability to repel/attract each other (a distinctive characteristic of cells), and therefore $\Delta P_{fw} = 0$. The cell capillary pressure function is determined from the fluid saturations, i.e. $\Delta P_{cw} = \Delta P_{cw}(\alpha_c, \alpha_f)$. We also assume that $\Lambda_C = \Lambda_C(C)$ and $\Lambda_H = \Lambda_H(H)$. This is slightly different from e.g. Evje (2017) where $\Lambda_C = \Lambda_C(C, \rho)$, thus also including the effect of *haptotaxis* (a mechanism similar to chemotaxis but where the cells follow concentration gradients of surface-bound substances).

Remark 2.5. *Note that the potential functions only enter the equations in* (2.20) *as gradients, and the purpose of these functions might become clearer if we rewrite them using the chain rule for differentiation. For example for chemokine, we can rewrite the gradient as:* $\nabla \Lambda_C(C) = \Lambda_C'(C) \cdot \nabla C$. *We see that the strength of the chemotaxis effect depends on the gradient of the chemokine concentration (in a product, such that the chemotactic response vanish when the gradient is zero), but also on the function* $\Lambda_C'(C)$. *By tuning the parameters of* $\Lambda_C(C)$ *we can control for which concentrations the chemotactic response should be stronger/weaker (for a given gradient). A special case*

would be $\Lambda_C(C) = A$ for some constant A, in which case chemotaxis would depend on the concentration gradient only. The form of the potential functions will be specified in greater detail later on when we will solve a simplified 1-D version of the model.

Remark 2.6. *It should be noted that the model* (2.20) *is given in dimensional form; however, using the dimensionless variables and parameters given in Appendix B, the equations will look exactly the same in dimensionless form. In the following, we are going to refer to this dimensionless version of the model; see Appendix B for further details.*

Summing up, the model (2.20) consists of ten equations: one mass and momentum balance for each of the three phases, i.e. a total of six equations, in addition to four transport-reaction equations describing the evolution of the chemical components and the ECM.

2.5 Rewritten Form of the Model

When solving the equations for flow of oil and water in an oil reservoir we use the mass balance equations in addition to explicit expressions for the phase velocities, represented by the Darcy law (Allen III et al., 1988). In this case, we have *implicit* expressions for the velocities, represented by the momentum balance equations $(2.20)_{4,5,6}$. We now want to replace these equations with explicit expressions for the phase velocities (see Appendix A for further details).

2.5.1 Explicit Expressions for Phase Velocities

Rewriting the momentum balance equations $(2.20)_{4,5,6}$ as

$$\begin{aligned} \alpha_c\nabla\Lambda_C + \alpha_c\nabla(\Delta P_{cw}) + \alpha_c\nabla P_w &= -(\hat{\zeta}_c + \hat{\zeta}_{cf})\mathbf{u}_c + \hat{\zeta}_{cf}\mathbf{u}_f \\ \alpha_f\nabla\Lambda_H + \alpha_f\nabla P_w &= \hat{\zeta}_{cf}\mathbf{u}_c - (\hat{\zeta}_f + \hat{\zeta}_{cf})\mathbf{u}_f \\ \alpha_w\nabla P_w &= -\hat{\zeta}_w\mathbf{u}_w, \end{aligned} \tag{2.21}$$

and solving the 3-by-3 linear system for the interstitial fluid velocities gives

$$\begin{aligned} \mathbf{u}_c = &- \frac{\alpha_f\hat{\zeta}_{cf} + \alpha_c(\hat{\zeta}_{cf} + \hat{\zeta}_f)}{\hat{\zeta}_c\hat{\zeta}_f + \hat{\zeta}_{cf}(\hat{\zeta}_c + \hat{\zeta}_f)}\nabla P_w \\ &- \frac{\alpha_c(\hat{\zeta}_{cf} + \hat{\zeta}_f)}{\hat{\zeta}_c\hat{\zeta}_f + \hat{\zeta}_{cf}(\hat{\zeta}_c + \hat{\zeta}_f)}\nabla(\Delta P_{cw} + \Lambda_C) \\ &- \frac{\alpha_f\hat{\zeta}_{cf}}{\hat{\zeta}_c\hat{\zeta}_f + \hat{\zeta}_{cf}(\hat{\zeta}_c + \hat{\zeta}_f)}\nabla\Lambda_H \end{aligned} \tag{2.22}$$

for the cell phase,

$$\begin{aligned}\mathbf{u}_f = &- \frac{\alpha_c\hat{\zeta}_{cf} + \alpha_f(\hat{\zeta}_c + \hat{\zeta}_{cf})}{\hat{\zeta}_c\hat{\zeta}_f + \hat{\zeta}_{cf}(\hat{\zeta}_c + \hat{\zeta}_f)}\nabla P_w \\ &- \frac{\alpha_c\hat{\zeta}_{cf}}{\hat{\zeta}_c\hat{\zeta}_f + \hat{\zeta}_{cf}(\hat{\zeta}_c + \hat{\zeta}_f)}\nabla(\Delta P_{cw} + \Lambda_C) \\ &- \frac{\alpha_f(\hat{\zeta}_c + \hat{\zeta}_{cf})}{\hat{\zeta}_c\hat{\zeta}_f + \hat{\zeta}_{cf}(\hat{\zeta}_c + \hat{\zeta}_f)}\nabla\Lambda_H\end{aligned} \tag{2.23}$$

for the fibroblast phase, and

$$\mathbf{u}_w = -\frac{\alpha_w}{\hat{\zeta}_w}\nabla P_w \tag{2.24}$$

for the IF phase. The corresponding Darcy/superficial velocities then follows directly from the definitions

$$\begin{aligned}\mathbf{U}_c := \alpha_c\mathbf{u}_c = &- \hat{\lambda}_c\nabla P_w \\ &- \left(\hat{\lambda}_c - \frac{\alpha_c\alpha_f\hat{\zeta}_{cf}}{\hat{\zeta}_c\hat{\zeta}_f + \hat{\zeta}_{cf}(\hat{\zeta}_c + \hat{\zeta}_f)}\right)\nabla(\Delta P_{cw} + \Lambda_C) \\ &- \frac{\alpha_c\alpha_f\hat{\zeta}_{cf}}{\hat{\zeta}_c\hat{\zeta}_f + \hat{\zeta}_{cf}(\hat{\zeta}_c + \hat{\zeta}_f)}\nabla\Lambda_H\end{aligned}$$

$$\begin{aligned}\mathbf{U}_f := \alpha_f\mathbf{u}_f = &- \hat{\lambda}_f\nabla P_w \\ &- \frac{\alpha_c\alpha_f\hat{\zeta}_{cf}}{\hat{\zeta}_c\hat{\zeta}_f + \hat{\zeta}_{cf}(\hat{\zeta}_c + \hat{\zeta}_f)}\nabla(\Delta P_{cw} + \Lambda_C) \\ &- \left(\hat{\lambda}_f - \frac{\alpha_c\alpha_f\hat{\zeta}_{cf}}{\hat{\zeta}_c\hat{\zeta}_f + \hat{\zeta}_{cf}(\hat{\zeta}_c + \hat{\zeta}_f)}\right)\nabla\Lambda_H\end{aligned} \tag{2.25}$$

$$\mathbf{U}_w := \alpha_w\mathbf{u}_w = - \hat{\lambda}_w\nabla P_w,$$

where we have introduced the generalized mobility functions

$$\begin{aligned}\hat{\lambda}_c &= \frac{\alpha_c[\alpha_c(\hat{\zeta}_{cf} + \hat{\zeta}_f) + \alpha_f\hat{\zeta}_{cf}]}{\hat{\zeta}_c\hat{\zeta}_f + \hat{\zeta}_{cf}(\hat{\zeta}_c + \hat{\zeta}_f)} \\ \hat{\lambda}_f &= \frac{\alpha_f[\alpha_c\hat{\zeta}_{cf} + \alpha_f(\hat{\zeta}_c + \hat{\zeta}_{cf})]}{\hat{\zeta}_c\hat{\zeta}_f + \hat{\zeta}_{cf}(\hat{\zeta}_c + \hat{\zeta}_f)} \\ \hat{\lambda}_w &= \frac{\alpha_w^2}{\hat{\zeta}_w} \\ \hat{\lambda}_T &= \frac{(\alpha_c + \alpha_f)^2\hat{\zeta}_{cf} + \alpha_c^2\hat{\zeta}_f + \alpha_f^2\hat{\zeta}_c + \frac{\alpha_w^2}{\hat{\zeta}_w}(\hat{\zeta}_c\hat{\zeta}_{cf} + \hat{\zeta}_c\hat{\zeta}_f + \hat{\zeta}_{cf}\hat{\zeta}_f)}{\hat{\zeta}_c\hat{\zeta}_f + \hat{\zeta}_{cf}(\hat{\zeta}_c + \hat{\zeta}_f)},\end{aligned} \tag{2.26}$$

allowing us to rewrite the coefficients in (2.22) and (2.23):

$$\begin{aligned}\frac{\alpha_c^2(\hat{\zeta}_{cf}+\hat{\zeta}_f)}{\hat{\zeta}_c\hat{\zeta}_f+\hat{\zeta}_{cf}(\hat{\zeta}_c+\hat{\zeta}_f)} &= \frac{\alpha_c\alpha_f\hat{\zeta}_{cf}+\alpha_c^2(\hat{\zeta}_{cf}+\hat{\zeta}_f)-\alpha_c\alpha_f\hat{\zeta}_{cf}}{\hat{\zeta}_c\hat{\zeta}_f+\hat{\zeta}_{cf}(\hat{\zeta}_c+\hat{\zeta}_f)} = \hat{\lambda}_c - \frac{\alpha_c\alpha_f\hat{\zeta}_{cf}}{\hat{\zeta}_c\hat{\zeta}_f+\hat{\zeta}_{cf}(\hat{\zeta}_c+\hat{\zeta}_f)} \\ \frac{\alpha_f^2(\hat{\zeta}_c+\hat{\zeta}_{cf})}{\hat{\zeta}_c\hat{\zeta}_f+\hat{\zeta}_{cf}(\hat{\zeta}_c+\hat{\zeta}_f)} &= \frac{\alpha_c\alpha_f\hat{\zeta}_{cf}+\alpha_f^2(\hat{\zeta}_c+\hat{\zeta}_{cf})-\alpha_c\alpha_f\hat{\zeta}_{cf}}{\hat{\zeta}_c\hat{\zeta}_f+\hat{\zeta}_{cf}(\hat{\zeta}_c+\hat{\zeta}_f)} = \hat{\lambda}_f - \frac{\alpha_c\alpha_f\hat{\zeta}_{cf}}{\hat{\zeta}_c\hat{\zeta}_f+\hat{\zeta}_{cf}(\hat{\zeta}_c+\hat{\zeta}_f)}.\end{aligned} \tag{2.27}$$

Remark 2.7. *Note that the Darcy velocities defined in* (2.25) *differs from the usual Darcy velocities used in the oil and gas industry in that they are defined as volumetric rate divided by porous area, instead of total area (which also includes the solid part of the cross-section). We also neglect any tortuosity of the pores, and assume flow along straight-line paths through the porous material. In addition, we do not take consideration of residual saturations.*

We now have explicit expressions for each of the phase velocities, given by (2.25), in addition to the mass balance equations given by $(2.20)_{1,2,3}$. This is also the starting point in the solution of the Buckley-Leverett (BL) equation describing two-phase flow of oil and water, where the explicit velocities are given by the Darcy equations (Buckley & Leverett, 1941). The next step in the solution of the BL equation is to sum the mass balance equations and derive an expression for the total velocity, using the constraint $S_w + S_o = 1$, S_w and S_o being the saturations of water and oil, respectively. Following a similar approach, we sum the three mass balance equations $(2.20)_{1,2,3}$ to get

$$\nabla \cdot \mathbf{U}_T = \nabla \cdot (\mathbf{U}_c + \mathbf{U}_f + \mathbf{U}_w) = Q_v - Q_l, \tag{2.28}$$

where we have made use of the relation $\alpha_c + \alpha_f + \alpha_w = 1$. This simplifies to the relation $\partial U_T/\partial x = 0$ used in BL when we have one-dimensional flow and no source terms. The next step is then to relate the total flux (total Darcy velocity) to the pressure gradient of the water/IF phase, by making use of the explicit expressions for the individual phase velocities. By summation of the equations in (2.25), we have that

$$\mathbf{U}_T = \mathbf{U}_c + \mathbf{U}_f + \mathbf{U}_w = -\hat{\lambda}_T\nabla P_w - \hat{\lambda}_c\nabla(\Delta P_{cw} + \Lambda_C) - \hat{\lambda}_f\nabla\Lambda_H, \tag{2.29}$$

which is similar to $U_T = -\lambda_T \partial P_w/\partial x$ in the BL case where chemotaxis and capillary pressure are not considered. By applying the divergence operator $(\nabla\cdot)$ on (2.29) and using (2.28), we get

$$-(Q_v - Q_l) - \nabla\cdot(\hat{\lambda}_c\nabla(\Delta P_{cw} + \Lambda_C)) - \nabla\cdot(\hat{\lambda}_f\nabla\Lambda_H) = \nabla\cdot(\hat{\lambda}_T\nabla P_w), \tag{2.30}$$

which is a more general version of the equation $\partial/\partial x(\lambda_T \partial P_w/\partial x) = 0$ used in the context of BL. This is an elliptic equation for P_w; knowing the pressure, we can calculate $\mathbf{U}_T$ from (2.29).

2.5.2 Elimination of IF Pressure Gradient

Following the procedure for solving the BL problem, the next step is now to eliminate the IF pressure gradient. We can solve for the pressure gradient using equation (2.29)

$$\nabla P_w = -\frac{\mathbf{U}_T}{\hat{\lambda}_T} - \frac{\hat{\lambda}_c}{\hat{\lambda}_T}\nabla(\Delta P_{cw} + \Lambda_C) - \frac{\hat{\lambda}_f}{\hat{\lambda}_T}\nabla\Lambda_H. \tag{2.31}$$

Substituting this expression into (2.25) we derive the following expressions for the superficial fluid velocities

$$\begin{aligned}
\mathbf{U}_c &= \hat{f}_c\mathbf{U}_T - (\hat{h}_1 + \hat{h}_2)\nabla(\Delta P_{cw} + \Lambda_C) + \hat{h}_2\nabla\Lambda_H \\
\mathbf{U}_f &= \hat{f}_f\mathbf{U}_T + \hat{h}_2\nabla(\Delta P_{cw} + \Lambda_C) - (\hat{h}_2 + \hat{h}_3)\nabla\Lambda_H \\
\mathbf{U}_w &= \hat{f}_w\mathbf{U}_T + \hat{h}_1\nabla(\Delta P_{cw} + \Lambda_C) + \hat{h}_3\nabla\Lambda_H,
\end{aligned} \tag{2.32}$$

where the fractional flow functions describing co-current flow are defined by

$$\begin{aligned}
\hat{f}_c(\alpha_c,\alpha_f) &:= \frac{\hat{\lambda}_c}{\hat{\lambda}_T} = \frac{\alpha_c[\alpha_f\hat{\zeta}_{cf} + \alpha_c(\hat{\zeta}_{cf} + \hat{\zeta}_f)]}{(\alpha_c+\alpha_f)^2\hat{\zeta}_{cf} + \alpha_c^2\hat{\zeta}_f + \alpha_f^2\hat{\zeta}_c + \frac{\alpha_w^2}{\hat{\zeta}_w}(\hat{\zeta}_c\hat{\zeta}_{cf} + \hat{\zeta}_c\hat{\zeta}_f + \hat{\zeta}_{cf}\hat{\zeta}_f)} \\
\hat{f}_f(\alpha_c,\alpha_f) &:= \frac{\hat{\lambda}_f}{\hat{\lambda}_T} = \frac{\alpha_f[\alpha_c\hat{\zeta}_{cf} + \alpha_f(\hat{\zeta}_{cf} + \hat{\zeta}_c)]}{(\alpha_c+\alpha_f)^2\hat{\zeta}_{cf} + \alpha_c^2\hat{\zeta}_f + \alpha_f^2\hat{\zeta}_c + \frac{\alpha_w^2}{\hat{\zeta}_w}(\hat{\zeta}_c\hat{\zeta}_{cf} + \hat{\zeta}_c\hat{\zeta}_f + \hat{\zeta}_{cf}\hat{\zeta}_f)} \\
\hat{f}_w(\alpha_c,\alpha_f) &:= \frac{\hat{\lambda}_w}{\hat{\lambda}_T} = \frac{\frac{\alpha_w^2}{\hat{\zeta}_w}(\hat{\zeta}_c\hat{\zeta}_{cf} + \hat{\zeta}_c\hat{\zeta}_f + \hat{\zeta}_{cf}\hat{\zeta}_f)}{(\alpha_c+\alpha_f)^2\hat{\zeta}_{cf} + \alpha_c^2\hat{\zeta}_f + \alpha_f^2\hat{\zeta}_c + \frac{\alpha_w^2}{\hat{\zeta}_w}(\hat{\zeta}_c\hat{\zeta}_{cf} + \hat{\zeta}_c\hat{\zeta}_f + \hat{\zeta}_{cf}\hat{\zeta}_f)},
\end{aligned} \tag{2.33}$$

and the h-functions describing counter-current flow are given by

$$\begin{aligned}
\hat{h}_1(\alpha_c,\alpha_f) &:= \frac{\hat{\lambda}_c\hat{\lambda}_w}{\hat{\lambda}_T} \\
&= \frac{\alpha_c\frac{\alpha_w^2}{\hat{\zeta}_w}[\alpha_c(\hat{\zeta}_f + \hat{\zeta}_{cf}) + \alpha_f\hat{\zeta}_{cf}]}{(\alpha_c+\alpha_f)^2\hat{\zeta}_{cf} + \alpha_c^2\hat{\zeta}_f + \alpha_f^2\hat{\zeta}_c + \frac{\alpha_w^2}{\hat{\zeta}_w}(\hat{\zeta}_c\hat{\zeta}_{cf} + \hat{\zeta}_c\hat{\zeta}_f + \hat{\zeta}_{cf}\hat{\zeta}_f)} \\
\hat{h}_2(\alpha_c,\alpha_f) &:= \frac{\hat{\lambda}_c\hat{\lambda}_f}{\hat{\lambda}_T} - \frac{\alpha_c\alpha_f\hat{\zeta}_{cf}}{\hat{\zeta}_c\hat{\zeta}_f + \hat{\zeta}_{cf}(\hat{\zeta}_c + \hat{\zeta}_f)} \\
&= \frac{\alpha_c\alpha_f(\alpha_c\alpha_f - \frac{\alpha_w^2}{\hat{\zeta}_w}\hat{\zeta}_{cf})}{(\alpha_c+\alpha_f)^2\hat{\zeta}_{cf} + \alpha_c^2\hat{\zeta}_f + \alpha_f^2\hat{\zeta}_c + \frac{\alpha_w^2}{\hat{\zeta}_w}(\hat{\zeta}_c\hat{\zeta}_{cf} + \hat{\zeta}_c\hat{\zeta}_f + \hat{\zeta}_{cf}\hat{\zeta}_f)} \\
\hat{h}_3(\alpha_c,\alpha_f) &:= \frac{\hat{\lambda}_f\hat{\lambda}_w}{\hat{\lambda}_T} \\
&= \frac{\alpha_f\frac{\alpha_w^2}{\hat{\zeta}_w}[\alpha_c\hat{\zeta}_{cf} + \alpha_f(\hat{\zeta}_c + \hat{\zeta}_{cf})]}{(\alpha_c+\alpha_f)^2\hat{\zeta}_{cf} + \alpha_c^2\hat{\zeta}_f + \alpha_f^2\hat{\zeta}_c + \frac{\alpha_w^2}{\hat{\zeta}_w}(\hat{\zeta}_c\hat{\zeta}_{cf} + \hat{\zeta}_c\hat{\zeta}_f + \hat{\zeta}_{cf}\hat{\zeta}_f)}.
\end{aligned} \tag{2.34}$$

Figure 2.2 illustrates graphically how the different phases are connected via the $\hat{h}$-functions.

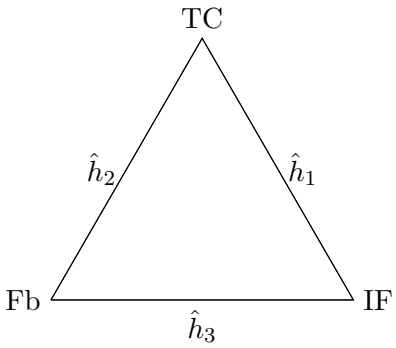

Figure 2.2: Graphical representation of how the different phases are coupled to each other via the counter-current flow coefficients. TC=tumor cell, Fb=fibroblast, IF=interstitial fluid.

Let us compare the equations in (2.32) to the oil-reservoir analogs. The equation for IF takes the following form in 1-D

$$U_w = \hat{f}_w U_T + \hat{h}_1(\Delta P_{cw})_x + \hat{h}_1 \Lambda_{Cx} + \hat{h}_3 \Lambda_{Hx}. \tag{2.35}$$

For two-phase flow of oil and water, including the effects of capillary pressure and gravity, we get the following water velocity using Darcy's law

$$U_w = f_w U_T + f_w \lambda_o \Delta\rho g + f_w \lambda_o P_{cx}, \tag{2.36}$$

or slightly different if we use the generalized mixture theory approach (Qiao et al., 2018)

$$U_w = \hat{f}_w U_T + W \Delta\rho g + W P_{cx}, \tag{2.37}$$

where also the viscous coupling between the two fluid phases has been taken into consideration. It should be clear from the last two equations, (2.36) and (2.37), that we get one term per transportation mechanism, in this case co-current flow, counter-current gravity and counter-current capillary pressure. Comparing these two equations with (2.35), we see that they are very similar, except that terms representing gravity are removed, whereas two extra (counter-current) terms, representing chemotaxis toward chemokine and TGF, have been added.

The expression for W in (2.37) is

$$W = \hat{f}_w \hat{\lambda}_o - \frac{\alpha_o \alpha_w \hat{\zeta}_{ow} \phi_e}{\hat{\zeta}_o \hat{\zeta}_w + \hat{\zeta}_{ow}(\hat{\zeta}_o + \hat{\zeta}_w)}, \tag{2.38}$$

which is similar to the coefficient $f_w \lambda_o$ in (2.36), except for the extra term accounting for viscous coupling between the oil and water phase. The coefficients $\hat{h}_1$ and $\hat{h}_3$ in (2.35)

describes how IF interacts with the cells and fibroblasts, see Figure 2.2. Since we have not included the effect of fluid-fluid interactions on the water phase (against either cells or fibroblasts), we should expect these two coefficients to be free for "viscous coupling effects", and therefore similar to the coefficient $f_w\lambda_o$ in (2.36). Indeed,

$$\hat{h}_1(\alpha_c,\alpha_f)=\frac{\hat{\lambda}_c\hat{\lambda}_w}{\hat{\lambda}_T}=\hat{f}_w\hat{\lambda}_c,\qquad \hat{h}_3(\alpha_c,\alpha_f)=\frac{\hat{\lambda}_f\hat{\lambda}_w}{\hat{\lambda}_T}=\hat{f}_w\hat{\lambda}_f,$$

similar to the counter-current coefficient in the equation for flow of oil and water when there is no viscous coupling between the phases. The factor $\hat{h}_2$, however, represent the counter-current coupling between cells and fibroblasts, where also the fluid-fluid interaction between the two phases have been taken into account. We should therefore expect this factor to be similar to W given in (2.38). Indeed,

$$\hat{h}_2(\alpha_c,\alpha_f)=\frac{\hat{\lambda}_c\hat{\lambda}_f}{\hat{\lambda}_T}-\frac{\alpha_c\alpha_f\hat{\zeta}_{cf}}{\hat{\zeta}_c\hat{\zeta}_f+\hat{\zeta}_{cf}(\hat{\zeta}_c+\hat{\zeta}_f)}=\hat{f}_f\hat{\lambda}_c-\frac{\alpha_c\alpha_f\hat{\zeta}_{cf}}{\hat{\zeta}_c\hat{\zeta}_f+\hat{\zeta}_{cf}(\hat{\zeta}_c+\hat{\zeta}_f)},$$

consistent with the expression in (2.38), except that the porosity was written explicitly in that case.

The expressions for the interstitial fluid velocities follows directly from (2.32)

$$\begin{aligned}
\mathbf{u}_c&=\frac{\hat{f}_c}{\alpha_c}\mathbf{U}_T-\frac{\hat{h}_1+\hat{h}_2}{\alpha_c}\nabla(\Delta P_{cw}+\Lambda_C)+\frac{\hat{h}_2}{\alpha_c}\nabla\Lambda_H\\
\mathbf{u}_f&=\frac{\hat{f}_f}{\alpha_f}\mathbf{U}_T+\frac{\hat{h}_2}{\alpha_f}\nabla(\Delta P_{cw}+\Lambda_C)-\frac{\hat{h}_2+\hat{h}_3}{\alpha_f}\nabla\Lambda_H\\
\mathbf{u}_w&=\frac{\hat{f}_w}{\alpha_w}\mathbf{U}_T+\frac{\hat{h}_1}{\alpha_w}\nabla(\Delta P_{cw}+\Lambda_C)+\frac{\hat{h}_3}{\alpha_w}\nabla\Lambda_H.
\end{aligned}\tag{2.39}$$

Note that each of the phase velocities consists of four different terms, representing contributions to the overall velocity of the phase from different mechanisms. Taking water, equation $(2.39)_3$ as an example, we have:

1. fluid-generated stress, $\frac{\hat{f}_w}{\alpha_w}\mathbf{U}_T$,
2. diffusion, $\frac{\hat{h}_1}{\alpha_w}\nabla(\Delta P_{cw})$,
3. chemotaxis of *cells* toward concentration gradients in *chemokine*, $\frac{\hat{h}_1}{\alpha_w}\nabla\Lambda_C$,
4. chemotaxis of *fibroblasts* toward concentration gradients in *TGF*, $\frac{\hat{h}_3}{\alpha_w}\nabla\Lambda_H$.

The fluid-generated stress depending on $\mathbf{U}_T$, represent a co-current transport effect, in which all of the phases flow in the same direction. This force is caused by the applied pressure gradient across the domain, causing a flow of IF, which in turn pushes the cells and fibroblasts in the same direction. If we do not have any source terms of IF, note that $\mathbf{U}_T$ will be divergence-free ($\nabla\cdot\mathbf{U}_T=0$), and therefore constant in a 1-D setting.

The fluid-generated stress on the phase is thus dependent only on the fractional flow function of that particular phase, being a function of the volume fractions.

The three remaining forces, dependent on $\hat{h}_1, \hat{h}_2$ and $\hat{h}_3$ represents counter-current flow. In the event that there is no viscous coupling between any of the three phases, the expressions in (2.34) simplify to

$$\begin{aligned}\hat{h}_1(\alpha_c, \alpha_f) &= \frac{\hat{\lambda}_c \hat{\lambda}_w}{\hat{\lambda}_T} \\ \hat{h}_2(\alpha_c, \alpha_f) &= \frac{\hat{\lambda}_c \hat{\lambda}_f}{\hat{\lambda}_T} \\ \hat{h}_3(\alpha_c, \alpha_f) &= \frac{\hat{\lambda}_f \hat{\lambda}_w}{\hat{\lambda}_T}.\end{aligned} \tag{2.40}$$

Note that these are all positive functions (since the mobilities are positive). We will also assume that $\Lambda'_C(C)$ and $\Lambda'_H(H)$ are negative, such that a positive gradient in for example TGF (H) will cause $\nabla\Lambda_H(H) = \Lambda'_H(H)\cdot\nabla H$ to be negative. Looking at $(2.39)_2$ we see that the velocity of the fibroblasts will get a positive contribution driving the fibroblasts in the direction of increasing concentration of TGF, consistent with Section 1.2. Looking at $(2.39)_{1,3}$ it is clear that the cell and IF phases will experience flow in the oppsite direction. Correspondingly, a positive gradient in chemokine (C), will increase the cell velocity in the downstream direction, while simultaneously trying to push the fibroblasts and IF in the upstream direction.

If we include the viscous coupling between cell and fibroblast, that is, setting $\hat{\zeta}_{cf} > 0$, then $(2.40)_{1,3}$ remains the same, but $\hat{h}_2$ now takes the following form:

$$\hat{h}_2(\alpha_c, \alpha_f) = \frac{\hat{\lambda}_c \hat{\lambda}_f}{\hat{\lambda}_T} - \frac{\alpha_c \alpha_f \hat{\zeta}_{cf}}{\hat{\zeta}_c\hat{\zeta}_f + \hat{\zeta}_c\hat{\zeta}_{cf} + \hat{\zeta}_f\hat{\zeta}_{cf}}.$$

Remark 2.8. *By increasing the strength of the cell-fibroblast interaction, $\hat{h}_2$ eventually becomes negative, thus making both cells and fibroblasts move in the direction of increasing concentration of TGF, forcing IF to move in the opposite direction (due to the counter-current nature of chemotactic migration). This is very different from the case without viscous coupling, where $\hat{h}_2 = \hat{f}_f\hat{\lambda}_c$ always will be positive. The terms in* (2.39) *describing chemotaxis toward chemokine and elevated cell pressure also behaves similarly, but they are directly affecting the cell phase, and indirectly the fibroblast and IF phases (contrary to chemotaxis toward TGF directly affecting the fibroblasts).*

Remark 2.9. *While it might seem that the only effect of including the fluid-fluid interaction lies in the second term of the $\hat{h}_2$ function, it should be mentioned that also the mobilities of the cell and fibroblast phases change. This affect the fractional flow functions as well.*

We will later see when specifying the form of the functions $\hat{f}_c, \hat{f}_f, \hat{f}_w, \hat{h}_1, \hat{h}_2$ and $\hat{h}_3$ that some terms in (2.39) are negligible, and by keeping only the terms representing the dominating effects we can further simplify the model.

2.6 Functional Forms of the Interaction Coefficients

Consistent with Waldeland and Evje (2018), we consider the following choices for the interaction coefficients

$$\begin{aligned}\hat{\zeta}_c &= I_c \hat{k}_c \alpha_c^{r_c} \\ \hat{\zeta}_f &= I_f \hat{k}_f \alpha_f^{r_f} \\ \hat{\zeta}_w &= I_w \hat{k}_w \alpha_w^{r_w} \\ \hat{\zeta}_{cf} &= I_{cf} \alpha_c^{r_{cf}} \alpha_f^{r_{fc}}.\end{aligned} \tag{2.41}$$

The parameters I_c, I_f and I_w represent static properties of the tissue, while $\hat{k}_c, \hat{k}_f$ and $\hat{k}_w$ can account for dynamic properties, related to for example ECM remodeling and fiber alignment, see Subsections 1.2.4 & 1.2.5. Reduction in the cell-ECM resistance force in the presence of fibroblasts could be attributed to $\hat{k}_c$. I_{cf} is a constant determining the order of magnitude of the cell-fibroblast interaction. The definitions in (2.41) emphasize the fact that the interaction forces should fade out when the phases disappear. In the case of single-phase flow of IF in one dimension, the momentum balance (2.14) reduces to

$$\frac{\partial P_w}{\partial x} = -I_w \hat{k}_w u_w.$$

Comparing this expression with the corresponding Darcy law

$$\frac{\partial P_w}{\partial x} = -\frac{\mu_w}{K} \phi u_w,$$

with K being the absolute permeability of the tissue, we get that

$$I_w \hat{k}_w = \frac{\mu_w}{K} \phi.$$

Initially, we are going to set $\hat{k}_l = 1, (l = c, f, w)$, implying that

$$I_w = \frac{\mu_w}{K} \phi,$$

i.e. proportional to the viscosity, as previously mentioned.

With the above-mentioned choices for the interaction coefficients, the fractional flow functions take the following forms

$$\begin{aligned}\hat{f}_c &= \frac{\alpha_c \alpha_f + \alpha_c^2 + R_f \alpha_c^{2-r_{cf}} \alpha_f^{r_f - r_{fc}}}{A(\alpha_c, \alpha_f)} \\ \hat{f}_f &= \frac{\alpha_c \alpha_f + \alpha_f^2 + R_c \alpha_c^{r_c - r_{cf}} \alpha_f^{2-r_{fc}}}{A(\alpha_c, \alpha_f)} \\ \hat{f}_w &= \frac{\alpha_w^{2-r_w}}{R_w} \frac{R_c \alpha_c^{r_c} + R_c R_f \alpha_c^{r_c - r_{cf}} \alpha_f^{r_f - r_{fc}} + R_f \alpha_f^{r_f}}{A(\alpha_c, \alpha_f)},\end{aligned} \tag{2.42}$$

while the expressions in (2.34) can be written

$$\begin{aligned}\hat{h}_1 &= \frac{\alpha_w^{2-r_w}}{I_w\hat{k}_w}\frac{R_f\alpha_c^{2-r_{cf}}\alpha_f^{r_f-r_{fc}}+\alpha_c^2+\alpha_c\alpha_f}{A(\alpha_c,\alpha_f)}\\ \hat{h}_2 &= \frac{1}{I_w\hat{k}_w}\frac{R_w\alpha_c^{2-r_{cf}}\alpha_f^{2-r_{fc}}-\alpha_c\alpha_f\alpha_w^{2-r_w}}{A(\alpha_c,\alpha_f)}\\ \hat{h}_3 &= \frac{\alpha_w^{2-r_w}}{I_w\hat{k}_w}\frac{\alpha_c\alpha_f+R_c\alpha_c^{r_c-r_cf}\alpha_f^{2-r_{fc}}+\alpha_f^2}{A(\alpha_c,\alpha_f)},\end{aligned} \tag{2.43}$$

with A given by

$$\begin{aligned}A(\alpha_c,\alpha_f) =&(\alpha_c+\alpha_f)^2+R_f\alpha_c^{2-r_{cf}}\alpha_f^{r_f-r_{fc}}+R_c\alpha_c^{r_c-r_{cf}}\alpha_f^{2-r_{fc}}\\ &+\frac{\alpha_w^{2-r_w}}{R_w}\left(R_c\alpha_c^{r_c}+R_cR_f\alpha_c^{r_c-r_{cf}}\alpha_f^{r_f-r_{fc}}+R_f\alpha_f^{r_f}\right),\end{aligned}$$

and the R-coefficients by

$$R_c=\frac{I_c\hat{k}_c}{I_{cf}},\qquad R_f=\frac{I_f\hat{k}_f}{I_{cf}},\qquad R_w=\frac{I_w\hat{k}_w}{I_{cf}}.$$

Remark 2.10. *The three coefficients R_l, $(l=c,f,w)$, indicate the relative strength of the different interaction forces, that is, fluid-ECM relative to fluid-fluid forces (i.e. the cell-fibroblast interaction, which is the only fluid-fluid force we are going to consider). For example, $R_c<1$ means that the cells are sticking more to the fibroblasts than the stationary ECM.*

Using the expressions for the flow functions given in (2.42) and (2.43), the parameters in Table 3.1, and letting $I_{cf}\to 0$, we get the plots in Figures 2.3-2.8.

2.7 One-Dimensional Version of the Model

The model (2.20) takes the following form in 1-D

$$\begin{aligned}\alpha_{ct}+(\alpha_c u_c)_x &= S_c\\ \alpha_{ft}+(\alpha_f u_f)_x &= S_f\\ \rho_t &= -\lambda_{21}G\rho+\rho\left(\lambda_{22}-\lambda_{23}\alpha_c-\lambda_{24}\frac{\rho}{\rho_M}\right)\\ G_t+(u_wG)_x &= D_GG_{xx}-\lambda_{31}G+\alpha_c\left(\lambda_{32}-\lambda_{33}\left(\frac{G}{G_M}\right)^{v_G}\right)\\ C_t+(u_wC)_x &= D_CC_{xx}+G\rho\left(\lambda_{41}-\lambda_{42}\left(\frac{C}{C_M}\right)^2-\lambda_{43}\left(\frac{C}{C_M}\right)^{v_C}\right)-\lambda_{44}\alpha_c\\ H_t+(u_wH)_x &= D_HH_{xx}-\lambda_{51}H+\alpha_f\left(\lambda_{52}-\lambda_{53}\left(\frac{H}{H_M}\right)^{v_H}\right),\end{aligned} \tag{2.44}$$

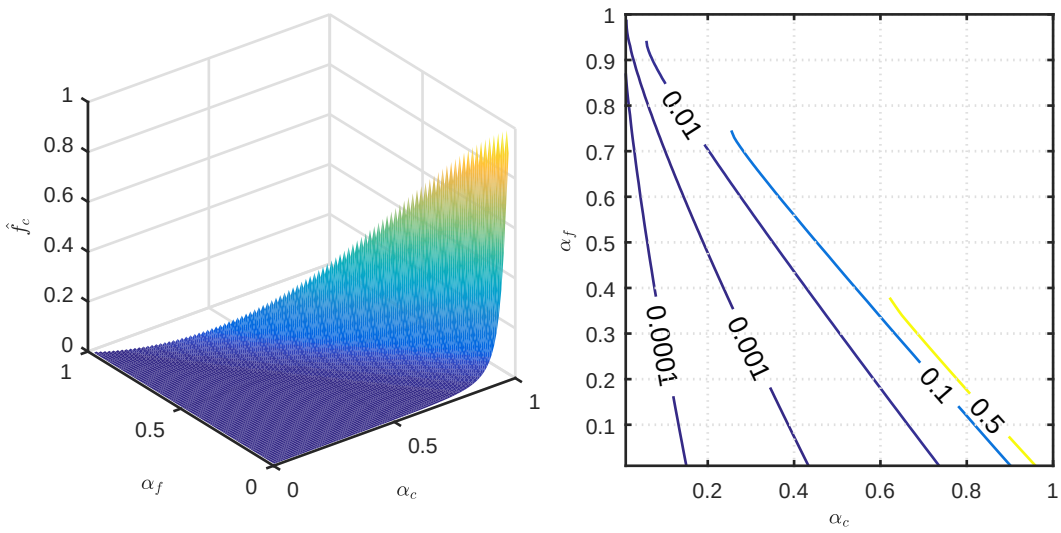

Figure 2.3: Fractional flow of cells as a function of the volume fraction of cells and fibroblasts (left). Contour plot (right).

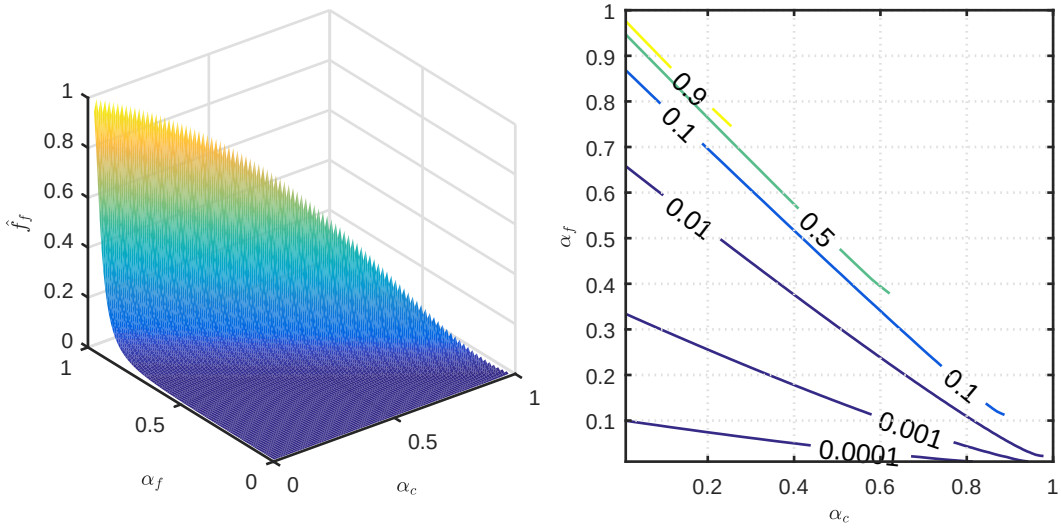

Figure 2.4: Fractional flow of fibroblasts as a function of the volume fraction of cells and fibroblasts (left). Contour plot (right).

using explicit expressions for the phase velocities. Equations for P_w and U_T (assuming $Q = 0$ and setting $\Delta P_{cw} = \Delta P$)

$$\begin{aligned} -(\hat{\lambda}_c(\Delta P + \Lambda_C)_x)_x - (\hat{\lambda}_f \Lambda_{Hx})_x &= (\hat{\lambda}_T P_{wx})_x \\ U_T &= -\hat{\lambda}_T P_{wx} - \hat{\lambda}_c(\Delta P + \Lambda_C)_x - \hat{\lambda}_f \Lambda_{Hx}, \end{aligned} \tag{2.45}$$

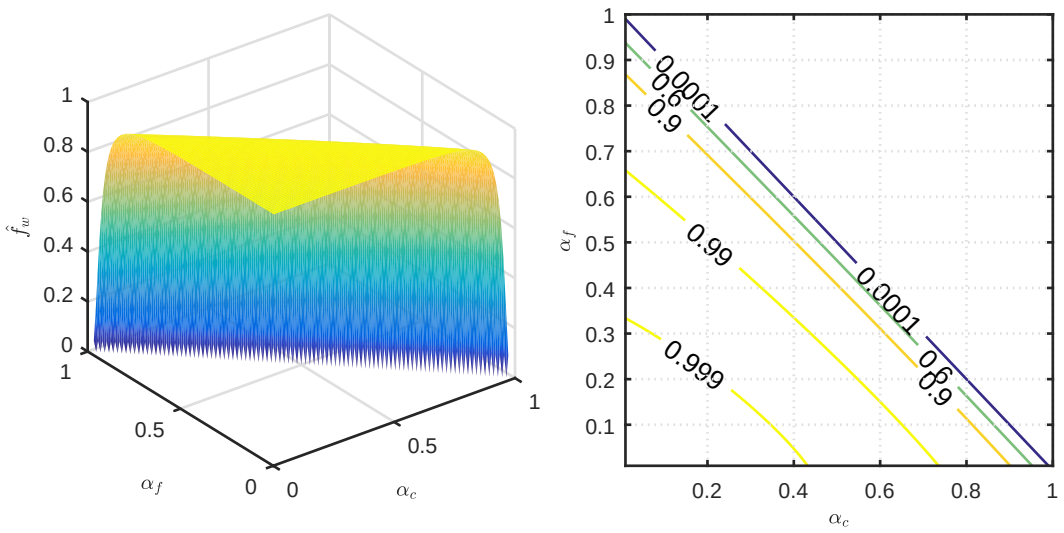

Figure 2.5: Fractional flow of IF as a function of the volume fraction of cells and fibroblasts (left). Contour plot (right).

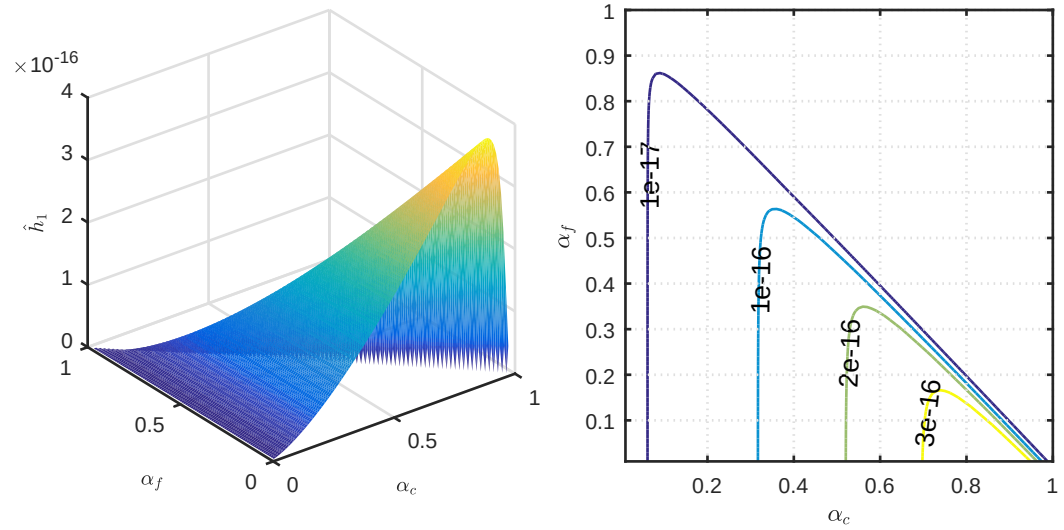

Figure 2.6: $\hat{h}_1$ as a function of the volume fraction of cells and fibroblasts (left). Contour plot (right).

with $\Lambda_C = \Lambda_C(C), \Lambda_H = \Lambda_H(H)$ and $\Delta P = \Delta P(\alpha_c)$. Superficial velocities

$$\begin{aligned} U_c &= \hat{f}_c U_T - (\hat{h}_1 + \hat{h}_2)(\Delta P + \Lambda_C)_x + \hat{h}_2 \Lambda_{Hx} \\ U_f &= \hat{f}_f U_T + \hat{h}_2(\Delta P + \Lambda_C)_x - (\hat{h}_2 + \hat{h}_3)\Lambda_{Hx} \\ U_w &= \hat{f}_w U_T + \hat{h}_1(\Delta P + \Lambda_C)_x + \hat{h}_3 \Lambda_{Hx}, \end{aligned} \tag{2.46}$$

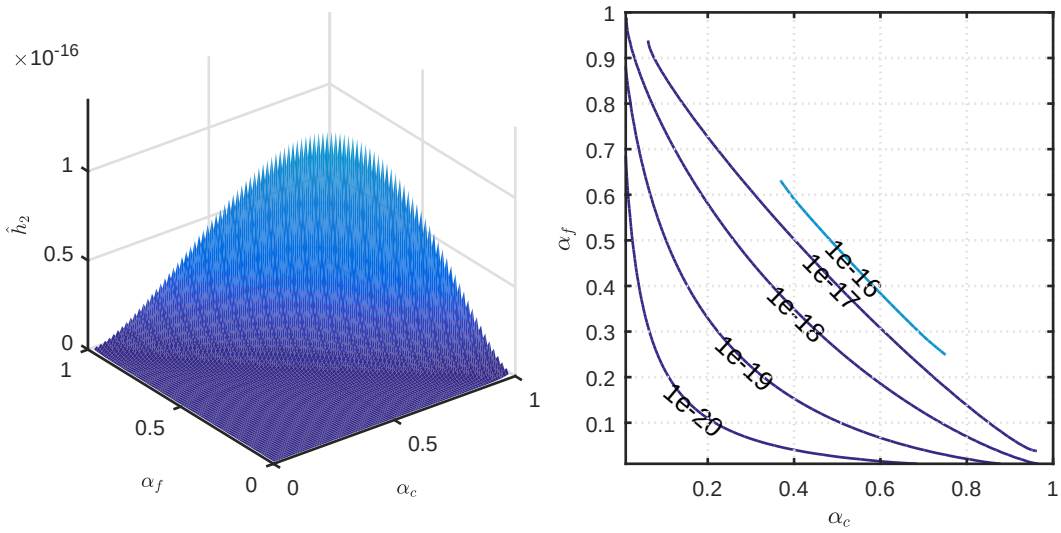

Figure 2.7: $\hat{h}_2$ as a function of the volume fraction of cells and fibroblasts (left). Contour plot (right).

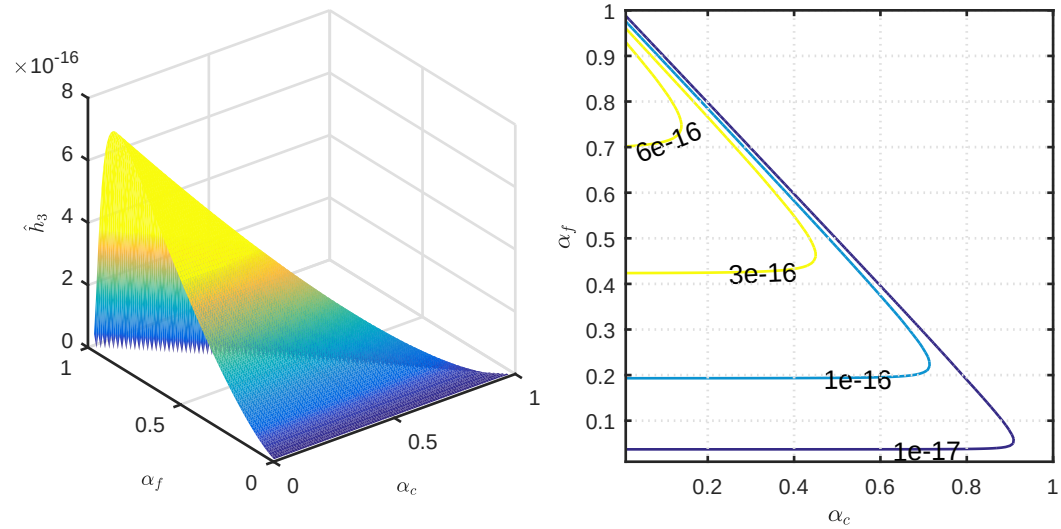

Figure 2.8: $\hat{h}_3$ as a function of the volume fraction of cells and fibroblasts (left). Contour plot (right).

interstitial velocities

$$u_c = \frac{\hat{f}_c}{\alpha_c} U_T - \frac{\hat{h}_1 + \hat{h}_2}{\alpha_c} (\Delta P + \Lambda_C)_x + \frac{\hat{h}_2}{\alpha_c} \Lambda_{Hx}$$
$$u_f = \frac{\hat{f}_f}{\alpha_f} U_T + \frac{\hat{h}_2}{\alpha_f} (\Delta P + \Lambda_C)_x - \frac{\hat{h}_2 + \hat{h}_3}{\alpha_f} \Lambda_{Hx} \tag{2.47}$$

$$u_w = \frac{\hat{f_w}}{\alpha_w} U_T + \frac{\hat{h}_1}{\alpha_w}(\Delta P + \Lambda_C)_x + \frac{\hat{h}_3}{\alpha_w}\Lambda_{Hx}.$$

The potential and capillary pressure functions are given by

$$\begin{aligned} \Lambda_C(C) &= \Lambda_{C0} - \frac{\Lambda_{C1}}{1 + \exp[-\xi_1(C - C_M)]} \\ \Lambda_H(H) &= \Lambda_{H0} - \frac{\Lambda_{H1}}{1 + \exp[-\xi_2(H - H_M)]} \\ \Delta P(\alpha_c) &= -\gamma \ln[\delta + (1 - \alpha_c)]. \end{aligned} \tag{2.48}$$

The form of the potential functions are similar to what was done by e.g. Waldeland and Evje (2018), whereas the function describing the elevated cell pressure due to cell-cell interactions are motivated by the approach commonly used in petroleum engineering. When the cells are closely packed (i.e. for large α_c) they experience stress and want to spread in order to reduce it (C. J. W. Breward, Byrne, & Lewis, 2002). For lower fractions they might want to attract themselves (cell aggregation), but we will only focus on the spreading effect occuring at higher fractions.

Here it is assumed that the capillary pressure is a function of the saturations only, justified by the fact that the interfacial geometry varies with saturation (Allen III et al., 1988; Green & Willhite, 1998; Leverett, 1940). The interfacial geometry, or more specifically the curvature of the interfaces, is directly related to the capillary pressure by the Young-Laplace equation (Green & Willhite, 1998; Kirby, 2010; Zolotukhin & Ursin, 2000)

$$\Delta P = \sigma \left(\frac{1}{R_1} + \frac{1}{R_2} \right),$$

where σ is the interfacial tension and R_1, R_2 the principal radii of curvature of the fluid-fluid interface at the position of capillary pressure determination.

A plot of the potential function for chemokine in $(2.48)_1$ and its derivative are given in Figure 2.9, using the parameters in Table 3.1. In the upper row ξ_1 ranges from 4 to 16 keeping Λ_{C1} constant at 2.5, while in the lower row we vary Λ_{C1} between 2-4 using $\xi_1 = 8$. Note that the magnitude of $\Lambda_C'(C)$ is greatest for $C = C_{max} = 0.3$.

A plot of the capillary pressure function given in $(2.48)_3$ and its derivative are shown in Figure 2.10, using different values of γ ranging from 0.05 to 0.15 and δ in the range 0.001 to 0.1. Note that the derivative takes low values except for very high cell concentrations. This suggests that the cell-cell interactions will be insignificant for the fractions of cells we'll be considering (less than 20 %).

Boundary and initial conditions. Boundary conditions

$$\begin{aligned} G_x|_{x=0,1} = 0, \qquad C_x|_{x=0,1} = 0, \qquad H_x|_{x=0,1} = 0, \qquad \hat{\lambda}_c|_{x=0,1} = 0, \qquad \hat{\lambda}_f|_{x=0,1} = 0, \\ P_w(0,t) = P_L^*, \qquad P_w(1,t) = P_R^*, \end{aligned}$$

initial data

$$\begin{aligned} \alpha_c(x,0) = \alpha_{c0}(x), \qquad \alpha_f(x,0) = \alpha_{f0}(x), \qquad \rho(x,0) = \rho_0(x), \\ G(x,0) = G_0(x), \qquad C(x,0) = C_0(x), \qquad H(x,0) = H_0(x). \end{aligned}$$

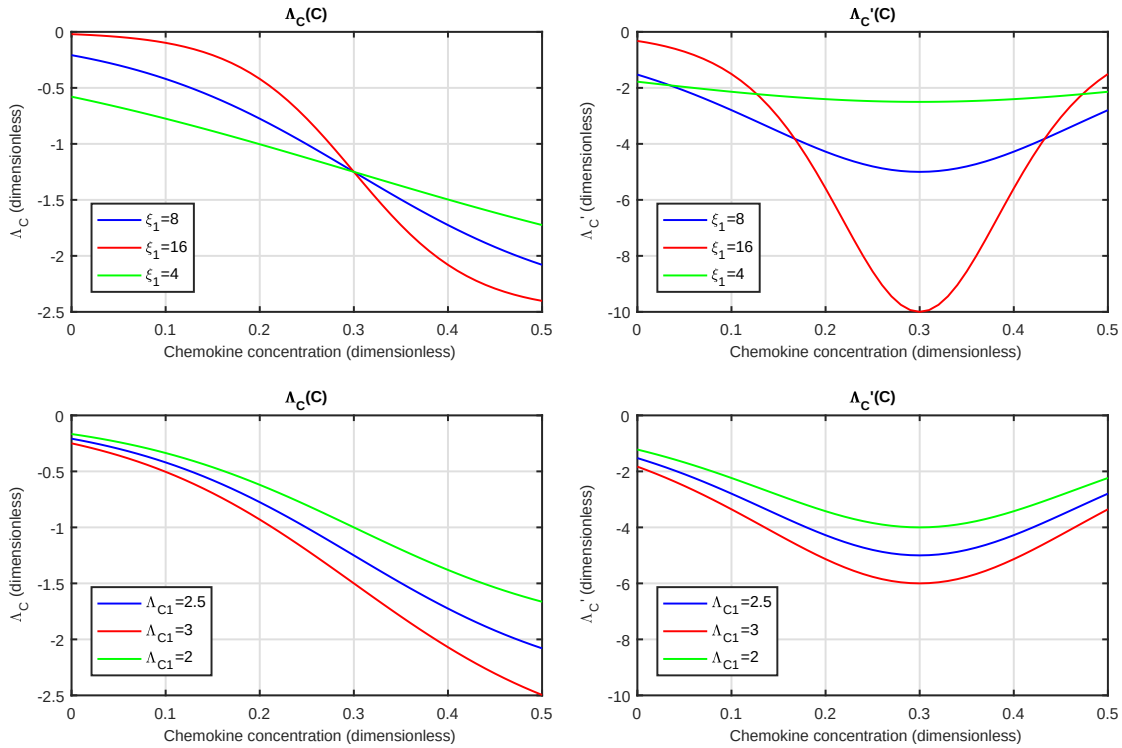

Figure 2.9: Plot of the chemokine potential function (left) and its derivative (right). The upper plots illustrate sensitivity with ξ_1 keeping $\Lambda_{C1} = 2.5$, and in the two lower plots we vary Λ_{C1} keeping $\xi_1 = 8$. Note that the magnitude of $\Lambda_C'(C)$ is greatest for $C = C_{max} = 0.3$.

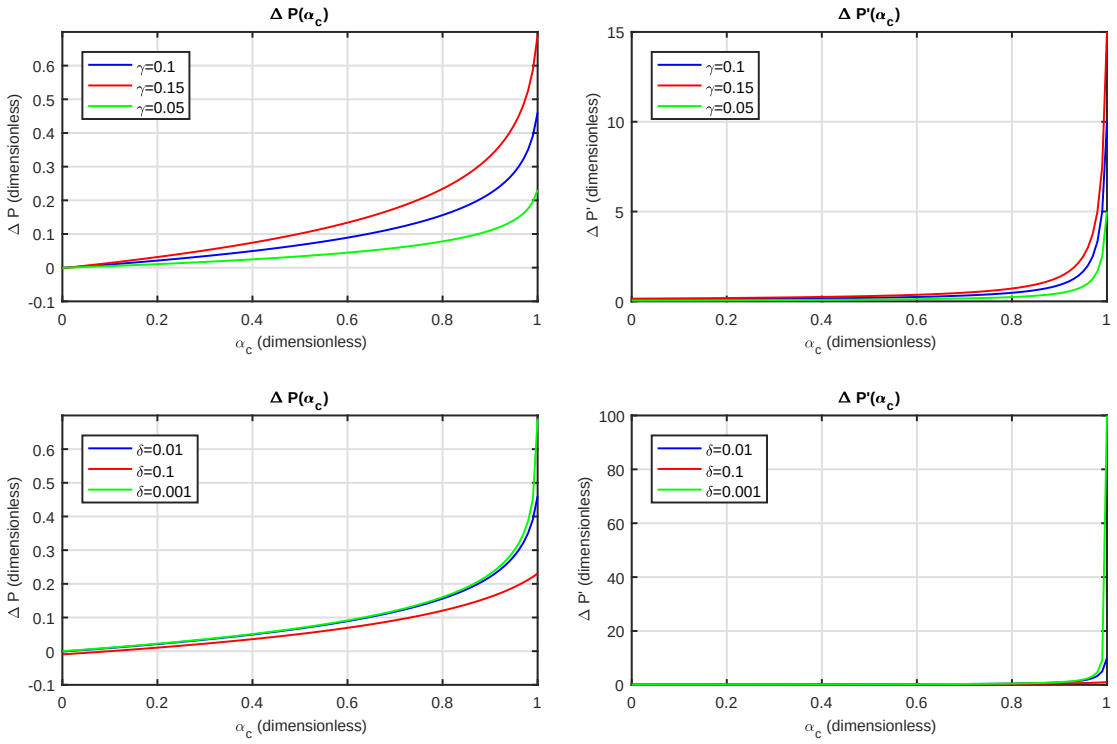

Figure 2.10: Plot of the capillary pressure function (left) and its derivative (right). In the two upper plots we use different values of γ (with $\delta = 0.01$), and in the lower plots we use values of δ ranging from 0.001 to 0.1 (keeping $\gamma = 0.1$).

Chapter 3

Numerical Solution

In this chapter we will develop a numerical solution procedure for the one-dimensional formulation of the three-phase model described in Section 2.7. To this end, we will employ a fractional-step or operator-splitting method called Strang Splitting (LeVeque, 2002). The idea is to split the equations into subproblems that can be solved independently.

The solution procedure has been implemented in a MATLAB script which will be used to solve the model for various parameters and initial conditions. We will start with a two-phase problem involving only cell and IF, similar to Figure 8 in the paper by Waldeland and Evje (2018). We will then gradually introduce the fibroblasts, neglecting TGF-dependent chemotaxis at first. Finally, we define an appropriate base case which will be used in the next chapter to test the model hypotheses stated in Subsection 1.2.6.

3.1 Steps in the Numerical Solution

Consider the following splitting of the one-dimensional model given by Equation (2.44) in Section 2.7 (Evje, 2017)

$$
\begin{aligned}
\alpha_{ct} &= S_c \\
\alpha_{ct} + (\alpha_c u_c)_x &= 0 \\
\alpha_{ft} &= S_f \\
\alpha_{ft} + (\alpha_f u_f)_x &= 0 \\
\rho_t &= -\lambda_{21} G\rho + \rho\left(\lambda_{22} - \lambda_{23}\alpha_c - \lambda_{24}\frac{\rho}{\rho_M}\right) \\
G_t + (u_w G)_x &= D_G G_{xx} - \lambda_{31} G + \alpha_c\left(\lambda_{32} - \lambda_{33}\left(\frac{G}{G_M}\right)^{v_G}\right) \\
C_t + (u_w C)_x &= D_C C_{xx} + G\rho\left(\lambda_{41} - \lambda_{42}\left(\frac{C}{C_M}\right)^2 - \lambda_{43}\left(\frac{C}{C_M}\right)^{v_C}\right) - \lambda_{44}\alpha_c
\end{aligned}
$$

$$H_t + (u_w H)_x = D_H H_{xx} - \lambda_{51} H + \alpha_f \left(\lambda_{52} - \lambda_{53} \left(\frac{H}{H_M} \right)^{v_H} \right),$$

where the mass transport equations have been splitted into one part accounting for reaction/source terms and another accounting for convection/transport. Let R_t be the solution operator associated with the subsystem

$$\begin{aligned} R_t : \qquad & \alpha_{ct} = S_c \\ & \alpha_{ft} = S_f \\ & \rho_t = -\lambda_{21} G \rho + \rho \left(\lambda_{22} - \lambda_{23} \alpha_c - \lambda_{24} \frac{\rho}{\rho_M} \right), \end{aligned} \tag{3.1}$$

and T_t to be associated with

$$\begin{aligned} T_t : \qquad & \alpha_{ct} + (\alpha_c u_c)_x = 0 \\ & \alpha_{ft} + (\alpha_f u_f)_x = 0 \\ & G_t + (u_w G)_x = D_G G_{xx} - \lambda_{31} G + \alpha_c \left(\lambda_{32} - \lambda_{33} \left(\frac{G}{G_M} \right)^{v_G} \right) \\ & C_t + (u_w C)_x = D_C C_{xx} + G\rho \left(\lambda_{41} - \lambda_{42} \left(\frac{C}{C_M} \right)^2 - \lambda_{43} \left(\frac{C}{C_M} \right)^{v_C} \right) - \lambda_{44} \alpha_c \\ & H_t + (u_w H)_x = D_H H_{xx} - \lambda_{51} H + \alpha_f \left(\lambda_{52} - \lambda_{53} \left(\frac{H}{H_M} \right)^{v_H} \right). \end{aligned} \tag{3.2}$$

The operator R_t accounts for the source term effects and T_t for the transport effects. Given an approximate solution S^n at time t^n, we find a new approximation at time t^{n+1} from the following sequential three-step procedure

$$S^{n+1} = (R_{\Delta t/2} T_{\Delta t} R_{\Delta t/2}) S^n.$$

3.1.1 Source Term Operator

The source term operator R_t is a system of ODE's (ordinary differential equations), differentiated with respect to time t only. We apply this operator over a time step of length $\Delta t/2$, discretizing $(3.1)_{1,2}$ in the following way

$$\frac{\Delta_t \alpha_l}{0.5\Delta t} = S^n_{l,j}, \qquad (l = c, f) \tag{3.3}$$

and $(3.1)_3$ as

$$\begin{aligned} \frac{\Delta_t \rho}{0.5\Delta t} &= -\lambda_{21} G^n_j \rho^{n+1}_j + \rho^n_j (\lambda_{22} - \lambda_{23} \alpha^n_{c,j} - \lambda_{24} \rho^n_j) \\ \rho^{n+1}_j &= \frac{\rho^n_j + 0.5\Delta t \rho^n_j \left(\lambda_{22} - \lambda_{23} \alpha^n_{c,j} - \lambda_{24} \frac{\rho^n_j}{\rho_M} \right)}{1 + 0.5\Delta t \lambda_{21} G^n_j}. \end{aligned}$$

Assuming $\lambda_{22} = \lambda_{44}$ and $\lambda_{23} = 0$, we get

$$\rho_j^{n+1} = \frac{\rho_j^n + 0.5\Delta t \lambda_{22} \rho_j^n \left(1 - \frac{\rho_j^n}{\rho_M}\right)}{1 + 0.5\Delta t \lambda_{21} G_j^n}. \tag{3.4}$$

3.1.2 Transport Operator

Using the new volume fractions we solve for P_w using the elliptic pressure equation

$$-(\hat{\lambda}_c(\Delta P + \Lambda_C)_x)_x - (\hat{\lambda}_f \Lambda_{Hx})_x = (\hat{\lambda}_T P_{wx})_x, \tag{3.5}$$

and find the total velocity using the explicit equation for U_T

$$U_T = -\hat{\lambda}_T P_{wx} - \hat{\lambda}_c(\Delta P + \Lambda_C)_x - \hat{\lambda}_f \Lambda_{Hx}. \tag{3.6}$$

Using the newly calculated volume fractions and total velocity, in addition to the concentrations of chemokine and TGF from previous time step, we find the superficial and interstitial velocities necessary for solving (3.2)

$$\begin{aligned}
U_c &= U_T \hat{f}_c - (\hat{h}_1 + \hat{h}_2)(\Delta P + \Lambda_C)_x + \hat{h}_2 \Lambda_{Hx} \\
U_f &= U_T \hat{f}_f + \hat{h}_2(\Delta P + \Lambda_C)_x - (\hat{h}_2 + \hat{h}_3)\Lambda_{Hx} \\
U_w &= U_T \hat{f}_w + \hat{h}_1(\Delta P + \Lambda_C)_x + \hat{h}_3 \Lambda_{Hx} \\
u_c &= U_T \frac{\hat{f}_c}{\alpha_c} - \frac{\hat{h}_1 + \hat{h}_2}{\alpha_c}(\Delta P + \Lambda_C)_x + \frac{\hat{h}_2}{\alpha_c}\Lambda_{Hx} \\
u_f &= U_T \frac{\hat{f}_f}{\alpha_f} + \frac{\hat{h}_2}{\alpha_f}(\Delta P + \Lambda_C)_x - \frac{\hat{h}_2 + \hat{h}_3}{\alpha_f}\Lambda_{Hx} \\
u_w &= U_T \frac{\hat{f}_w}{\alpha_w} + \frac{\hat{h}_1}{\alpha_w}(\Delta P + \Lambda_C)_x + \frac{\hat{h}_3}{\alpha_w}\Lambda_{Hx}.
\end{aligned} \tag{3.7}$$

Finally, we apply the operator T_t over a time step of length Δt and spatial interval of length Δx. We use the following discretization of Equations (3.5) and (3.6)

$$\begin{aligned}
\delta_x \hat{\lambda}_T \delta_x P_w &= -\delta_x \hat{\lambda}_c \delta_x \Delta P - \delta_x \hat{\lambda}_c \delta_x \Lambda_C - \delta_x \hat{\lambda}_f \delta_x \Lambda_H \\
U_T &= -\frac{\hat{\lambda}_T \delta_x P_w + \hat{\lambda}_c \delta_x \Delta P + \hat{\lambda}_c \delta_x \Lambda_C + \hat{\lambda}_f \delta_x \Lambda_H}{\Delta x},
\end{aligned} \tag{3.8}$$

where

$$\delta_x \hat{\lambda}_T \delta_x P_w = \hat{\Lambda}_{T,j+1/2}(P_{w,j+1} - P_{w,j}) - \hat{\Lambda}_{T,j-1/2}(P_{w,j} - P_{w,j-1}),$$

and similarly for the other terms. The boundary conditions are specified as

$$\begin{aligned}
\hat{\lambda}_{l,1/2} = \hat{\lambda}_{l,N+1/2} = 0, \qquad (l = c, f), \\
P_{w,1/2} = P_L^*, \qquad P_{w,N+1/2} = P_R^*.
\end{aligned}$$

Equation (3.7) takes the following discretized form

$$
\begin{aligned}
U_c &= \hat{f}_c U_T - \frac{\hat{h}_1+\hat{h}_2}{\Delta x}\delta_x(\Delta P+\Lambda_C) + \frac{\hat{h}_2}{\Delta x}\delta_x\Lambda_H \\
U_f &= \hat{f}_f U_T + \frac{\hat{h}_2}{\Delta x}\delta_x(\Delta P+\Lambda_C) - \frac{\hat{h}_2+\hat{h}_3}{\Delta x}\delta_x\Lambda_H \\
U_w &= \hat{f}_w U_T + \frac{\hat{h}_1}{\Delta x}\delta_x(\Delta P+\Lambda_C) + \frac{\hat{h}_3}{\Delta x}\delta_x\Lambda_H \\
u_c &= \frac{\hat{f}_c}{\alpha_c}U_T - \frac{1}{\Delta x}\frac{\hat{h}_1+\hat{h}_2}{\alpha_c}\delta_x(\Delta P+\Lambda_C) + \frac{1}{\Delta x}\frac{\hat{h}_2}{\alpha_c}\delta_x\Lambda_H \\
u_f &= \frac{\hat{f}_f}{\alpha_f}U_T + \frac{1}{\Delta x}\frac{\hat{h}_2}{\alpha_f}\delta_x(\Delta P+\Lambda_C) - \frac{1}{\Delta x}\frac{\hat{h}_2+\hat{h}_3}{\alpha_f}\delta_x\Lambda_H \\
u_w &= \frac{\hat{f}_w}{\alpha_w}U_T + \frac{1}{\Delta x}\frac{\hat{h}_1}{\alpha_w}\delta_x(\Delta P+\Lambda_C) + \frac{1}{\Delta x}\frac{\hat{h}_3}{\alpha_w}\delta_x\Lambda_H.
\end{aligned}
\tag{3.9}
$$

The mass balances $(3.2)_{1,2}$ become

$$
\Delta_t\alpha_l = -\frac{\Delta t}{\Delta x}\delta_x(\alpha_l u_l), \qquad (l=c,f) \tag{3.10}
$$

with advective terms treated explicitly (at time level t^n). For the evolution of the chemical components we use the discretized forms of $(3.2)_{3,4,5}$ given as

$$
\begin{aligned}
\Delta_t G + \lambda\delta_x(u_w G) &= D_G\gamma\delta_x^2 G - \Delta t\lambda_{31}G_j^n + \Delta t\alpha_c\left(\lambda_{32}-\lambda_{33}\left(\frac{G_j^n}{G_M}\right)^{\nu_G}\right) \\
\Delta_t C + \lambda\delta_x(u_w C) &= D_C\gamma\delta_x^2 C + \Delta t G\rho\left(\lambda_{41}-\lambda_{42}\left(\frac{C_j^n}{C_M}\right)^2-\lambda_{43}\left(\frac{C_j^n}{C_M}\right)^{\nu_C}\right) - \Delta t\lambda_{44}\alpha_c \\
\Delta_t H + \lambda\delta_x(u_w H) &= D_H\gamma\delta_x^2 H - \Delta t\lambda_{51}H_j^n + \Delta t\alpha_f\left(\lambda_{52}-\lambda_{53}\left(\frac{H_j^n}{H_M}\right)^{\nu_H}\right),
\end{aligned}
\tag{3.11}
$$

where the advective and diffusive terms are treated explicitly and implicitly, respectively. The boundary conditions are specified as

$$
G_1 = G_2,\ G_{N-1} = G_N, \qquad C_1 = C_2,\ C_{N-1} = C_N, \qquad H_1 = H_2,\ H_{N-1} = H_N,
$$

i.e. no flux of the chemical components at the left and right boundary.

3.2 Case Without Fibroblasts

In this section we will take a look at the case for flow of tumor cells and interstitial fluid, without fibroblasts. The parameters are chosen to be the same as in Figure 8 in the paper by Waldeland and Evje (2018), repeated in Table 3.1.

Table 3.1: Parameters for case without fibroblasts

Parameter	Description	Value	Unit
General parameters			
L	length of domain	$1 \cdot 10^{-2}$	m
T	simulation time	$5 \cdot 10^{5}$	s
P_{atm}	reference pressure (atmospheric)	$1.01325 \cdot 10^{5}$	Pa
Discretization parameters			
N	number of grid blocks	$2 \cdot 10^{2}$	-
N_{time}	number of time steps	$2 \cdot 10^{4}$	-
Material constants			
D_G	diffusion coefficient of protease	$8 \cdot 10^{-12}$	m^2/s
D_C	diffusion coefficient of chemokine	$7 \cdot 10^{-14}$	m^2/s
Production/decay rates			
λ_{21}	degradation of ECM	10	m^3/kgs
λ_{22}	reconstruction of ECM	$1.25 \cdot 10^{-3}$	1/s
λ_{23}	release of ECM	0	1/s
λ_{24}	release of ECM	$1.25 \cdot 10^{-3}$	1/s
ρ_M	maximum density of ECM	1	kg/m^3
λ_{31}	decay of protease	$2.5 \cdot 10^{-3}$	1/s
λ_{32}	cell production of protease	$2 \cdot 10^{-6}$	kg/m^3s
λ_{33}	logistic term constant (protease)	$2 \cdot 10^{-6}$	kg/m^3s
ν_G	exponent in logistic function of protease	1	-
G_M	maximum concentration of protease	$5 \cdot 10^{-5}$	kg/m^3
λ_{41}	proteolytically freed chemokine	$3.2 \cdot 10^{-3}$	m^3/kgs
λ_{42}	logistic term constant (chemokine)	$1.44 \cdot 10^{-4}$	m^3/kgs
λ_{43}	logistic term constant (chemokine)	$3.2 \cdot 10^{-3}$	m^3/kgs
λ_{44}	cell consumption of chemokine	$1 \cdot 10^{-9}$	kg/m^3s
ν_C	exponent in logistic function of chemokine	0.2	-
C_M	maximum concentration of chemokine	$3 \cdot 10^{-5}$	kg/m^3
Interaction parameters			
I_w	IF-ECM resistance force	$2 \cdot 10^{12}$	Pas/m^2
I_c/I_w	ratio between cell- and IF-ECM interaction	10^3	-
r_c	parameter controlling cell-ECM interaction	0.6	-
r_w	parameter controlling IF-ECM interaction	0	-
Potential function, chemokine			
ξ_1	parameter characterizing Λ_C	$8 \cdot 10^{4}$	m^3/kg
Λ_{C0}	parameter characterizing Λ_C	0	Pa
Λ_{C1}	parameter characterizing Λ_C	$2.5 \cdot 10^{4}$	Pa
Capillary pressure function			
γ	parameter characterizing ΔP	10^3	Pa

δ	parameter characterizing ΔP	0.01	-

The boundary conditions are given by

$$G_x|_{x=0,1} = 0, \qquad C_x|_{x=0,1} = 0, \qquad H_x|_{x=0,1} = 0, \qquad \hat{\lambda}_c|_{x=0,1} = 0, \qquad \hat{\lambda}_f|_{x=0,1} = 0,$$
$$P_w(0,t) = P_{atm} + 10^4 \text{ Pa}, \qquad P_w(1,t) = P_{atm},$$

and the initial data

$$\alpha_{c0}(x) = 0.2e^{-[25(x-0.5)]^2}, \qquad \alpha_f(x,0) = 0, \qquad \rho_0(x) = 1 - 0.5\alpha_{c0}(x),$$
$$G_0(x) = 0, \qquad C_0(x) = 0, \qquad H_0(x) = 0. \tag{3.12}$$

In this case we have a cell aggregate in the center, exposed to a global pressure difference of 10 kPa. This causes a total flow of 0.5 μm/s, consistent with Shieh et al. (2011).

Remark 3.1. *While $r_w = 0$ might seem a little odd since it implies $\hat{\zeta}_w$ being constant according to $(2.41)_3$, it will actually produce the same result as Darcy's law using Corey relative permeabilities with $n_w = 2$, i.e. $k_{rw} = S_w^2$ (Evje, 2017; Waldeland & Evje, 2018). The reason is that there is already one α_w on the left side of $(2.20)_6$, and another coming from the relation $\mathbf{u}_w = \mathbf{U}_w/\alpha_w$.*

Figure 3.1 shows a plot of the initial solution at time T=0. Note that all of the subplots are plotted against dimensionless distance, ranging from zero (left end) to one (right end, corresponding to L=1 cm). A brief explanation of the different subplots are given in the following, numbered from top left, top right, middle left, and so forth:

1. The first subplot shows the volume fractions of cell and fibroblast. The fibroblast fraction is set to zero, while there is a concentration of cells at the center. The IF volume fraction is given by the no-voids constraint: $\alpha_{w0}(x) = 1 - \alpha_{c0}(x) - \alpha_{f0}(x)$.

2. This plot shows the (dimensionless) pressure in each phase across the domain. A value of zero corresponds to atmospheric pressure, which is what we have at the right end. The gradient is fairly constant in those parts of the domain where only IF is present, in the center however, the gradient is larger (i.e. more negative), as seen by the steeper pressure profile here. This is due to the presence of cells, which tend to decrease the total mobility (because $I_c >> I_w$), and therefore also increases the magnitude of the gradient in accordance with $U_T = -\hat{\lambda}_T P_{wx} - \hat{\lambda}_c(\Delta P)_x$ (Equation $(2.45)_2$ with terms involving chemotaxis ignored since there are no chemoattractants present initially, ref. (3.12)). Note that there is a discrepancy between the cell and IF pressures due to the cell-cell interactions described by $\Delta P(\alpha_c)$.

3. The third subplot shows the (dimensionless) velocity of the cells, with values on the y-axis ranging from zero (stationary) to one (corresponding to 1 μm/s). Naturally, this velocity drops to zero outside of the domain (0.4, 0.6), since there are no cells present in this region. The total velocity is also included for reference, and since we

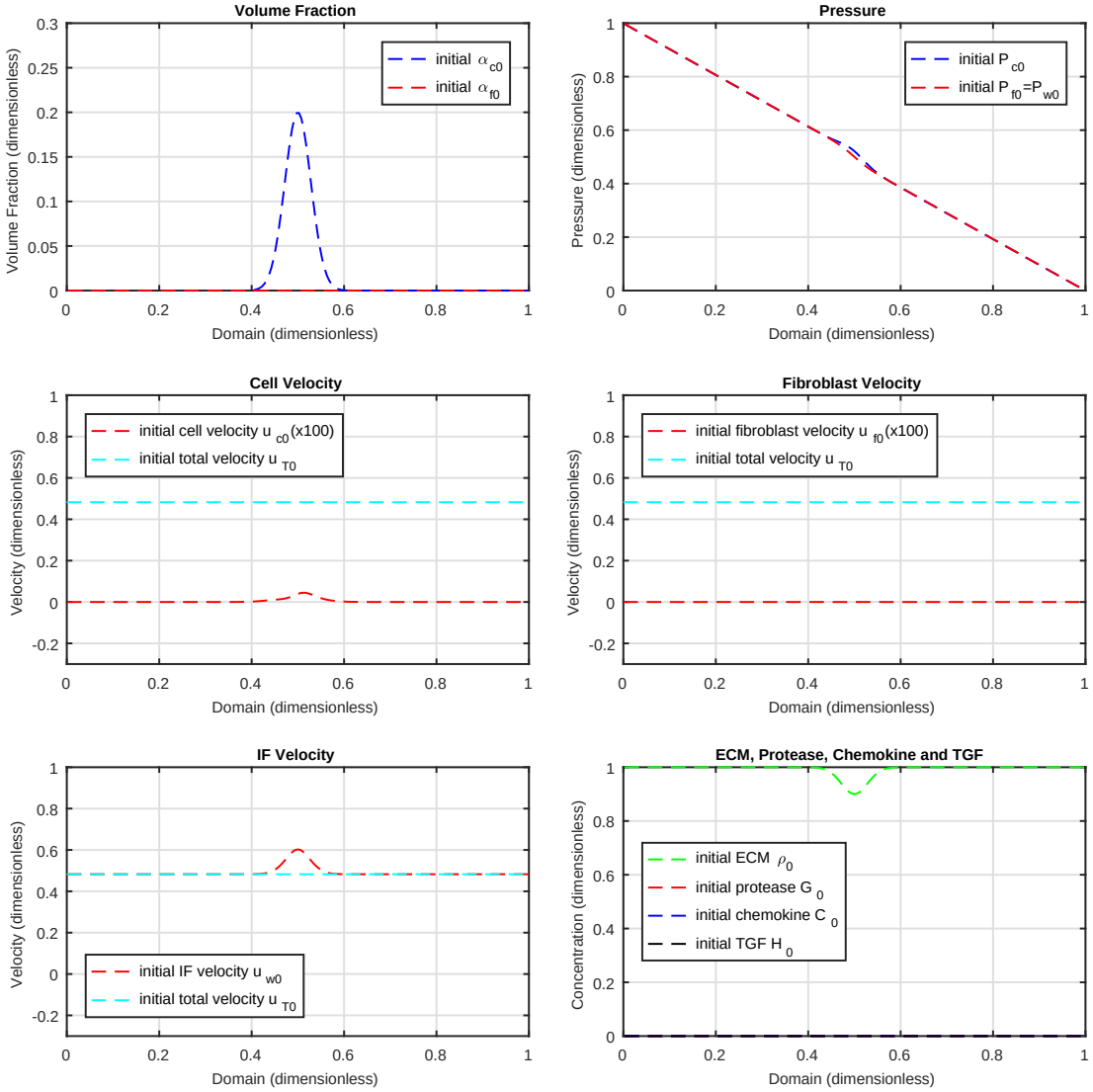

Figure 3.1: Initial solution of case without fibroblasts (T=0)

have set all the source terms to zero ($S_c = S_f = Q_v = Q_l = 0$), the total velocity will be divergence-free according to Equation (2.28). In the present 1-D setting, this implies a constant velocity (in space). Note that the cell velocity has been multiplied by a factor of 100 to include it in the same figure as the total velocity.

4. This plot is exactly identical to plot number three, but showing the velocity of fibroblasts. Again, the total velocity has been included for reference, and the fibroblast velocity has been multiplied by a factor of 100.

5. This is a plot of the IF velocity, but otherwise similar to the two previous plots.

Note that the magnitude of the IF velocity is comparable to the total velocity, therefore any scaling has not been necessary.

6. Plot showing the concentration of the chemical components; protease (G), chemokine (C) and TGF (H). The density of the ECM (ρ) is also included. It is assumed that the ECM has already been reacting with the tumor cells, and therefore the density is less than unity in the middle of the domain.

Similar plots are show in Figure 3.2 after $T = 5 \cdot 10^5$ s, corresponding to approximately 5.8 days. Some comments related to the figure:

1. The cells have migrated to the right, i.e. in the direction of flow. Since we have neglected proliferation and death of tumor cells by setting $S_c = 0$, the total amount of cells are still the same, meaning that the area under the blue curve is preserved. The average cell migration downstream can be expressed by the "cell volume center", $\bar{x}_c$, calculated using the following equation

$$\bar{x}_c = \frac{\int_0^1 \alpha_c x dx}{\int_0^1 \alpha_c dx} = 0.56.$$

2. The main difference seen in this figure compared with the initial solution is a shift in the pressure profiles from left to right, consistent with the shift of the cell volume fraction shown in the first subplot.

3. The plot showing the cell velocity has some new features. As before, the cell and total velocities are included, but also the decomposition of the cell velocity into its constituent terms according to Equation (2.39), are shown. *Flow* represents the momentum transfer to the cell phase due to push and drag from the flow of IF. The magnitude of this term depends on $\hat{f}_c/\alpha_c$, which is a function of the cell volume fraction only. Consequently, there is a clear connection to the volume fractions in subplot one. *Diffusion* is the velocity component resulting from cell-cell interactions, and the label is explained by the diffusional behavior resulting from these forces. The most significant contributor to the overall cell velocity is the term labeled *chemokine*, which describes the cell migration in the direction of increasing concentration of chemokine by chemotaxis. Since this is a counter-current effect, we see that the IF velocity in subplot five suffers from a negative chemokine contribution. Finally, *TGF* denotes chemotaxis of fibroblasts toward increasing concentration of TGF, or strictly speaking, the (possibly counter-current) effect this will have on the cell velocity. For this particular case the term is zero, due to a lack of fibroblasts. See also the discussion on page 24.

4. This figure has all of the same features as subplot three, but given for the fibroblasts. Note that *chemokine*, in this case, is the indirect, possibly counter-current, effect representing momentum transfer from cells to fibroblasts as a result of cells moving in the gradient-direction of chemokine. *TGF*, however, is a direct effect

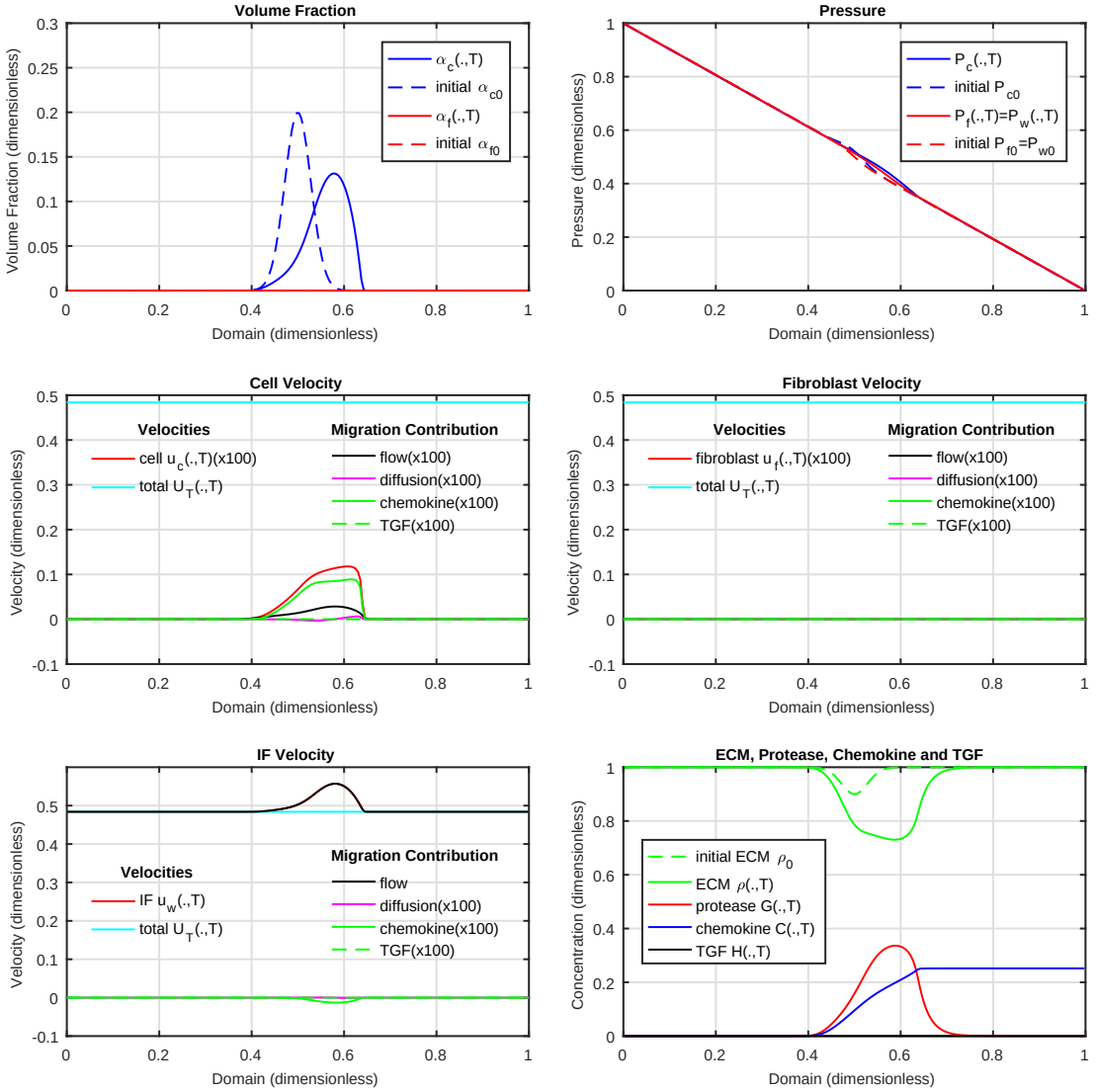

Figure 3.2: Solution of case without fibroblasts at T=5.8 days. The red and black curves in subplot 5 are overlapping.

in this case. All the velocities appear as zero since we have not yet included the fibroblasts.

5. In this plot both *chemokine* and *TGF* are indirect effects, since IF does not chemotact toward any of these chemicals. We should therefore expect both of them to be negative (TGF is of course zero in this particular case since we have omitted fibroblasts from the simulation). Note that *flow* is the by far most dominating mechanism, and it's shown in the figure without any scaling.

6. Protease is produced by the cells, but the concentration profile is skewed in the flow direction due to advection. For $x > 0.7$ the concentration drops to zero as a result of decay, since there are no cells present to maintain the high concentration levels. The chemokine concentration is also skewed in the direction of flow, but levels off at a fairly high concentration for $x > 0.65$. This happens because there are no cells present in this area, and therefore no consumption of chemokine either (the decay rate is very low).

3.3 Case With Fibroblasts

We will now include the fibroblasts in the simulation, using the same parameters as given in Table 3.1, in addition to the new fibroblast-specific parameters given in Table 3.2. We are only interested in the influence of the mere presence of fibroblasts, so we remove all special features they might possess, such as chemotaxis (toward TGF), viscous coupling to cells, and ECM remodeling.

Table 3.2: Fibroblast- and TGF-specific parameters

Parameter	Description	Value	Unit
Material constants			
D_H	diffusion coefficient of TGF	$8 \cdot 10^{-12}$	m^2/s
Production/decay rates			
λ_{51}	decay of TGF	0	1/s
λ_{52}	production of TGF	$1.7 \cdot 10^{-6}$	kg/m^3s
λ_{53}	logistic term constant (TGF)	$2 \cdot 10^{-6}$	kg/m^3s
ν_H	exponent in logistic function of TGF	0.2	-
H_M	maximum concentration of TGF	$5 \cdot 10^{-5}$	kg/m^3
Interaction parameters			
I_f/I_w	parameter controlling fibroblast-ECM interaction	$5 \cdot 10^2$	-
r_f	parameter controlling fibroblast-ECM interaction	0.6	-

The boundary conditions are given by

$$G_x|_{x=0,1} = 0, \qquad C_x|_{x=0,1} = 0, \qquad H_x|_{x=0,1} = 0, \qquad \hat{\lambda}_c|_{x=0,1} = 0, \qquad \hat{\lambda}_f|_{x=0,1} = 0,$$
$$P_w(0,t) = P_{atm} + 10000 \text{ Pa}, \qquad P_w(1,t) = P_{atm},$$

and the initial data

$$\alpha_{c0}(x) = 0.2e^{-[25(x-0.5)]^2}, \qquad \alpha_f(x,0) = 0.1e^{-3\cdot 10^5\cdot(x-0.5)^{12}}, \qquad \rho_0(x) = 1 - 0.5\alpha_{c0}(x),$$
$$G_0(x) = 0, \qquad C_0(x) = 0, \qquad H_0(x) = 0. \tag{3.13}$$

Since fibroblasts are a vital part of the tissue, we assume that it'll be uniformly distributed throughout the domain, as shown in the top left plot in Figure 3.3. Explanation

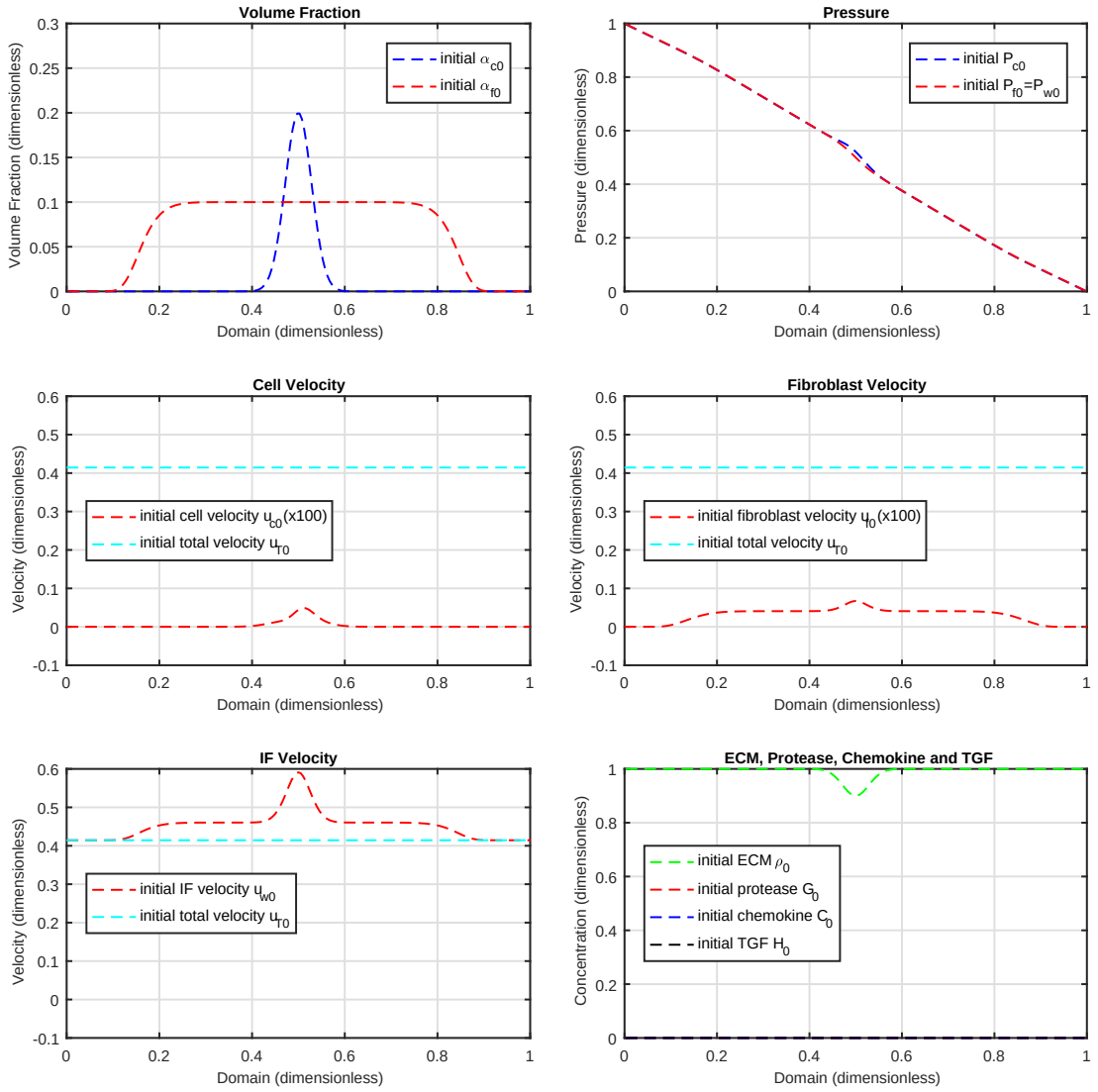

Figure 3.3: Solution of case with fibroblasts at T=0. Blocking of TGF.

of results:

1. The first plot shows the initial data consistent with (3.13). The volume fraction of cells is the same as before, but in addition we have a uniform density of fibroblasts occupying 10 % of the pore volume.

2. The pressure profile(s) are also the same as before. Note that the pressures in the fibroblast and IF phases are equal because fibroblast cells do not exert any interactions among themselves.

3. First note that the total velocity is slightly lower than in the case without fibrob-

lasts. The reason for this is that IF had to be expelled from the pores of the tissue in order to give room for the less mobile fibroblasts (the cell fraction is the same as before). This decreases the (average) total mobility of the porous medium, and therefore the total fluid velocity suffers (the global pressure gradient is the same). The cell velocity still correlates with the cell volume fraction, as before.

4. The velocity profile of the fibroblasts also correlates well with the associated volume fraction, but it seems to be affected by the volume fraction of the cells as well. This can be explained by looking at the fractional flow function of the fibroblasts as a function of the cell volume fraction, ref. Figure 3.4. Here we have plotted $\hat{f}_f(\alpha_c, \alpha_f)$ as a function of α_c at $\alpha_f = 0.1$. We see that the function is monotonically increasing. The reason for this is that as the cell volume fraction increases, the IF will gradually be replaced by the less mobile cell phase, thus improving the fibroblasts' fraction of the total mobility (i.e. the fractional flow).

5. Only IF is flowing at the left and right ends, and consequently its speed is identical to the total fluid velocity. As a response to lower volume fractions in the middle of the domain, the interstitial velocity increases.

6. Consistent with initial data and identical to Figure 3.1 (subplot no. 6).

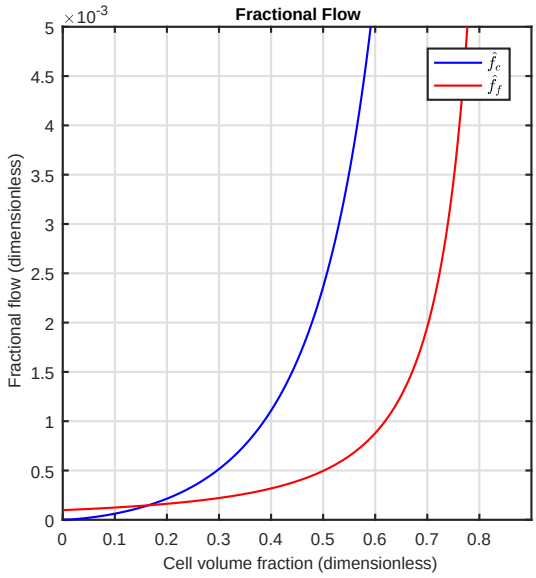

Figure 3.4: Fractional flow of cells and fibroblasts as a function of α_c when $\alpha_f = 0.1$.

Figure 3.5 include the results of the simulation after 5.8 days. Comments to the different subplots:

1. The cell fraction does not seem to be significantly affected by the presence of fibroblasts. The plot in Figure 3.6 (left) also confirms this, with the final cell

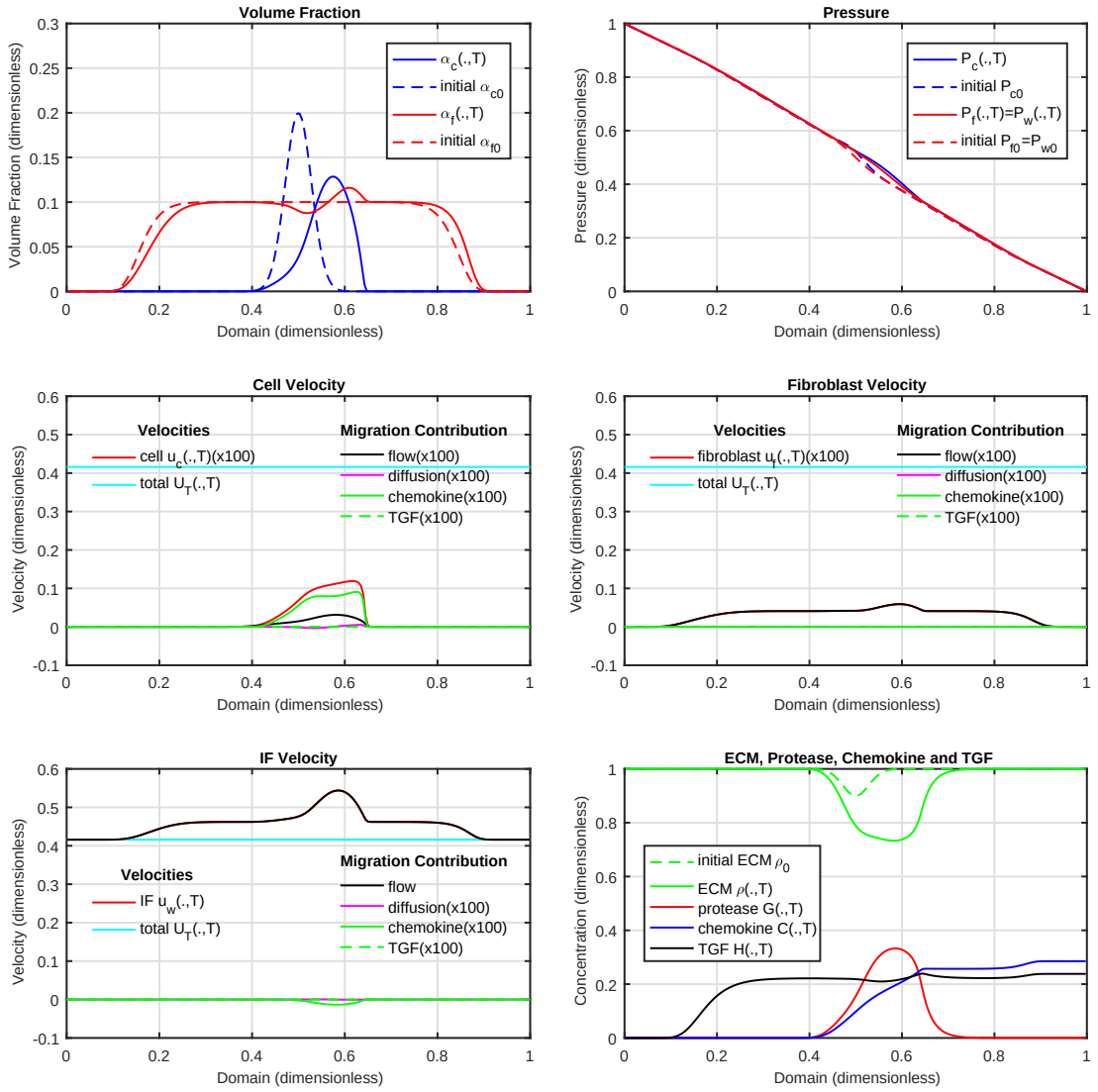

Figure 3.5: Solution of case with fibroblasts at T=5.8 days. Blocking of TGF. The red and black curves in subplot 4 and 5 are overlapping.

volume fraction being almost the same in the two cases. The cell volume center is still $\bar{x}_c = 0.56$, just as before. Note that the fibroblast fraction have shifted in the downstream direction, so the issue is not related to the mobility of the fibroblasts. This suggests that we have to include some other mechanism(s) such as chemotaxis against TGF, viscous coupling or ECM remodeling, in order to get the behavior observed in experiments. This is also consistent with pt. 2 in Subsection 1.2.4. The fibroblast fraction is however clearly affected by the presence of cells, see Figure 3.6 (right). As noted before, an increasing concentration of cells has a positive effect

on the velocity of the fibroblasts. We observe accumulation of fibroblasts in regions of decreasing fibroblast velocity, and depletion in areas of increasing velocity.

2. The pressure profiles has shifted to the right in accordance with the volume fractions.

3. The cells move in the downstream direction, mainly due to chemotaxis.

4. Since $\hat{f}_f$ is a function of α_c (in addition to α_f), we observe a bump in the velocity profile according to the volume fraction of cells. This effect would not be observed in a two-phase simulation where cells are absent, since the (fibroblast) velocity is then only a function of the fibroblast fraction.

5. Note that the phase velocity of IF experiences a (small) negative contribution from chemokine.

6. The concentration of protease correlates well with the cell volume fraction. The concentration of chemokine starts increasing at x=0.4, consistent with the profile of protease (which is necessary for the production of chemokine). It then increases until x=0.58, which is the location of the maximum level of protease. Somewhat unexpectedly, the concentration profile steepens after this, but this is due to increased density of ECM, in addition to reduced velocity of IF. The profile is then constant, but around x=0.85 it increases, again due to lowered IF velocity, and stabilizes at a new, elevated level. The TGF profile correlates with the fibroblast volume fraction, and also experience an increase at x=0.85 due to reduced IF velocity.

3.4 Base Case

We are now going to include the TGF-dependent chemotaxis of the fibroblasts. We then need to specify parameters belonging to the new potential function, $\Lambda_H(H)$, see Table 3.3. We are going to define the data given in Tables 3.1-3.3 as the base case. See also Table 3.4 for a summary of the data in *dimensionless* form. The initial data in Figure 3.7 are the same as in Figure 3.3, since initially we do not have any gradients in TGF.

Table 3.3: Parameters describing TGF-dependent chemotaxis of fibroblasts.

Parameter	Description	Value	Unit
Potential function, TGF			
ξ_2	parameter characterizing Λ_H	$8 \cdot 10^4$	m^3/kg
Λ_{H0}	parameter characterizing Λ_H	0	Pa
Λ_{H1}	parameter characterizing Λ_H	$2.5 \cdot 10^4$	Pa

The results after 5.8 days are shown in Figure 3.8, and the main findings are summarized in the following list:

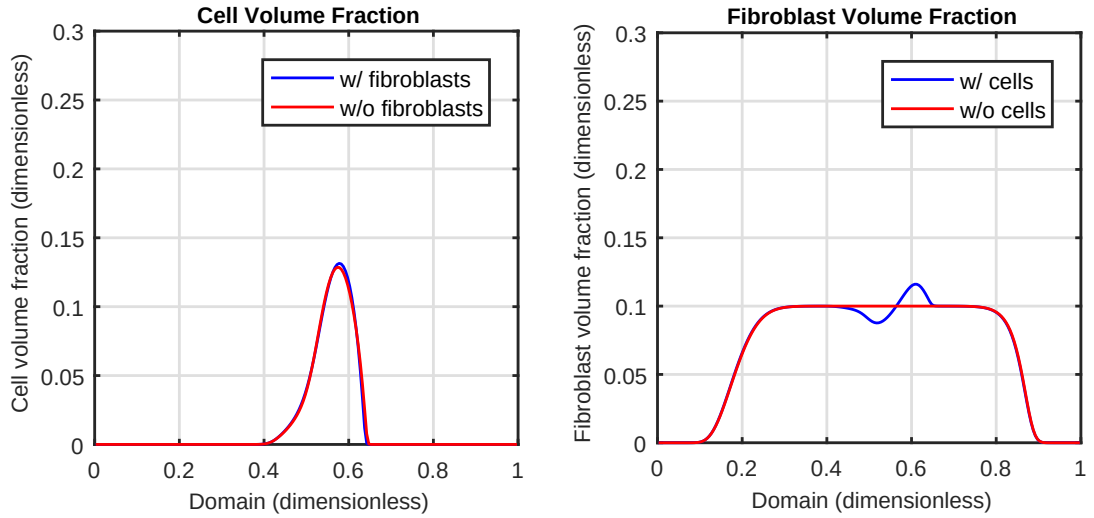

Figure 3.6: *Left:* Comparison of cell volume fraction after T=5.8 days, for cases with and without fibroblasts. The fibroblasts does not seem to have any impact on the migration of tumor cells in the absence of special effects such as viscous coupling and/or ECM remodeling. *Right:* Comparison of fibroblast volume fraction after T=5.8 days, for cases with and without cells. The cells do seem to have an impact on the migration of fibroblasts.

Table 3.4: Dimensionless parameters for base case.

Parameter	Value	Parameter	Value	Parameter	Value
L	1	T	50	ΔP	1
D_G	$8 \cdot 10^{-4}$	D_C	$7 \cdot 10^{-6}$	D_H	$8 \cdot 10^{-4}$
λ_{21}	10	λ_{22}	12.5	λ_{23}	0
λ_{24}	12.5	ρ_M	1	λ_{31}	25
λ_{32}	$2 \cdot 10^2$	λ_{33}	$2 \cdot 10^2$	ν_G	1
G_M	0.5	λ_{41}	32	λ_{42}	1.44
λ_{43}	32	λ_{44}	0.1	ν_C	0.2
C_M	0.3	λ_{51}	0	λ_{52}	$1.7 \cdot 10^2$
λ_{53}	$2 \cdot 10^2$	ν_H	0.2	H_M	0.5
I_w	2	I_c/I_w	10^3	I_f/I_w	$5 \cdot 10^2$
r_c	0.6	r_f	0.6	r_w	0
ξ_1	8	Λ_{C0}	0	Λ_{C1}	2.5
ξ_2	8	Λ_{H0}	0	Λ_{H1}	2.5
γ	0.1	δ	0.01		

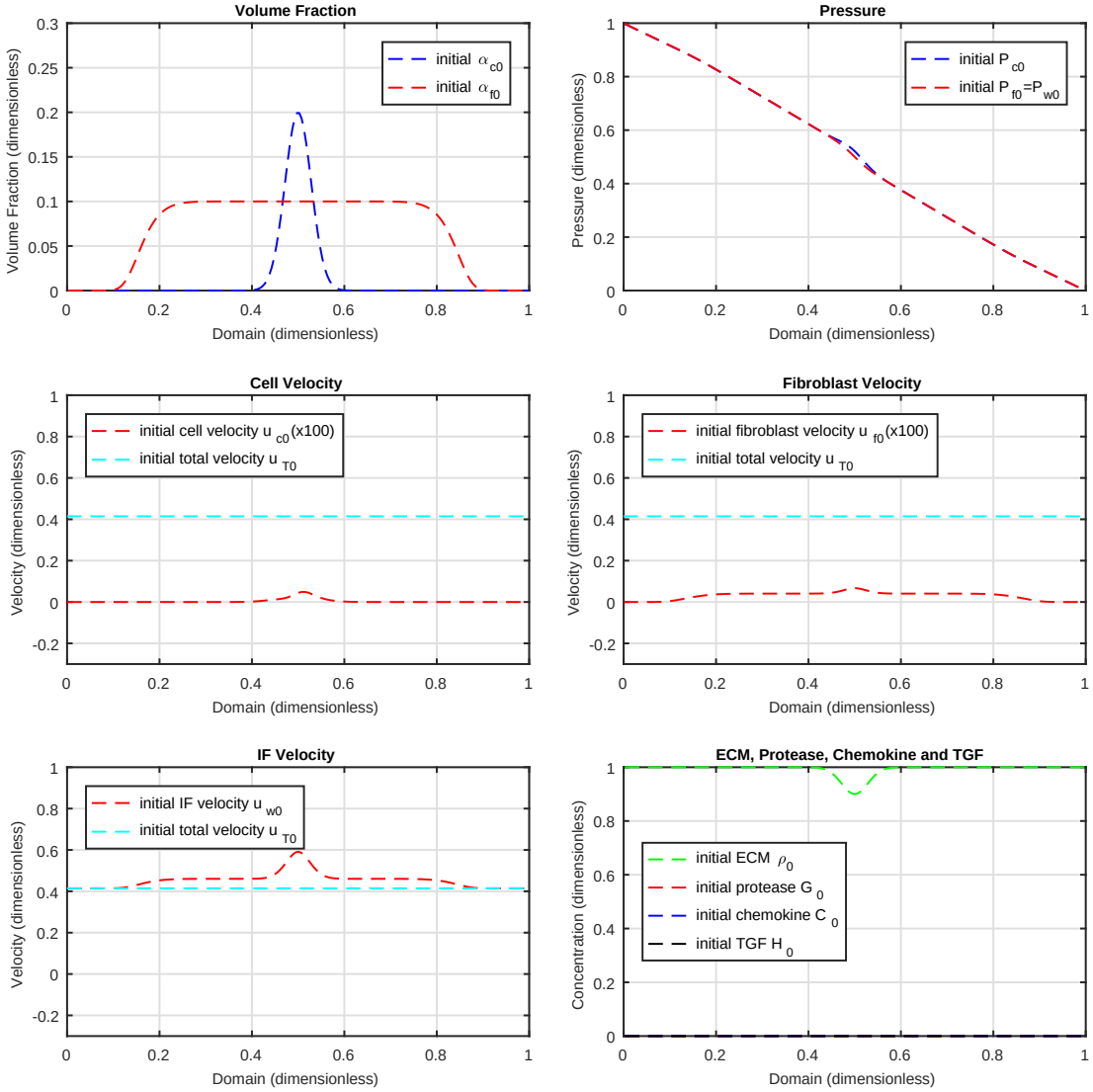

Figure 3.7: Initial solution of case with fibroblasts and TGF (base case) at T=0.

1. The cell fraction has still not changed very much compared to the other cases. The cell volume center is still at $\bar{x}_c = 0.56$, but there is less spreading. A comparison of the cell volume fraction in each case after T=5.8 days is shown in Figure 3.9. The fibroblasts are more volatile, with more peaks and valleys in the saturation profile. The final fibroblast volume fraction for different cases are shown in Figure 3.10. Note that the combined effects of both tumor cells and TGF is equal to the effect of TGF plus the effect of the tumor cells (magnified).

2. The pressure response at x=0.3 is due to the fibroblast peak forming at the back.

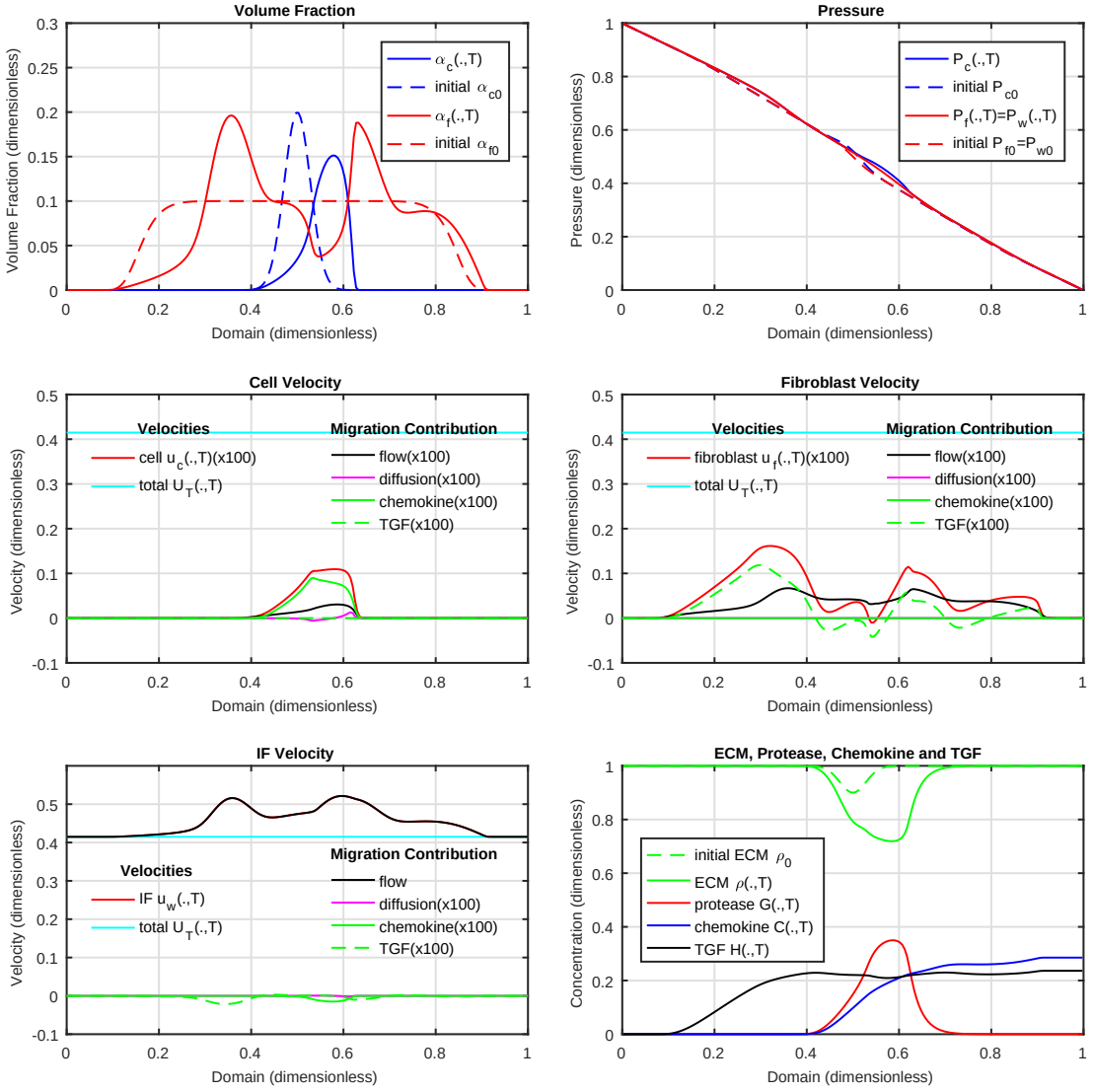

Figure 3.8: Solution of case with fibroblasts and TGF (base case) at T=5.8 days. The red and black curves in figure 5 are overlapping.

3. The total cell velocity still remains the same, around 0.001 μm/s.

4. The peak forming on the left side is due to TGF-dependent chemotaxis, see Figure 3.10, subplot 3 and 4. The concentration of TGF explains the peak forming; H(.,T) is concave at first, meaning that its derivative increases and therefore also the TGF-dependent velocity-component, thus depleting material (fibroblasts) in this region. Further downstream the concentration profile becomes concave in shape and consequently there is accumulation of material. The second valley-peak pair is also evident in the case where TGF is neglected, see Figure 3.10, subplot

2, and is due to the presence of cells in this area, as explained before. In this case this "S" shape have become somewhat magnified. The explanation for this is that since TGF is produced by the fibroblasts themselves, the concentration of TGF will be higher in areas where there is a high fraction of fibroblasts, and lower where fibroblasts are low/lacking. Therefore, also the concentration of the chemoattractant will have this S-shape, but skewed in the downstream direction as a result of flow, see 3.10, subplot 4. In the "valley part" of $\alpha_f(.,T)$, $H(.,T)$ is convex, causing further depletion. The concentration of TGF is however concave to the right of the point where $\alpha_f(.,T)$ peaks, causing accumulation.

5. IF is pushed to the left by both chemokine- and TGF-dependent chemotaxis.

6. Results can be explained on the basis of subplot 1 and 5.

Note that Figure 3.10 confirms the experimental observation that not only do fibroblasts influence the invasion of tumor cells, but the tumor cells also affect the migration of fibroblasts (under flow conditions), see Figure 1.2B (right).

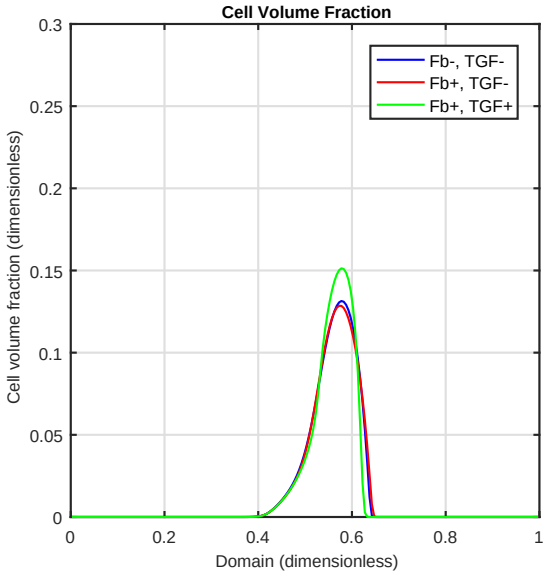

Figure 3.9: Comparison of cell volume fraction after T=5.8 days, for cases with and without fibroblasts and TGF. Fb=fibroblast, TGF=transforming growth factor.

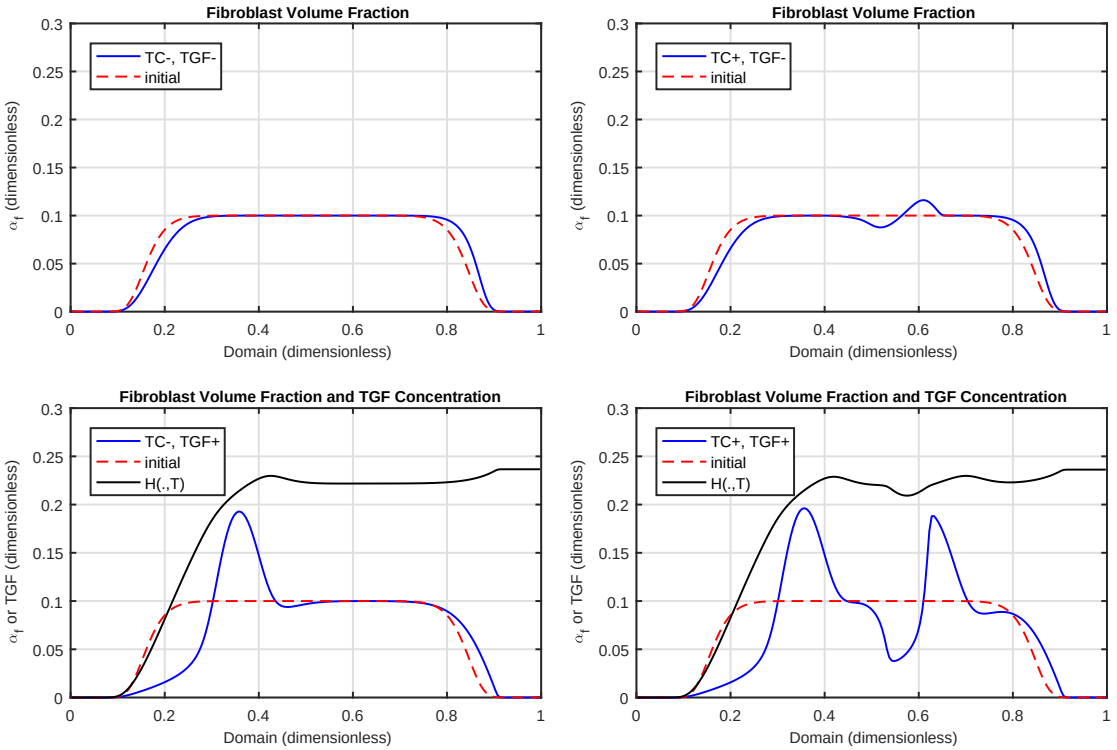

Figure 3.10: Comparison of fibroblast volume fraction after T=5.8 days, for cases with and without cells and TGF. TC=tumor cells, TGF=transforming growth factor.

Chapter 4

Testing Model Hypotheses

4.1 Viscous Coupling Between Cells and Fibroblasts

4.1.1 Strong Interaction

Previously we have worked with cases where $I_{cf} = 0$, but let us now consider the other extreme by letting $I_{cf} \to \infty$ (resembling the mechanism proposed by Labernadie et al. (2017)). The parameters necessary for modeling the fluid-fluid interaction as given by Equation $(2.41)_4$ are given in Table 4.1, while all the other parameters remain the same as in the base case, Section 3.4. As mentioned previously, increased viscous

Table 4.1: Viscous coupling-specific parameters

Parameter	Description	Value	Unit
Interaction parameters			
I_{cf}/I_w	parameter controlling viscous coupling	$5 \cdot 10^2$	-
r_{cf}	parameter controlling viscous coupling	0.5	-
r_{fc}	parameter controlling viscous coupling	0.5	-

coupling manifests itself in the $\hat{h}_2$-function, which may become negative for large values of I_{cf}. See Figure 4.1 for a plot of $\hat{h}_2$ as a function of α_c, keeping the fibroblast fraction constant at $\alpha_f = 0.2$. Note that for $I_{cf} = \infty$ (green curve), $\hat{h}_2 = 0$ for $\alpha_c = 0$ and $\alpha_c = 0.8$. Remember that $\hat{h}_2$ describes the counter-current interaction between the cells and fibroblasts, and since there can be no interaction between the two phases when the cells are missing ($\alpha_c = 0$), it becomes zero. For a cell volume fraction of 0.8; however, both cells and fibroblasts are present, but IF is missing. Since $\hat{h}_2$ describes a *counter-current* effect, it means that cells and fibroblasts have to flow in different directions (when IF is present, fibroblasts and cell might flow in the *same* direction, provided the IF moves in the opposite direction). Consequently, any value of $\hat{h}_2$ different from zero means they flow in opposite directions, but since they are completely locked to each other; that will be impossible.

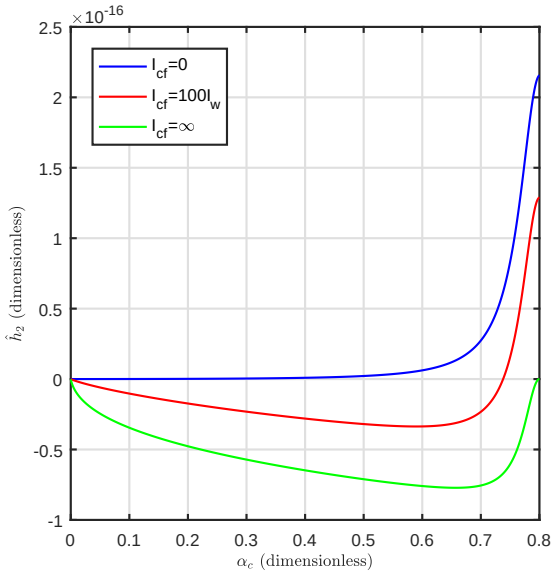

Figure 4.1: Plot of $\hat{h}_2$ as a function of α_c for $\alpha_f = 0.1$, using different values of I_{cf}.

The initial data are the same as before, and presented in Figure 4.2 together with the initial solution of phase pressures and velocities. Brief explanation of the initial results:

1. Initial volume fractions identical to the base case.

2. The initial pressure profiles are also the same as before, when comparing with Figure 3.7. The IF pressure is calculated from the equation $-(\hat{\lambda}_c \Delta P_x)_x = (\hat{\lambda}_T P_{wx})_x$, and since α_{c0} and α_{f0} are the same as in the base case, then also $\Delta P(x)$ will be the same as before. However, $\hat{\lambda}_c$ and $\hat{\lambda}_T$ have changed since they feel the effect of I_{cf}. Consequently, the pressure profiles do change, but the resolution of the graphs prevent us from noticing it. The mobility functions are plotted in Figure 4.3 as a function of α_c when $\alpha_f = 0.1$. Note that at $\alpha_c = 0.57$ both the cell and fibroblast mobilities are unaffected by I_{cf}. In a situation where flow-generated stress is the only prevailing flow mechanism, we find from Equation (2.47) that $u_c = u_f$. Consequently, there can be no momentum transfer between the two phases no matter how strong the interaction coefficient is. For lower cell volume fractions (when the cell phase is the slower fluid), the cells experience an increased mobility given the opportunity to mechanically couple to and tag along with the fibroblasts. Consequently, the fibroblast mobility is reduced. For higher cell volume fractions the opposite is true, because the faster flowing fluid is the cell phase.

3. First, comparing subplot 3 and 4, we see that the cell and fibroblast velocities are the same, since the two phases are coupled together, flowing as a single phase. Second, the combined velocity is somewhere between the "free" cell and fibroblast velocities without any coupling, see Figure 4.4. Note that there is an overall

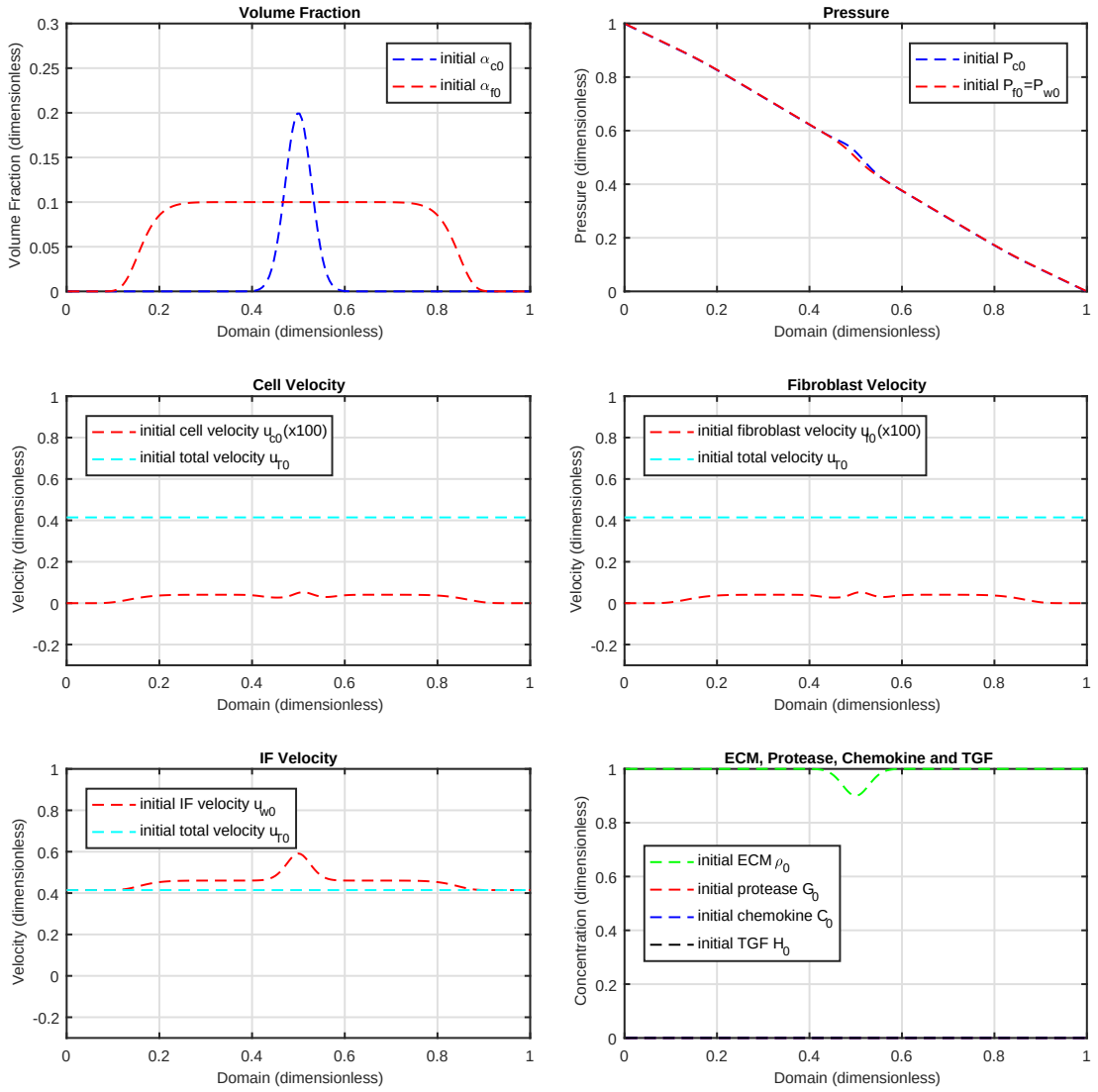

Figure 4.2: Initial solution of case with infinite viscous coupling.

increase in the cell velocity, and especially at the right and left "foot" where the velocity was close to zero before.

The final solution after 5.8 days is shown in Figure 4.5. Explanation of results:

1. One of the main differences seen in this plot compared to the base case is the increased mobility of the lower cell fractions, whereas the net effect of cell migration is similar to before, with $\bar{x}_c = 0.55$. See also Figure 4.6 for a comparison of the cell volume fraction for cases with and without mechanical coupling. Left figure at T=5.8 days, and the right after twice that time. Also here we observe that

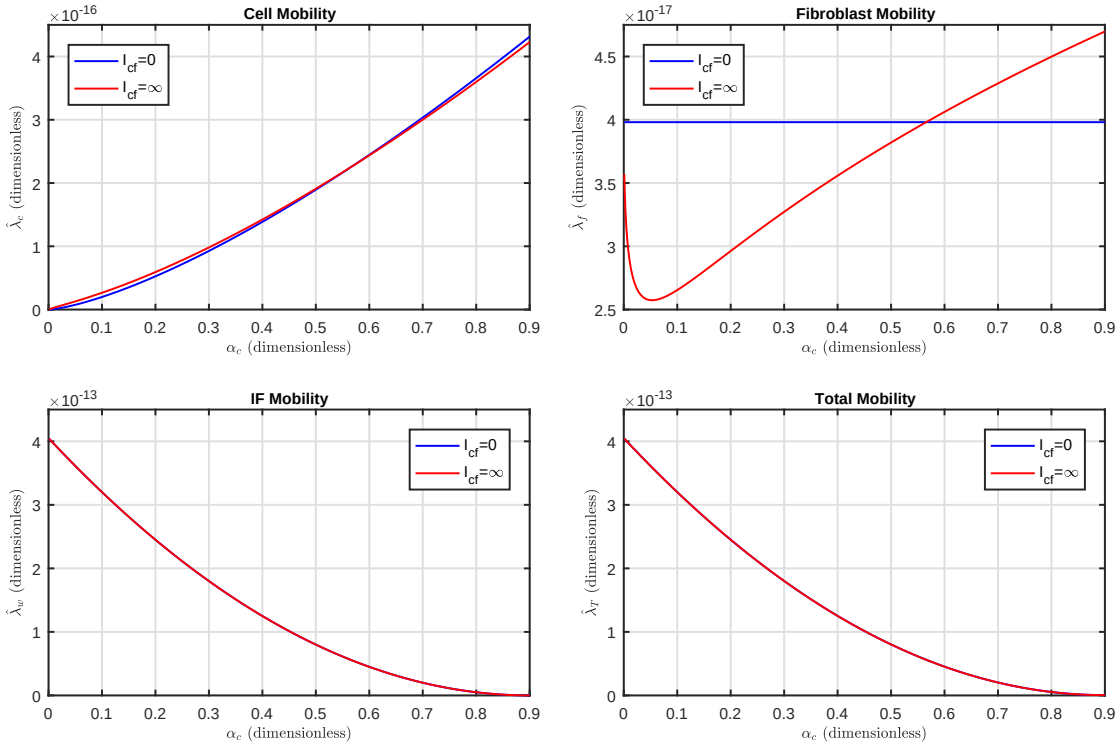

Figure 4.3: Phase and total mobilities plotted as a function of the cell volume fraction α_c, keeping the fibroblast fraction constant at $\alpha_f = 0.1$. The two curves are overlapping in the lower plots.

the lower volume fractions have progressed further in the downstream direction in the presence of fluid-fluid interactions. Another thing to note is that there is some asymmetry in the α_c profile in the presence of fluid-fluid interactions after 11.6 days, i.e. the black curve in the right figure. This is because the fibroblasts coming from behind catches up with the cell aggregate and the cell flux $\alpha_c u_c$ will be influenced by TGF. Previously, the velocity component due to TGF was outside the domain where cells are present, and therefore had no effect on the cell flux (but it did have an effect on the velocity).

2. The pressure profiles are similar to what we have seen before.

3. Again, notice that the velocity of cells and fibroblasts are equal. Neglecting diffusion, the velocity can be decomposed into three terms; flow, which is fairly uniform, chemokine, having a maximum located in the center of the domain (zero elsewhere), and TGF, having its maximum in the left part of the domain (approximately zero elsewhere). This explains the shape of the total cell velocity; TGF+flow (left), chemokine+flow (middle) and flow only (right), giving rise to the three "bumps" seen. Essentially only the middle peak drives the invasion of

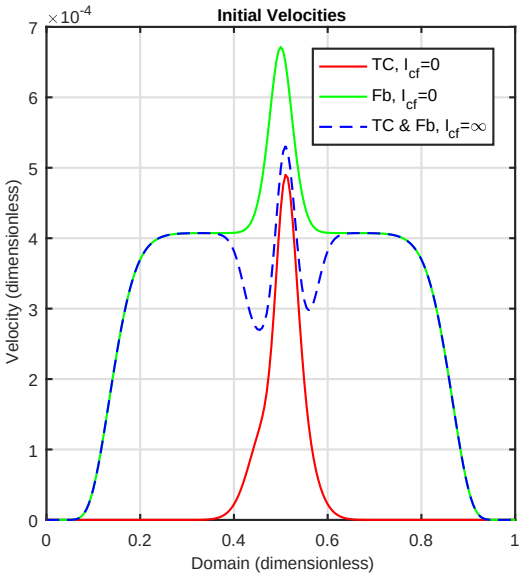

Figure 4.4: Initial velocity of "free" cells and fibroblasts when $I_{cf} = 0$, and combined velocity when $I_{cf} = \infty$. Fb=fibroblast, TC=tumor cell.

tumor cells, because here we have $\alpha_c > 0$, thus creating a flux $\alpha_c u_c$ transporting tumor cells downstream. What has happened in Figure 4.7 is that the left peak have catched up with the middle, and therefore it has started to influence the flux of cells. Consequently, the volume fraction is affected through Equation $(2.44)_1$.

4. See point 3.

5. Notice that the two positive peaks due to chemokine and TGF acting on the (combined) cell/fibroblast phase, becomes negative because of the counter-current nature of these forces.

6. The concentration profiles are quite similar to the base case.

4.1.2 Increased Fibroblast Mobility

While fluid-fluid interactions had some effect on the invasion of tumor cells in the previous case, it does not explain the prominent cell aggressiveness seen in Figure 1.2B (left) when fibroblasts are present. One possible explanation is related to the mobility of the fibroblasts being too low. We want to test this possibility by reducing the fibroblast-ECM interaction described through the term I_f. Since the velocity of the fibroblasts will increase, the potential for momentum transfer to the cells should improve.

Using the same parameters as in the previous case, but setting $I_f = 100$, we get the initial data in Figure 4.8. There are no significant differences compared to Subsection 4.1.1, but there are a few comments to be made:

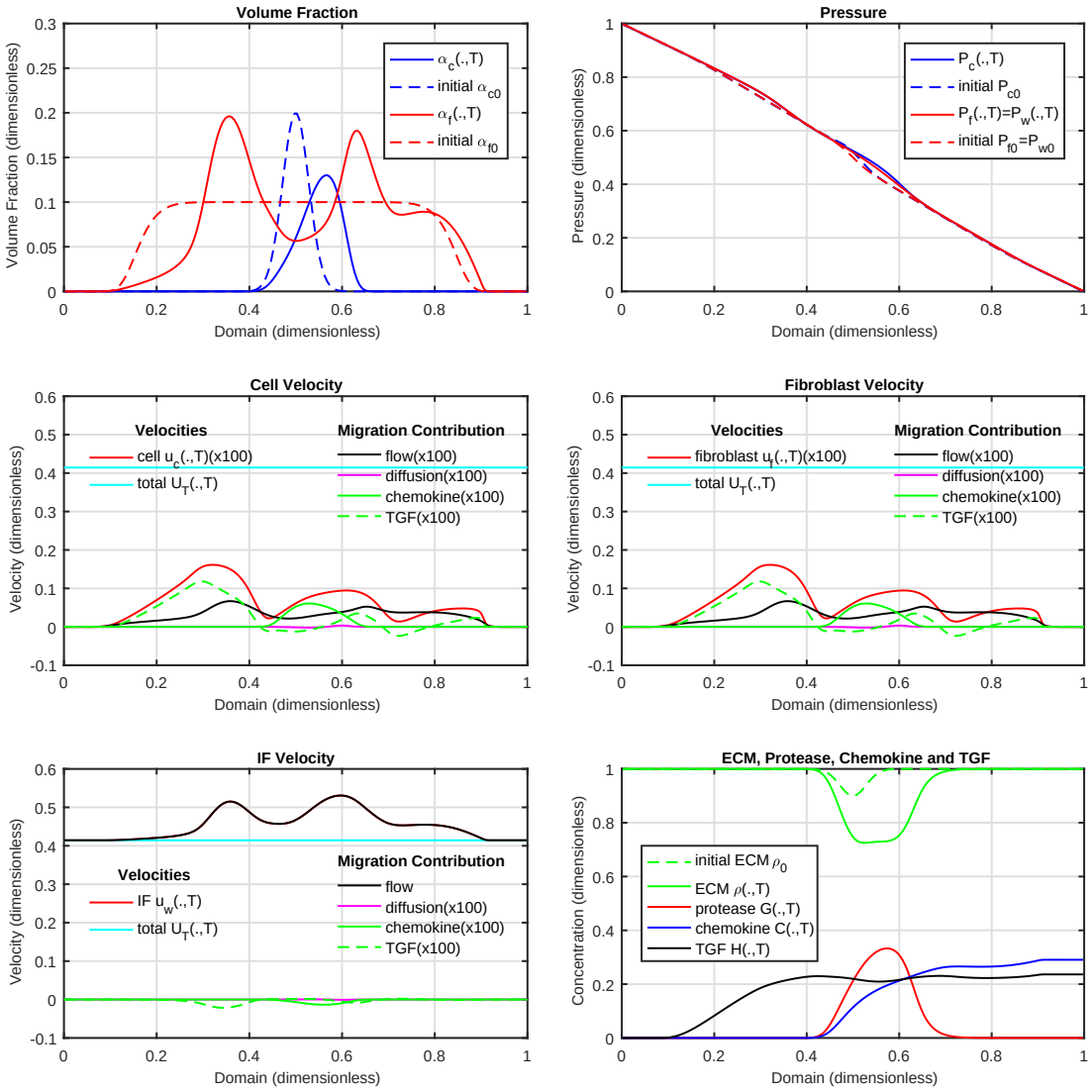

Figure 4.5: Final solution of case with infinite viscous coupling. T=5.8 days.

1. Same initial fractions as in Figure 4.2.
2. Identical to Figure 4.2.
3. Not surprisingly the velocity of the cell/fibroblast phase has increased quite a lot, compared with Figure 4.2. Note the reduced velocity in the center where cells are present. The cells, resisting flow by sticking to the ECM, is acting as an anchor. The same effect is of course seen for the fibroblast velocity in subplot 4 (since $I_{cf} = \infty$).

The final solution after 5.8 days are shown in Figure 4.9. Characteristics of the solution:

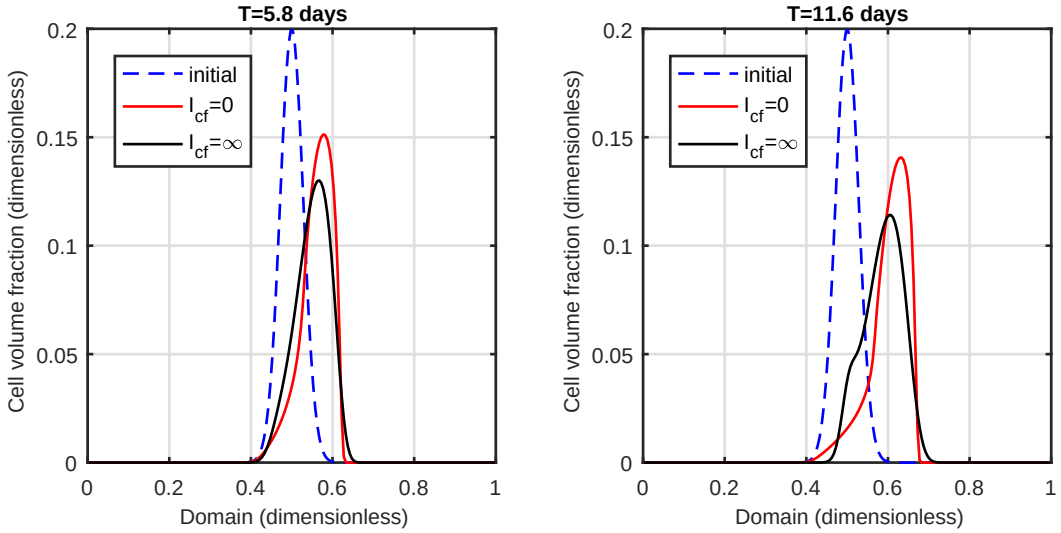

Figure 4.6: Cell volume fraction with and without fluid-fluid interactions. T=5.8 days (left) and T=11.6 days (right).

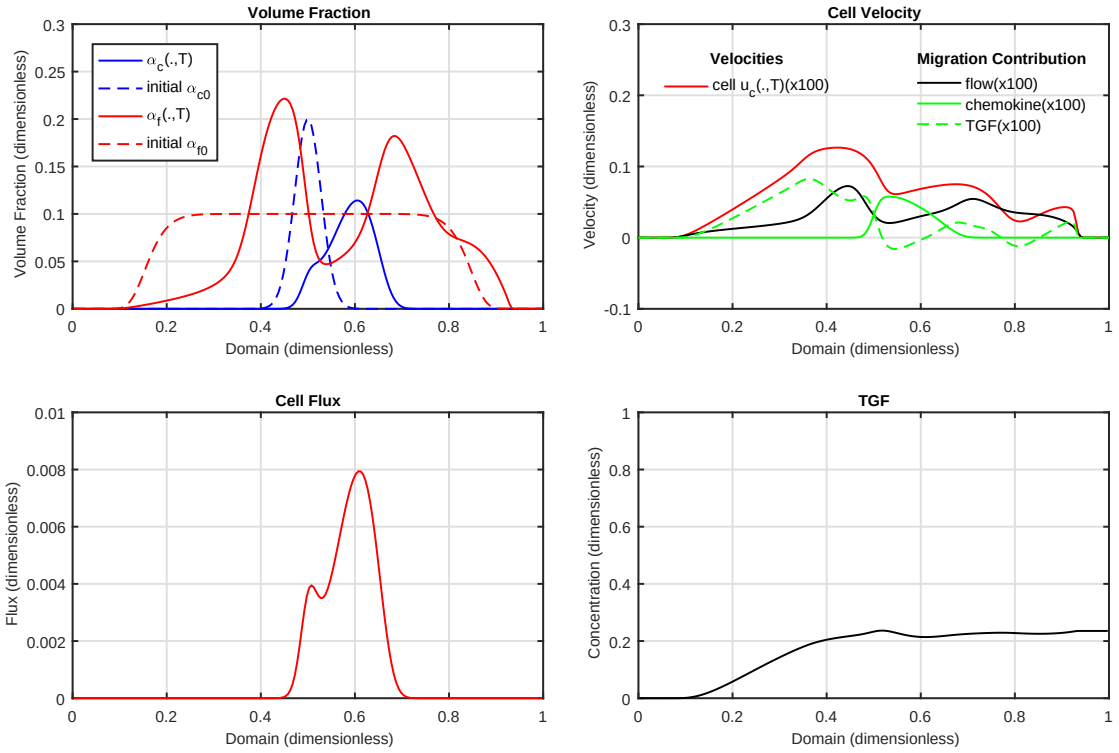

Figure 4.7: Final solution of case with infinite viscous coupling. T=11.6 days.

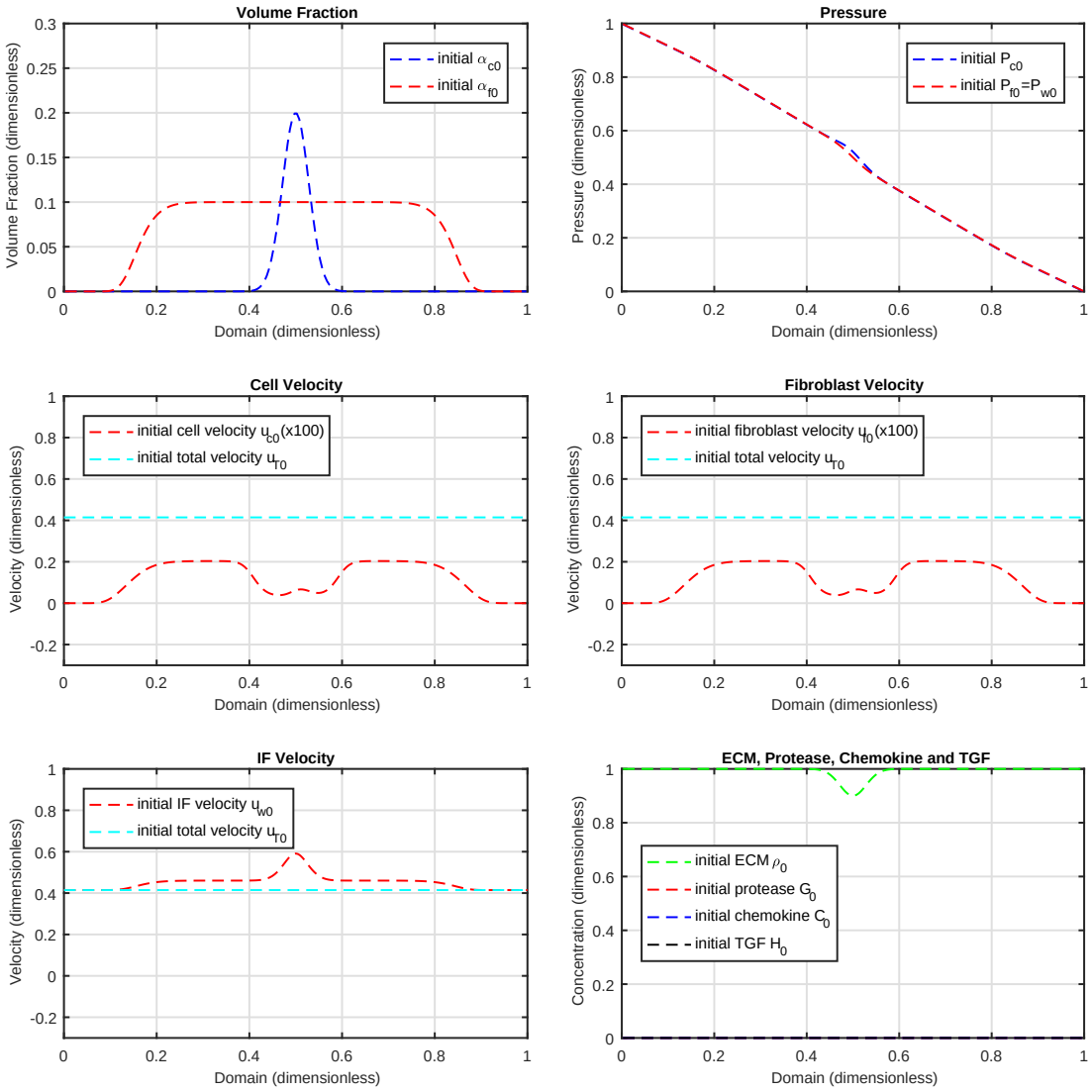

Figure 4.8: Initial solution of case with infinite viscous coupling and increased fibroblast mobility.

1. The fibroblast volume fraction is similar to what is seen in Subplot 1 of Figure 4.5, the main difference being that the fibroblasts have migrated further downstream due to decreased I_f, and as a consequence the peak that had previously starting to form at the back have catched up with the second peak, and they are now starting to interact and combine. The most important thing to notice is the cell fraction; $\alpha_c(., T)$ shows an almost uniform movement of cells for all volume fractions, with $\bar{x}_c = 0.61$, a considerable increase compared to the previous case(s). Pay particular attention to the lower fractions, which are much more mobile than they normally

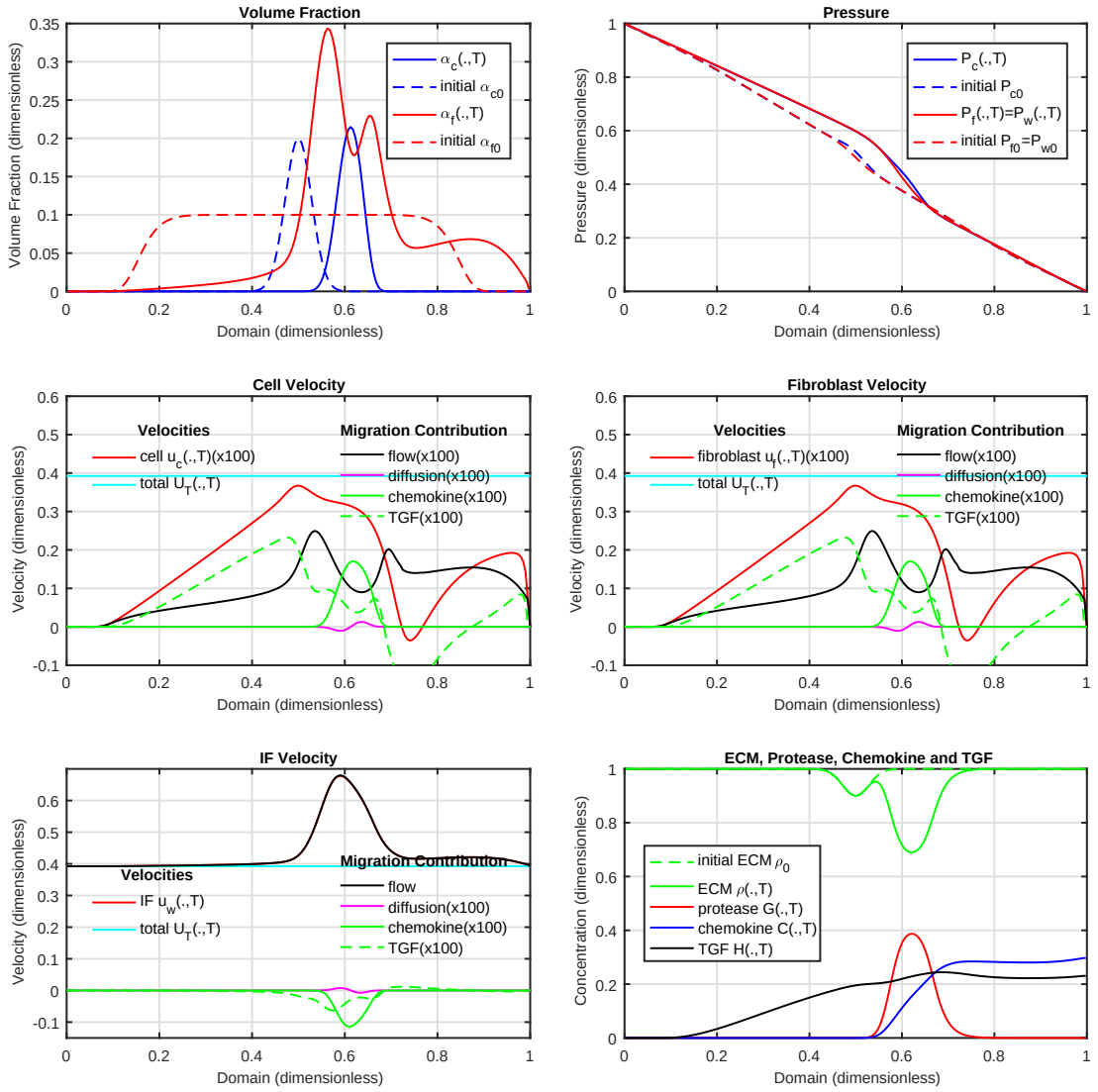

Figure 4.9: Final solution of case with infinite viscous coupling and increased fibroblast mobility. T=5.8 days.

would be. This can be explained by taking a look at the cell fractional flow curve, plotted in Figure 4.10. Usually, the flow contribution will be zero when $\alpha_c = 0$, due to $\frac{\partial \hat{f}_c}{\partial \alpha_c}(0, \alpha_f)$ being zero. Looking at the red curve ($I_{cf} = \infty$) in Figure 4.10, we can clearly see that the slope is greater than zero, and this is driving the small volume fractions.

2. The pressure profiles clearly illustrate how the cell clusters have advanced in the downstream direction.

3. The left and center velocity peaks mentioned in conjunction with Figure 4.5 have now merged into one, dominated by TGF+chemokine+flow.

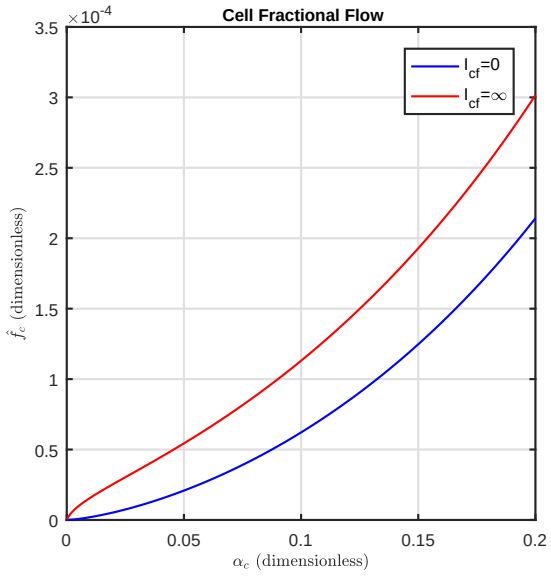

Figure 4.10: Fractional flow of cells with and without viscous coupling, when the fibroblasts have increased mobility compared to the base case. Notice the non-zero slope at $\alpha_c = 0$ for $I_{cf} = \infty$.

Summing up, taking a look at the cell fraction in the two-phase case, Figure 3.9 (blue curve), it's clear that the left end at $x = 0.4$ is stationary. Including the fibroblasts (without TGF-dependent chemotaxis) (red curve), did not have any effect, nor did the inclusion of TGF (green curve). Including viscous coupling had some effect, although not that clear after 5.8 days, ref. Figure 4.6 (left). After 11.6 days however, some sharpening of the cell fraction is seen at the left side, Figure 4.6 (right). This is due to the high concentration of fibroblasts approaching from the left, which is kind of sweeping up the cells and carrying them downstream. This becomes very clear in the current case, with $\alpha_c(., T)$ showing an almost uniform movement of cells for all volume fractions.

Note that even if the cell migration seem to be kind of uniform in the present 1-D case, that might not apply in a 2-D or 3-D setting. The simulation done here could represent maybe one cross-section (a two-dimensional "strip") in a two-dimensional simulation, such that even if the translation is uniform in each cross-section, the net effect in 2-D might not be. Further investigations in two and three dimensions could be suggested for future work.

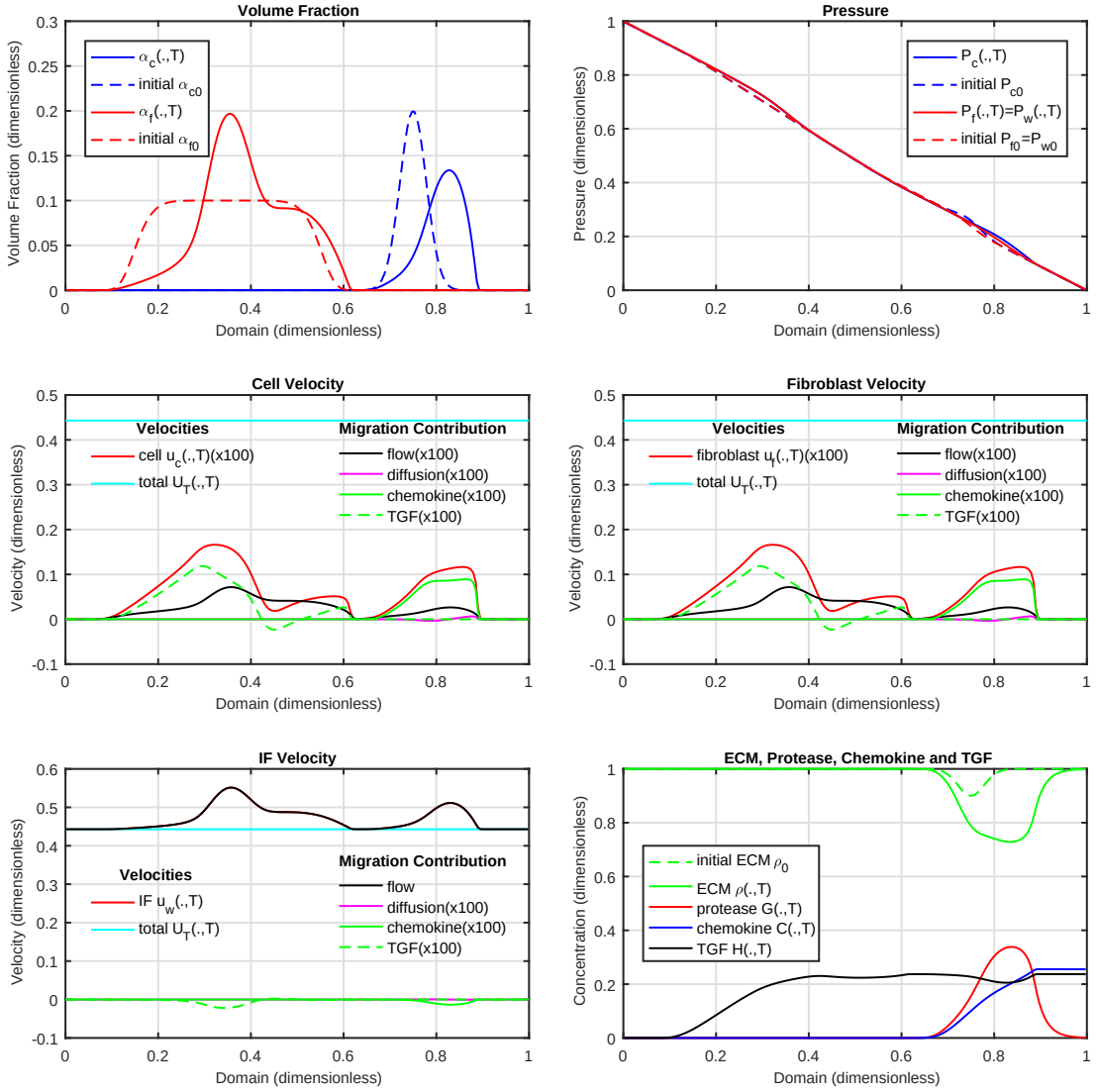

Figure 4.11: Final solution of case with fibroblasts cultured upstream. T=5.8 days.

4.2 Fibroblasts Cultured Upstream

Re-running the case described in Section 4.1.1 (infinite viscous coupling), but with different initial conditions given by

$$\alpha_{c0}(x) = 0.2e^{-[25(x-0.75)]^2}, \qquad \alpha_f(x,0) = 0.1e^{-3\cdot 10^5\cdot(x-0.35)^8},$$

produced the results in Figure 4.11. The initial data are chosen such to achieve upstream-cultured fibroblasts (with respect to the cells). Note that the right "foot" of the fibroblast aggregate have a hard time moving downstream, due to low volume fractions keeping

the flow contribution down, and the IF being saturated with TGF (preventing gradients and chemotaxis). Thus the fibroblasts are not able to reach the downstream-positioned cells.

Comparing the cell volume fraction in this three-phase case (including TGF-dependent chemotaxis and viscous coupling) with the corresponding results from the two-phase simulation in Section 3.2, we see that the difference is none/negligible, Figure 4.12. Thus we conclude that fibroblasts cultured upstream does not have any effect on the invasion of tumor cells, in accordance with Figure 1.2B (left). This is also a result of tumor cells not responding to TGF, and therefore supports this assumption.

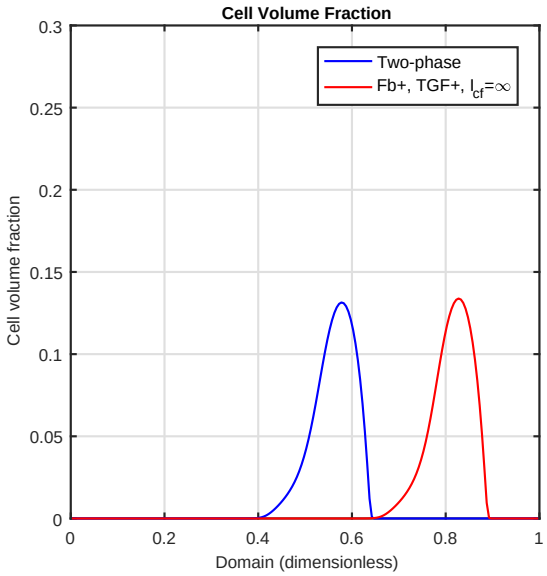

Figure 4.12: Comparison of final cell volume fraction in two-phase case and case with fibroblasts cultured upstream. T=5.8 days.

4.3 ECM Remodeling

We are now going to test the other hypothesis mentioned in Subsection 1.2.6, namely that flow- and fibroblast-enhanced tumor cell invasion is a result of indirect interactions between the two cell types through remodeling of the ECM. The fibroblasts are more mobile, flowing ahead of the cells and priming the matrix by pulling the collagen fibers of the ECM, thus increasing the mediums permeability to tumor cells.

We are going to model this dynamic permeability behavior through the term $\hat{k}_c$. The simplest model would be one that determines $\hat{k}_c$ as a function of the fibroblast volume fraction α_f alone, for instance in the following way

$$\hat{k}_c = 1 - A\left(1 - e^{-B\alpha_f}\right). \tag{4.1}$$

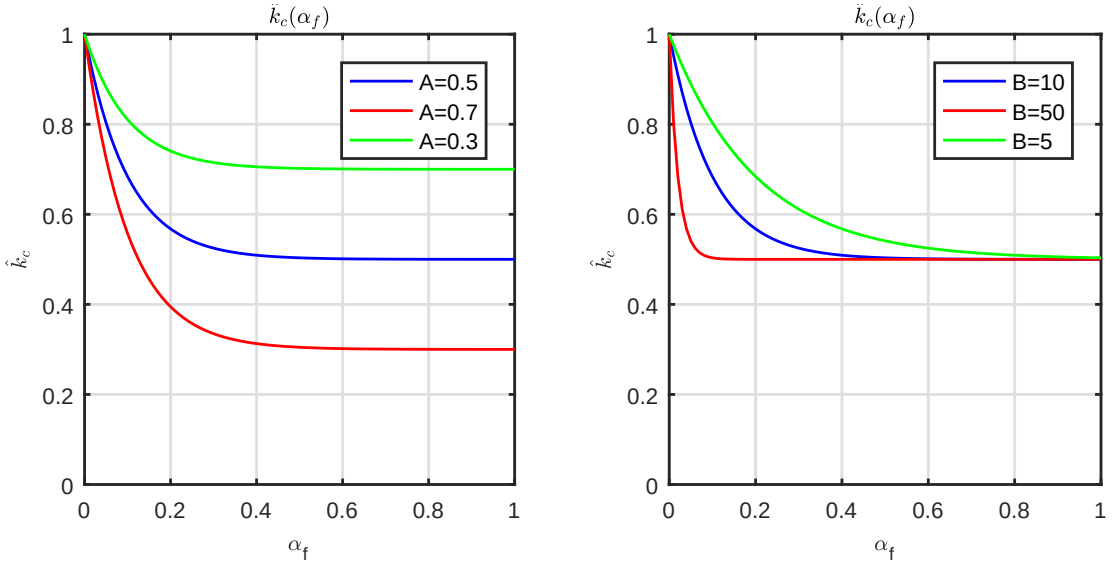

Figure 4.13: Plot of $\hat{k}_c$ against the fibroblast volume fraction α_f. In the *left* plot we use different values of A (with B=10), and in the *right* plot we use values of B ranging from 5 to 50 (keeping A=0.5).

We should expect $\hat{k}_c$ to be a function of other variables as well, at least the velocity; when the fibroblasts flow in a certain direction, the collagen fibers of the ECM preferentially align themselves parallel to the direction of flow, increasing the permeability in that direction. At the same time we would expect it to *decrease* in the direction perpendicular to flow. Still, we are going to make this simplifying assumption (which might not be that unrealistic given we're in a 1-D setting).

The motivation for choosing the functional form given in (4.1) is due to Figure 1.2D; note that $\hat{k}_c$ represent resistance to flow, and therefore the conductivity is proportional to $1/\hat{k}_c$, now taking the same form as the figure. A plot of (4.1) using different values of the parameters A and B, are shown in Figure 4.13.

The final solution after 5.8 days are shown in Figure 4.14. The results are summarized in the following points:

- The cell fraction is less uniform compared to the viscous-coupling-case. Note that the left "foot" is stagnant, while the larger volume fractions, including the right foot, have a significant distance covered. The total migration is the largest for all cases simulated, with $\bar{x}_c = 0.65$. We can conclude that this is an efficient way for cells to invade the surrounding tissue.

- The pressure profiles clearly demonstrate that there has been significant movement in the downstream direction.

- First, note that the cell and fibroblast velocities are no longer identical. The velocity profile actually looks similar to the base case, dropping to zero where cells

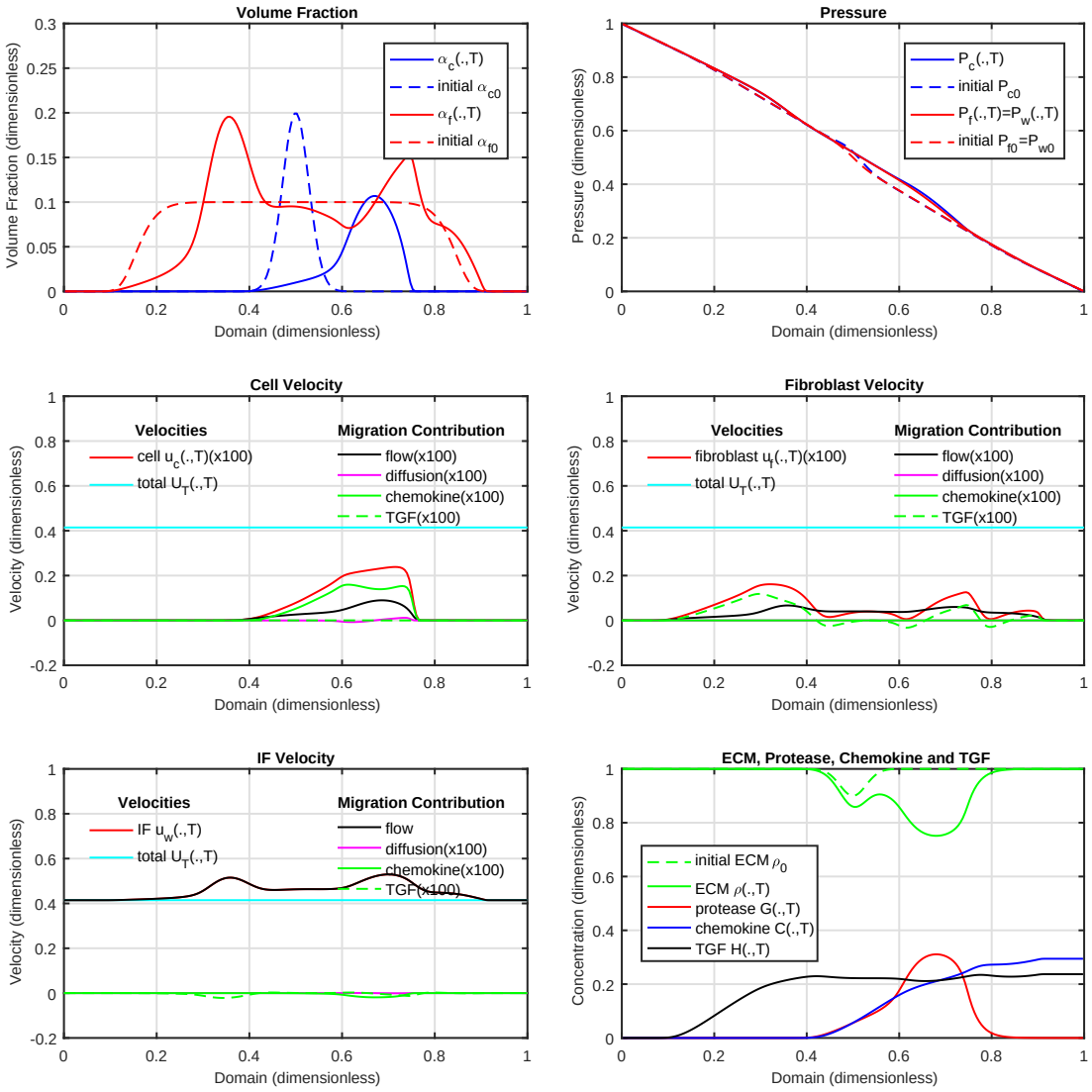

Figure 4.14: Final solution of case with ECM remodeling. T=5.8 days. A=0.7, B=50.

are lacking.

Chapter 5

Conclusion

It has been demonstrated that both viscous coupling and ECM remodeling (or even a combination of the two) might explain fibroblast-enhanced tumor cell invasion. A significant difference between the two is that the former has the ability to mobilize the small volume fractions on the left end of the initial cell aggregate, and causing a more or less uniform movement cells (at least in a 1-D setting), whereas ECM remodeling significantly increases the movement of the larger fractions, while the left end of the initial aggregate remains stagnant.

It is hard to say which one seems more realistic based on the experimental results given by Shieh et al. (2011), and we may conclude that either (or both) seem reasonable.

5.1 Concluding Remarks

The following list is a summary of the results obtained throughout this thesis:

- Fibroblasts without any special effects such as ECM remodeling and/or viscous coupling did not affect the tumor cell invasion at all.
- Tumor cells had a significant impact on the migration of fibroblasts, consistent with experimental results.
- When fibroblasts were given the ability to either remodel the ECM or mechanically couple to the cells, tumor cell invasion experienced a significant increase (in the presence of flow). This is consistent with experimental results.
- Viscous coupling tend to increase the velocity of all cell volume fractions, even the lower ones when $\alpha_c \approx 0$. It manifests itself in the flow functions mainly by increasing the derivative of the cell fractional flow function at zero volume fraction, and by causing a negative $\hat{h}_2$ coupling between the cells and fibroblasts. The effect depends on the mobility of the fibroblasts, such that increased fibroblast mobility also increased the fibroblast-enhanced tumor cell invasion.
- ECM remodeling accelerated mainly the larger cell volume fractions.

- Fibroblasts cultured upstream does not have an effect on the migration of cancer cells, even if TGF-dependent chemotaxis, ECM remodeling and/or viscous coupling are included, consistent with experimental results.

5.2 Suggestions for Future Work

Some suggestions for future work are listed below:

- Perform numerical simulations in 2-D and 3-D, especially to see if the effect of mechanical coupling retains the uniform behavior shown in the 1-D case.
- Production of TGF could be modeled in a manner similar to the production/release of chemokine, by letting fibroblasts secrete their own protease that can react with the ECM to release surface-bound, latent TGF, into the IF.
- Include source terms S_c and S_f to account for proliferation and apoptosis of cancer cells and fibroblasts.
- Investigate effects of including mechanisms such as haptotaxis or compressibility. The phases could possibly be modeled as slightly compressible fluids.
- Experiment with alternative models for ECM remodeling. In this thesis only a simple expression were used, but more sophisticated models involving e.g. the velocities could have been used. Possibly even more relevant in a 2-D or 3-D setting.
- Perform numerical investigations on simplified versions of the model, thus reducing the number of parameters and mechanisms at play, which somewhat clutters the picture when becoming too many. An example could be two-phase flow of fibroblasts and IF, particularly if there exist experimental data to compare against.

References

Ahamed, J., Burg, N., Yoshinaga, K., Janczak, C. A., Rifkin, D. B., & Coller, B. S. (2008). In vitro and in vivo evidence for shear-induced activation of latent transforming growth factor-β1. *Blood*, *112*(9), 3650–3660.

Allen III, M. B. (1985). Numerical modelling of multiphase flow in porous media. *Advances in Water Resources*, *8*, 162–187.

Allen III, M. B., Behie, G. A., & Trangenstein, J. A. (1988). *Multiphase flow in porous media: mechanics, mathematics , and numerics* (Vol. 34). Springer-Verlag New York Inc., New York, NY.

Ambrosi, D., & Preziosi, L. (2002). On the closure of mass balance models for tumor growth. *Mathematical Models and Methods in Applied Sciences*, *12*(05), 737–754.

Ambrosi, D., & Preziosi, L. (2009). Cell adhesion mechanisms and stress relaxation in the mechanics of tumours. *Biomechanics and modeling in mechanobiology*, *8*(5), 397.

Bear, J. (1988). *Dynamics of fluids in porous media*. Dover Publications.

Breward, C. J., Byrne, H. M., & Lewis, C. E. (2003). A multiphase model describing vascular tumour growth. *Bulletin of mathematical biology*, *65*(4), 609–640.

Breward, C. J. W., Byrne, H. M., & Lewis, C. E. (2002). The role of cell-cell interactions in a two-phase model for avascular tumour growth. *Journal of Mathematical Biology*, *45*(2), 125–152.

Buckley, S. E., & Leverett, M. C. (1941). Mechanism of fluid displacement in sands. *Transactions of the AIME*, *146*(01), 107–116.

Byrne, H. M., & Owen, M. R. (2004). A new interpretation of the Keller-Segel model based on multiphase modelling. *Journal of mathematical biology*, *49*(6), 604–626.

Ertekin, T., Abou-Kassem, J. H., & King, G. R. (2001). *Basic applied reservoir simulation*.

Evje, S. (2017). An integrative multiphase model for cancer cell migration under influence of physical cues from the microenvironment. *Chemical Engineering Science*, *165*, 240–259.

Fleury, M. E., Boardman, K. C., & Swartz, M. A. (2006). Autologous morphogen gradients by subtle interstitial flow and matrix interactions. *Biophysical journal*, *91*(1), 113–121.

Green, D. W., & Willhite, G. P. (1998). *Enhanced oil recovery* (Vol. 6). Henry L. Doherty Memorial Fund of AIME, Society of Petroleum Engineers Richardson, TX.

Helmlinger, G., Netti, P. A., Lichtenbeld, H. C., Melder, R. J., & Jain, R. K. (1997). Solid stress inhibits the growth of multicellular tumor spheroids. *Nature biotechnology*, *15*(8), 778.

Hilfer, R. (1998). Macroscopic equations of motion for two-phase flow in porous media. *Physical Review E*, *58*(2), 2090.

Jain, R. K., Martin, J. D., & Stylianopoulos, T. (2014). The role of mechanical forces in tumor growth and therapy. *Annual review of biomedical engineering*, *16*, 321–346.

Jambhekar, V. A. (2011). Forchheimer porous-media flow models-numerical investigation and comparison with experimental data. *Published Master Thesis. Stuttgart: Universität Stuttgart-Institut für Wasserund Umweltsystemmodellierung*.

Kim, A., Lakshman, N., & Petroll, W. M. (2006). Quantitative assessment of local collagen matrix remodeling in 3-D culture: the role of Rho kinase. *Experimental cell research*, *312*(18), 3683–3692.

Kirby, B. J. (2010). *Micro-and nanoscale fluid mechanics: transport in microfluidic devices*. Cambridge university press.

Labernadie, A., Kato, T., Brugués, A., Serra-Picamal, X., Derzsi, S., Arwert, E., ... Trepat, X. (2017). A mechanically active heterotypic E-cadherin/N-cadherin adhesion enables fibroblasts to drive cancer cell invasion. *Nature cell biology*, *19*(3), 224.

Lemon, G., King, J. R., Byrne, H. M., Jensen, O. E., & Shakesheff, K. M. (2006). Mathematical modelling of engineered tissue growth using a multiphase porous flow mixture theory. *Journal of mathematical biology*, *52*(5), 571–594.

LeVeque, R. J. (2002). *Finite volume methods for hyperbolic problems* (Vol. 31). Cambridge university press.

Leverett, M. (1940). Capillary behavior in porous solids. *Transactions of the AIME*, *142*(01), 152–169.

Muskat, M., Wyckoff, R., Botset, H., & Meres, M. (1937). Flow of gas-liquid mixtures through sands. *Transactions of the AIME*, *123*(01), 69–96.

Qiao, Y., Andersen, P., Evje, S., & Standnes, D. (2018). A mixture theory approach to model co-and counter-current two-phase flow in porous media accounting for viscous coupling. *Advances in Water Resources*, *112*, 170–188.

Shieh, A. C., Rozansky, H. A., Hinz, B., & Swartz, M. A. (2011). Tumor cell invasion is promoted by interstitial flow-induced matrix priming by stromal fibroblasts. *Cancer research*, *71*(3), 790–800.

Shieh, A. C., & Swartz, M. A. (2011). Regulation of tumor invasion by interstitial fluid flow. *Physical biology*, *8*(1), 015012.

Shields, J. D., Fleury, M. E., Yong, C., Tomei, A. A., Randolph, G. J., & Swartz, M. A. (2007). Autologous chemotaxis as a mechanism of tumor cell homing to lymphatics via interstitial flow and autocrine CCR7 signaling. *Cancer cell*, *11*(6), 526–538.

Swartz, M. A., & Fleury, M. E. (2007). Interstitial flow and its effects in soft tissues. *Annu. Rev. Biomed. Eng.*, *9*, 229–256.

Teng, H., & Zhao, T. (2000). An extension of Darcy's law to non-Stokes flow in porous media. *Chemical engineering science*, *55*(14), 2727–2735.

Waldeland, J.-O., & Evje, S. (2018). A multiphase model for exploring cancer cell migration driven by autologous chemotaxis (submitted for publication).

Wipff, P.-J., Rifkin, D. B., Meister, J.-J., & Hinz, B. (2007). Myofibroblast contraction activates latent tgf-β1 from the extracellular matrix. *The Journal of cell biology*, *179*(6), 1311–1323.

Zolotukhin, A. B., & Ursin, J.-R. (2000). *Introduction to petroleum reservoir engineering*. Norwegien Academic Press (HóyskoleForlaget).

Appendix A

Explicit Expressions for Phase Velocities

In this chapter we present more of the details involved in the calculation of the explicit phase velocities in Section 2.5.

A.1 Interstitial Velocities

In this section we show the calculations leading to the expressions (2.22)-(2.24) in subsection 2.5.1. We start out with the rewritten momentum balance equations given by (2.21)

$$\begin{aligned} \alpha_c \nabla \Lambda_C + \alpha_c \nabla(\Delta P_{cw}) + \alpha_c \nabla P_w &= -(\hat{\zeta}_c + \hat{\zeta}_{cf})\mathbf{u}_c + \hat{\zeta}_{cf}\mathbf{u}_f \\ \alpha_f \nabla \Lambda_H + \alpha_f \nabla P_w &= \hat{\zeta}_{cf}\mathbf{u}_c - (\hat{\zeta}_f + \hat{\zeta}_{cf})\mathbf{u}_f \\ \alpha_w \nabla P_w &= -\hat{\zeta}_w \mathbf{u}_w, \end{aligned} \tag{A.1}$$

and want to solve for $\mathbf{u}_c, \mathbf{u}_f$ and $\mathbf{u}_w$. The IF velocity is easily solved for, and using $(\text{A.1})_3$ we find that

$$\mathbf{u}_w = -\frac{\alpha_w}{\hat{\zeta}_w} \nabla P_w. \tag{A.2}$$

It remains to solve the 2-by-2 linear system given by $(\text{A.1})_{1,2}$ for the unknows $\mathbf{u}_c$ and $\mathbf{u}_f$. Solving the first equation for the fibroblast velocity, we find that

$$\mathbf{u}_f = \frac{\alpha_c \nabla(\Lambda_C + \Delta P_{cw}) + \alpha_c \nabla P_w + (\hat{\zeta}_c + \hat{\zeta}_{cf})\mathbf{u}_c}{\hat{\zeta}_{cf}}, \tag{A.3}$$

and by inserting this expression into $(\text{A.1})_2$, we get

$$\alpha_f \nabla \Lambda_H + \alpha_f \nabla P_w = \hat{\zeta}_{cf}\mathbf{u}_c - \frac{\hat{\zeta}_f + \hat{\zeta}_{cf}}{\hat{\zeta}_{cf}} \left(\alpha_c \nabla(\Lambda_C + \Delta P_{cw}) + \alpha_c \nabla P_w + (\hat{\zeta}_c + \hat{\zeta}_{cf})\mathbf{u}_c \right).$$

Rearranging the last expression, we find the cell velocity

$$\begin{aligned}\mathbf{u}_c\frac{\hat{\zeta}_f\hat{\zeta}_c+\hat{\zeta}_f\hat{\zeta}_{cf}+\hat{\zeta}_c\hat{\zeta}_{cf}}{\hat{\zeta}_{cf}} =& -\frac{\alpha_c(\hat{\zeta}_f+\hat{\zeta}_{cf})+\alpha_f\hat{\zeta}_{cf}}{\hat{\zeta}_{cf}}\nabla P_w\\ &-\frac{\alpha_c(\hat{\zeta}_f+\hat{\zeta}_{cf})}{\hat{\zeta}_{cf}}\nabla\left(\Delta P_{cw}+\Lambda_C\right)-\alpha_f\nabla\Lambda_H,\end{aligned}$$

or

$$\begin{aligned}\mathbf{u}_c =& -\frac{\alpha_f\hat{\zeta}_{cf}+\alpha_c(\hat{\zeta}_{cf}+\hat{\zeta}_f)}{\hat{\zeta}_c\hat{\zeta}_f+\hat{\zeta}_{cf}(\hat{\zeta}_c+\hat{\zeta}_f)}\nabla P_w\\ &-\frac{\alpha_c(\hat{\zeta}_{cf}+\hat{\zeta}_f)}{\hat{\zeta}_c\hat{\zeta}_f+\hat{\zeta}_{cf}(\hat{\zeta}_c+\hat{\zeta}_f)}\nabla\left(\Delta P_{cw}+\Lambda_C\right)\\ &-\frac{\alpha_f\hat{\zeta}_{cf}}{\hat{\zeta}_c\hat{\zeta}_f+\hat{\zeta}_{cf}(\hat{\zeta}_c+\hat{\zeta}_f)}\nabla\Lambda_H,\end{aligned}\tag{A.4}$$

which is the expression given in (2.22). Inserting this expression into (A.3), we find the fibroblast velocity

$$\begin{aligned}\mathbf{u}_f\hat{\zeta}_{cf} =&\alpha_c\nabla(\Lambda_C+\Delta P_{cw})+\alpha_c\nabla P_w+(\hat{\zeta}_c+\hat{\zeta}_{cf})\mathbf{u}_c\\ =&\alpha_c\nabla(\Lambda_C+\Delta P_{cw})+\alpha_c\nabla P_w\\ &-(\hat{\zeta}_c+\hat{\zeta}_{cf})\frac{\alpha_f\hat{\zeta}_{cf}+\alpha_c(\hat{\zeta}_{cf}+\hat{\zeta}_f)}{\hat{\zeta}_c\hat{\zeta}_f+\hat{\zeta}_{cf}(\hat{\zeta}_c+\hat{\zeta}_f)}\nabla P_w\\ &-(\hat{\zeta}_c+\hat{\zeta}_{cf})\frac{\alpha_c(\hat{\zeta}_{cf}+\hat{\zeta}_f)}{\hat{\zeta}_c\hat{\zeta}_f+\hat{\zeta}_{cf}(\hat{\zeta}_c+\hat{\zeta}_f)}\nabla\left(\Delta P_{cw}+\Lambda_C\right)\\ &-(\hat{\zeta}_c+\hat{\zeta}_{cf})\frac{\alpha_f\hat{\zeta}_{cf}}{\hat{\zeta}_c\hat{\zeta}_f+\hat{\zeta}_{cf}(\hat{\zeta}_c+\hat{\zeta}_f)}\nabla\Lambda_H,\end{aligned}$$

which can be rearranged into

$$\begin{aligned}\mathbf{u}_f\hat{\zeta}_{cf} =& -\frac{\alpha_c\hat{\zeta}_{cf}^2+\alpha_f\hat{\zeta}_{cf}(\hat{\zeta}_c+\hat{\zeta}_{cf})}{\hat{\zeta}_c\hat{\zeta}_f+\hat{\zeta}_{cf}(\hat{\zeta}_c+\hat{\zeta}_f)}\nabla P_w\\ &-\frac{\alpha_c\hat{\zeta}_{cf}^2}{\hat{\zeta}_c\hat{\zeta}_f+\hat{\zeta}_{cf}(\hat{\zeta}_c+\hat{\zeta}_f)}\nabla(\Delta P_{cw}+\Lambda_C)\\ &-\frac{\alpha_f(\hat{\zeta}_c+\hat{\zeta}_{cf})\hat{\zeta}_{cf}}{\hat{\zeta}_c\hat{\zeta}_f+\hat{\zeta}_{cf}(\hat{\zeta}_c+\hat{\zeta}_f)}\nabla\Lambda_H,\end{aligned}$$

or

$$\begin{aligned}\mathbf{u}_f = &- \frac{\alpha_c\hat{\zeta}_{cf} + \alpha_f(\hat{\zeta}_c + \hat{\zeta}_{cf})}{\hat{\zeta}_c\hat{\zeta}_f + \hat{\zeta}_{cf}(\hat{\zeta}_c + \hat{\zeta}_f)}\nabla P_w \\ &- \frac{\alpha_c\hat{\zeta}_{cf}}{\hat{\zeta}_c\hat{\zeta}_f + \hat{\zeta}_{cf}(\hat{\zeta}_c + \hat{\zeta}_f)}\nabla(\Delta P_{cw} + \Lambda_C) \\ &- \frac{\alpha_f(\hat{\zeta}_c + \hat{\zeta}_{cf})}{\hat{\zeta}_c\hat{\zeta}_f + \hat{\zeta}_{cf}(\hat{\zeta}_c + \hat{\zeta}_f)}\nabla\Lambda_H.\end{aligned} \tag{A.5}$$

This is the same fibroblast velocity as given by (2.23) in Subsection 2.5.1.

A.2 Superficial Velocities

The superficial velocity are given as the product of the interstitial velocity and the volume fraction, i.e.

$$\begin{aligned}\mathbf{U}_c := \alpha_c\mathbf{u}_c = &- \frac{\alpha_c\alpha_f\hat{\zeta}_{cf} + \alpha_c^2(\hat{\zeta}_{cf} + \hat{\zeta}_f)}{\hat{\zeta}_c\hat{\zeta}_f + \hat{\zeta}_{cf}(\hat{\zeta}_c + \hat{\zeta}_f)}\nabla P_w \\ &- \frac{\alpha_c^2(\hat{\zeta}_{cf} + \hat{\zeta}_f)}{\hat{\zeta}_c\hat{\zeta}_f + \hat{\zeta}_{cf}(\hat{\zeta}_c + \hat{\zeta}_f)}\nabla\left(\Delta P_{cw} + \Lambda_C\right) \\ &- \frac{\alpha_c\alpha_f\hat{\zeta}_{cf}}{\hat{\zeta}_c\hat{\zeta}_f + \hat{\zeta}_{cf}(\hat{\zeta}_c + \hat{\zeta}_f)}\nabla\Lambda_H, \\ \mathbf{U}_f := \alpha_f\mathbf{u}_f = &- \frac{\alpha_c\alpha_f\hat{\zeta}_{cf} + \alpha_f^2(\hat{\zeta}_c + \hat{\zeta}_{cf})}{\hat{\zeta}_c\hat{\zeta}_f + \hat{\zeta}_{cf}(\hat{\zeta}_c + \hat{\zeta}_f)}\nabla P_w \\ &- \frac{\alpha_c\alpha_f\hat{\zeta}_{cf}}{\hat{\zeta}_c\hat{\zeta}_f + \hat{\zeta}_{cf}(\hat{\zeta}_c + \hat{\zeta}_f)}\nabla(\Delta P_{cw} + \Lambda_C) \\ &- \frac{\alpha_f^2(\hat{\zeta}_c + \hat{\zeta}_{cf})}{\hat{\zeta}_c\hat{\zeta}_f + \hat{\zeta}_{cf}(\hat{\zeta}_c + \hat{\zeta}_f)}\nabla\Lambda_H. \\ \mathbf{U}_w := \alpha_w\mathbf{u}_w = &- \frac{\alpha_w^2}{\hat{\zeta}_w}\nabla P_w,\end{aligned} \tag{A.6}$$

using the interstitial velocities calculated in the previous section. By defining the coefficients in front of ∇P_w as the phase *mobilities*, i.e.

$$\begin{aligned}\hat{\lambda}_c &= \frac{\alpha_c\alpha_f\hat{\zeta}_{cf} + \alpha_c^2(\hat{\zeta}_{cf} + \hat{\zeta}_f)}{\hat{\zeta}_c\hat{\zeta}_f + \hat{\zeta}_{cf}(\hat{\zeta}_c + \hat{\zeta}_f)} \\ \hat{\lambda}_f &= \frac{\alpha_c\alpha_f\hat{\zeta}_{cf} + \alpha_f^2(\hat{\zeta}_c + \hat{\zeta}_{cf})}{\hat{\zeta}_c\hat{\zeta}_f + \hat{\zeta}_{cf}(\hat{\zeta}_c + \hat{\zeta}_f)} \\ \hat{\lambda}_w &= \frac{\alpha_w^2}{\hat{\zeta}_w},\end{aligned} \tag{A.7}$$

we can write

$$\begin{aligned}\frac{\alpha_c^2(\hat{\zeta}_{cf}+\hat{\zeta}_f)}{\hat{\zeta}_c\hat{\zeta}_f+\hat{\zeta}_{cf}(\hat{\zeta}_c+\hat{\zeta}_f)} &= \frac{\alpha_c\alpha_f\hat{\zeta}_{cf}+\alpha_c^2(\hat{\zeta}_{cf}+\hat{\zeta}_f)-\alpha_c\alpha_f\hat{\zeta}_{cf}}{\hat{\zeta}_c\hat{\zeta}_f+\hat{\zeta}_{cf}(\hat{\zeta}_c+\hat{\zeta}_f)} = \hat{\lambda}_c - \frac{\alpha_c\alpha_f\hat{\zeta}_{cf}}{\hat{\zeta}_c\hat{\zeta}_f+\hat{\zeta}_{cf}(\hat{\zeta}_c+\hat{\zeta}_f)} \\ \frac{\alpha_f^2(\hat{\zeta}_c+\hat{\zeta}_{cf})}{\hat{\zeta}_c\hat{\zeta}_f+\hat{\zeta}_{cf}(\hat{\zeta}_c+\hat{\zeta}_f)} &= \frac{\alpha_c\alpha_f\hat{\zeta}_{cf}+\alpha_f^2(\hat{\zeta}_c+\hat{\zeta}_{cf})-\alpha_c\alpha_f\hat{\zeta}_{cf}}{\hat{\zeta}_c\hat{\zeta}_f+\hat{\zeta}_{cf}(\hat{\zeta}_c+\hat{\zeta}_f)} = \hat{\lambda}_f - \frac{\alpha_c\alpha_f\hat{\zeta}_{cf}}{\hat{\zeta}_c\hat{\zeta}_f+\hat{\zeta}_{cf}(\hat{\zeta}_c+\hat{\zeta}_f)}.\end{aligned} \tag{A.8}$$

Using (A.7) and (A.8), we can rewrite (A.6) as

$$\begin{aligned}\mathbf{U}_c =& -\hat{\lambda}_c\nabla P_w \\ &- \left(\hat{\lambda}_c - \frac{\alpha_c\alpha_f\hat{\zeta}_{cf}}{\hat{\zeta}_c\hat{\zeta}_f+\hat{\zeta}_{cf}(\hat{\zeta}_c+\hat{\zeta}_f)}\right)\nabla\left(\Delta P_{cw}+\Lambda_C\right) \\ &- \frac{\alpha_c\alpha_f\hat{\zeta}_{cf}}{\hat{\zeta}_c\hat{\zeta}_f+\hat{\zeta}_{cf}(\hat{\zeta}_c+\hat{\zeta}_f)}\nabla\Lambda_H \\ \mathbf{U}_f =& -\hat{\lambda}_f\nabla P_w \\ &- \frac{\alpha_c\alpha_f\hat{\zeta}_{cf}}{\hat{\zeta}_c\hat{\zeta}_f+\hat{\zeta}_{cf}(\hat{\zeta}_c+\hat{\zeta}_f)}\nabla(\Delta P_{cw}+\Lambda_C) \\ &- \left(\hat{\lambda}_f - \frac{\alpha_c\alpha_f\hat{\zeta}_{cf}}{\hat{\zeta}_c\hat{\zeta}_f+\hat{\zeta}_{cf}(\hat{\zeta}_c+\hat{\zeta}_f)}\right)\nabla\Lambda_H \\ \mathbf{U}_w =& -\hat{\lambda}_w\nabla P_w,\end{aligned} \tag{A.9}$$

which is the expression in (2.25). Next, we want to replace the IF pressure gradient, so that we can express the phase velocities using the total Darcy velocity instead.

A.3 Elimination of IF Pressure Gradient

The next step is to get rid of the gradient of the IF pressure, by substituting the expression (2.31)

$$\nabla P_w = -\frac{\mathbf{U}_T}{\hat{\lambda}_T} - \frac{\hat{\lambda}_c}{\hat{\lambda}_T}\nabla(\Delta P_{cw}+\Lambda_C) - \frac{\hat{\lambda}_f}{\hat{\lambda}_T}\nabla\Lambda_H,$$

into (A.9). Taking the cells as an example, we see that the Darcy velocity can be written as

$$\begin{aligned}
\mathbf{U}_c =& -\hat{\lambda}_c\left(-\frac{\mathbf{U}_T}{\hat{\lambda}_T}-\frac{\hat{\lambda}_c}{\hat{\lambda}_T}\nabla(\Delta P_{cw}+\Lambda_C)-\frac{\hat{\lambda}_f}{\hat{\lambda}_T}\nabla\Lambda_H\right)\\
&-\left(\hat{\lambda}_c-\frac{\alpha_c\alpha_f\hat{\zeta}_{cf}}{\hat{\zeta}_c\hat{\zeta}_f+\hat{\zeta}_{cf}(\hat{\zeta}_c+\hat{\zeta}_f)}\right)\nabla\left(\Delta P_{cw}+\Lambda_C\right)\\
&-\frac{\alpha_c\alpha_f\hat{\zeta}_{cf}}{\hat{\zeta}_c\hat{\zeta}_f+\hat{\zeta}_{cf}(\hat{\zeta}_c+\hat{\zeta}_f)}\nabla\Lambda_H\\
=&\frac{\hat{\lambda}_c}{\hat{\lambda}_T}\mathbf{U}_T+\frac{\hat{\lambda}_c^2}{\hat{\lambda}_T}\nabla(\Delta P_{cw}+\Lambda_C)+\frac{\hat{\lambda}_c\hat{\lambda}_f}{\hat{\lambda}_T}\nabla\Lambda_H\\
&-\left(\hat{\lambda}_c-\frac{\alpha_c\alpha_f\hat{\zeta}_{cf}}{\hat{\zeta}_c\hat{\zeta}_f+\hat{\zeta}_{cf}(\hat{\zeta}_c+\hat{\zeta}_f)}\right)\nabla\left(\Delta P_{cw}+\Lambda_C\right)\\
&-\frac{\alpha_c\alpha_f\hat{\zeta}_{cf}}{\hat{\zeta}_c\hat{\zeta}_f+\hat{\zeta}_{cf}(\hat{\zeta}_c+\hat{\zeta}_f)}\nabla\Lambda_H\\
=&\frac{\hat{\lambda}_c}{\hat{\lambda}_T}\mathbf{U}_T\\
&-\left(\hat{\lambda}_c-\frac{\hat{\lambda}_c^2}{\hat{\lambda}_T}-\frac{\alpha_c\alpha_f\hat{\zeta}_{cf}}{\hat{\zeta}_c\hat{\zeta}_f+\hat{\zeta}_{cf}(\hat{\zeta}_c+\hat{\zeta}_f)}\right)\nabla\left(\Delta P_{cw}+\Lambda_C\right)\\
&+\left(\frac{\hat{\lambda}_c\hat{\lambda}_f}{\hat{\lambda}_T}-\frac{\alpha_c\alpha_f\hat{\zeta}_{cf}}{\hat{\zeta}_c\hat{\zeta}_f+\hat{\zeta}_{cf}(\hat{\zeta}_c+\hat{\zeta}_f)}\right)\nabla\Lambda_H.
\end{aligned}\tag{A.10}$$

We now make use of the following relation

$$\hat{\lambda}_c-\frac{\hat{\lambda}_c^2}{\hat{\lambda}_T}=\frac{\hat{\lambda}_c\hat{\lambda}_T}{\hat{\lambda}_T}-\frac{\hat{\lambda}_c^2}{\hat{\lambda}_T}=\frac{\hat{\lambda}_c(\hat{\lambda}_c+\hat{\lambda}_f+\hat{\lambda}_w)-\hat{\lambda}_c^2}{\hat{\lambda}_T}=\frac{\hat{\lambda}_c\hat{\lambda}_f+\hat{\lambda}_c\hat{\lambda}_w}{\hat{\lambda}_T}=\frac{\hat{\lambda}_c\hat{\lambda}_f}{\hat{\lambda}_T}+\frac{\hat{\lambda}_c\hat{\lambda}_w}{\hat{\lambda}_T},$$

which allows us to rewrite (A.10) in the following way

$$\begin{aligned}
\mathbf{U}_c =&\frac{\hat{\lambda}_c}{\hat{\lambda}_T}\mathbf{U}_T\\
&-\left(\frac{\hat{\lambda}_c\hat{\lambda}_f}{\hat{\lambda}_T}+\frac{\hat{\lambda}_c\hat{\lambda}_w}{\hat{\lambda}_T}-\frac{\alpha_c\alpha_f\hat{\zeta}_{cf}}{\hat{\zeta}_c\hat{\zeta}_f+\hat{\zeta}_{cf}(\hat{\zeta}_c+\hat{\zeta}_f)}\right)\nabla\left(\Delta P_{cw}+\Lambda_C\right)\\
&+\left(\frac{\hat{\lambda}_c\hat{\lambda}_f}{\hat{\lambda}_T}-\frac{\alpha_c\alpha_f\hat{\zeta}_{cf}}{\hat{\zeta}_c\hat{\zeta}_f+\hat{\zeta}_{cf}(\hat{\zeta}_c+\hat{\zeta}_f)}\right)\nabla\Lambda_H\\
=&\hat{f}_c\mathbf{U}_T-(\hat{h}_1+\hat{h}_2)\nabla\left(\Delta P_{cw}+\Lambda_C\right)+\hat{h}_2\nabla\Lambda_H.
\end{aligned}\tag{A.11}$$

This relation is the same as $(2.32)_1$, just as we wanted. The expressions for the fibroblast and IF velocities are derived following a similar procedure.

Appendix B

Non-Dimensionalization

In this chapter we show how to obtain a dimensionless version of the model (2.20). We start by introducing the reference parameters given in Table B.1, denoted by an asterisk (*). The parameters are taken from Waldeland and Evje (2018), and represents the order-of-magnitude of the different variables, with e.g. L^* being equal to the length of the domain which will be used in the subsequent simulations, P^* having the same magnitude as the global pressure difference and u^* having the same order-of-magnitude as the total flow velocity.

Table B.1: Reference parameters for non-dimensionalization.

Parameter	Description	Value	Unit
L^*	length	10^{-2}	m
T^*	time	10^4	s
P^*	pressure	10^4	Pa
$u^* = L^*/T^*$	velocity	10^{-6}	m/s
$D^* = (L^*)^2/T^*$	diffusion	10^{-8}	m^2/s
ρ^*	ECM density	1	kg/m^3
G^*	protease	10^{-4}	kg/m^3
C^*	chemokine	10^{-4}	kg/m^3
H^*	TGF	10^{-4}	kg/m^3

Using these parameters we introduce the dimensionless space and time variables

$$\tilde{x} = \frac{x}{L^*}, \quad \tilde{x} \in [0,1], \qquad \tilde{t} = \frac{t}{T^*}, \quad \tilde{t} > 0,$$

where the tilde emphasizes that it is a dimensionless variable. In addition, we choose dimensionless variables related to the concentrations of the chemical components, the

phase pressures and velocities, in the following way

$$\tilde{\rho} = \frac{\rho}{\rho^*}, \qquad \tilde{G} = \frac{G}{G^*}, \qquad \tilde{C} = \frac{C}{C^*}, \qquad \tilde{H} = \frac{H}{H^*},$$
$$\tilde{D}_G = \frac{D_G}{D^*}, \qquad \tilde{D}_C = \frac{D_C}{D^*}, \qquad \tilde{D}_H = \frac{D_H}{D^*},$$
$$\tilde{P}_l = \frac{P_l}{P^*}, \qquad \tilde{\mathbf{u}}_l = \frac{\mathbf{u}_l}{u^*}, \qquad (l = c, f, w).$$

For production, decay and consumption of the chemical agents, we are going to use the following set of dimensionless expressions

$$\begin{aligned}
\rho: \quad & \tilde{\lambda}_{21} = \lambda_{21} T^* G^*, && \tilde{\lambda}_{22} = \lambda_{22} T^*, && \tilde{\lambda}_{23} = \lambda_{23} T^*, && \tilde{\lambda}_{24} = \lambda_{24} T^*, \\
G: \quad & \tilde{\lambda}_{31} = \lambda_{31} T^*, && \tilde{\lambda}_{32} = \frac{\lambda_{32} T^*}{G^*}, && \tilde{\lambda}_{33} = \frac{\lambda_{33} T^*}{G^*}, && \\
C: \quad & \tilde{\lambda}_{41} = \frac{\lambda_{41} T^* G^* \rho^*}{C^*}, && \tilde{\lambda}_{42} = \frac{\lambda_{42} T^* G^* \rho^*}{C^*}, && \tilde{\lambda}_{43} = \frac{\lambda_{43} T^* G^* \rho^*}{C^*}, && \tilde{\lambda}_{44} = \frac{\lambda_{44} T^*}{C^*}, \\
H: \quad & \tilde{\lambda}_{51} = \lambda_{51} T^*, && \tilde{\lambda}_{52} = \frac{\lambda_{52} T^*}{H^*}, && \tilde{\lambda}_{53} = \frac{\lambda_{53} T^*}{H^*}. &&
\end{aligned}$$

The potential and capillary pressure functions are having units of pressure, and therefore they can be made dimensionless by dividing by the reference pressure, P^*:

$$\begin{aligned}
\tilde{\Lambda}_C &= \frac{\Lambda_C}{P^*}, & \tilde{\Lambda}_{C0} &= \frac{\Lambda_{C0}}{P^*}, & \tilde{\Lambda}_{C1} &= \frac{\Lambda_{C1}}{P^*}, & \tilde{\xi}_1 &= \xi_1 C^*, \\
\tilde{\Lambda}_C &= \frac{\Lambda_C}{P^*}, & \tilde{\Lambda}_{H0} &= \frac{\Lambda_{H0}}{P^*}, & \tilde{\Lambda}_{H1} &= \frac{\Lambda_{H1}}{P^*}, & \tilde{\xi}_2 &= \xi_2 H^*, \\
\Delta\tilde{P}_{cw} &= \frac{\Delta P_{cw}}{P^*}, & \tilde{\gamma} &= \frac{\gamma}{P^*}. & & & &
\end{aligned}$$

Note that using $(2.48)_1$ the chemokine potential function can now be written (similar for TGF)

$$\begin{aligned}
\tilde{\Lambda}_C = \frac{\Lambda_C}{P^*} &= \tilde{\Lambda}_{C0} - \frac{\tilde{\Lambda}_{C1}}{1 + \exp[-\xi_1 (C - C_M)]} \\
&= \tilde{\Lambda}_{C0} - \frac{\tilde{\Lambda}_{C1}}{1 + \exp[-\tilde{\xi}_1 (\tilde{C} - \tilde{C}_M)]}.
\end{aligned}$$

Interaction coefficients

$$\tilde{\hat{\zeta}}_c = \hat{\zeta}_c \frac{D^*}{P^*}, \qquad \tilde{\hat{\zeta}}_f = \hat{\zeta}_f \frac{D^*}{P^*}, \qquad \tilde{\hat{\zeta}}_w = \hat{\zeta}_w \frac{D^*}{P^*}, \qquad \tilde{\hat{\zeta}}_{cf} = \hat{\zeta}_{cf} \frac{D^*}{P^*}.$$

Let's proceed with the details of rewriting the model (2.20) using the newly defined (dimensionless) parameters. We demonstrate with one mass and momentum equation,

and one of the transport-reaction equations. First, for the mass balance of cell, Equation $(2.20)_1$, we have (introducing the notation ∇_x and $\nabla_{\tilde{x}}$ to state explicitly which spatial variable we are referring to)

$$\begin{aligned}
\alpha_{ct} + \nabla_x \cdot (\alpha_c \mathbf{u}_c) &= S_c \\
\alpha_{c\tilde{t}} \frac{\partial \tilde{t}}{\partial t} + \nabla_x \cdot (\alpha_c \tilde{\mathbf{u}}_c u^*) &= S_c \\
\frac{1}{T^*} \alpha_{c\tilde{t}} + \frac{L^*}{T^*} \nabla_x \cdot (\alpha_c \tilde{\mathbf{u}}_c) &= S_c \\
\alpha_{c\tilde{t}} + L^* \frac{\partial \tilde{x}}{\partial x} \nabla_{\tilde{x}} \cdot (\alpha_c \tilde{\mathbf{u}}_c) &= S_c T^* \\
\alpha_{c\tilde{t}} + L^* \frac{1}{L^*} \nabla_{\tilde{x}} \cdot (\alpha_c \tilde{\mathbf{u}}_c) &= \tilde{S}_c \\
\alpha_{c\tilde{t}} + \nabla_{\tilde{x}} \cdot (\alpha_c \tilde{\mathbf{u}}_c) &= \tilde{S}_c,
\end{aligned}$$

where we have defined the dimensionless cell source term $\tilde{S}_c = S_c T^*$. The momentum balance of IF, Equation $(2.20)_6$, takes the form

$$\begin{aligned}
\alpha_w \nabla_x P_w &= -\hat{\zeta}_w \mathbf{u}_w \\
\alpha_w \frac{\partial \tilde{x}}{\partial x} \nabla_{\tilde{x}} \left(\tilde{P}_w P^* \right) &= -\tilde{\hat{\zeta}}_w \frac{P^*}{D^*} \tilde{\mathbf{u}}_w u^* \\
\alpha_w \frac{P^*}{L^*} \nabla_{\tilde{x}} \tilde{P}_w &= -\tilde{\hat{\zeta}}_w \frac{P^* T^*}{(L^*)^2} \tilde{\mathbf{u}}_w \frac{L^*}{T^*} \\
\alpha_w \nabla_{\tilde{x}} \tilde{P}_w &= -\tilde{\hat{\zeta}}_w \tilde{\mathbf{u}}_w.
\end{aligned}$$

For the chemical agents, say TGF, we get from $(2.20)_{10}$

$$\begin{aligned}
H_t + \nabla_x \cdot (\mathbf{u}_w H) =& \nabla_x \cdot (D_H \nabla_x H) - \lambda_{51} H + \alpha_f \left(\lambda_{52} - \lambda_{53} \left(\frac{H}{H_M} \right)^{v_H} \right) \\
(\tilde{H} H^*)_{\tilde{t}} \frac{\partial \tilde{t}}{\partial t} + \frac{\partial \tilde{x}}{\partial x} \nabla_{\tilde{x}} \cdot (\tilde{\mathbf{u}}_w u^* \tilde{H} H^*) =& \frac{\partial \tilde{x}}{\partial x} \nabla_{\tilde{x}} \cdot (\tilde{D}_H D^* \frac{\partial \tilde{x}}{\partial x} \nabla_{\tilde{x}} (\tilde{H} H^*)) \\
& - \lambda_{51} \tilde{H} H^* + \alpha_f \left(\lambda_{52} - \lambda_{53} \left(\frac{\tilde{H}}{\tilde{H}_M} \right)^{v_H} \right) \\
\frac{\tilde{H}_{\tilde{t}}}{T^*} + \frac{1}{T^*} \nabla_{\tilde{x}} \cdot (\tilde{\mathbf{u}}_w \tilde{H}) =& \frac{1}{T^*} \nabla_{\tilde{x}} \cdot (\tilde{D}_H \nabla_{\tilde{x}} \tilde{H}) \\
& - \lambda_{51} \tilde{H} + \alpha_f \left(\frac{\lambda_{52}}{H^*} - \frac{\lambda_{53}}{H^*} \left(\frac{\tilde{H}}{\tilde{H}_M} \right)^{v_H} \right) \\
\tilde{H}_{\tilde{t}} + \nabla_{\tilde{x}} \cdot (\tilde{\mathbf{u}}_w \tilde{H}) =& \nabla_{\tilde{x}} \cdot (\tilde{D}_H \nabla_{\tilde{x}} \tilde{H}) \\
& - \lambda_{51} T^* \tilde{H} + \alpha_f \left(\frac{\lambda_{52} T^*}{H^*} - \frac{\lambda_{53} T^*}{H^*} \left(\frac{\tilde{H}}{\tilde{H}_M} \right)^{v_H} \right) \\
\tilde{H}_{\tilde{t}} + \nabla_{\tilde{x}} \cdot (\tilde{\mathbf{u}}_w \tilde{H}) =& \nabla_{\tilde{x}} \cdot (\tilde{D}_H \nabla_{\tilde{x}} \tilde{H}) - \tilde{\lambda}_{51} \tilde{H} + \alpha_f \left(\tilde{\lambda}_{52} - \tilde{\lambda}_{53} \left(\frac{\tilde{H}}{\tilde{H}_M} \right)^{v_H} \right).
\end{aligned}$$

Note that the equations have the same form whether we write them using dimensionless or dimensional variables. Dropping the tilde notation, this means that we can use Equation (2.20) to represent the dimensionless model as well.